

https://dspace.org/

Finding the sweet-spot of a cricket bat using a mathematical approach

Rogers, Langton

2016-09-13

http://hdl.handle.net/10539/21020

Rogers, Langton (2016) Finding the sweet-spot of a cricket bat using a mathematical approach, University of Witwatersrand, Johannesburg, < http://wiredspace.wits.ac.za/handle/10539/21020>

Downloaded from a DSpace repository. https://dspace.org/

Finding The Sweet-Spot Of A Cricket Bat Using A Mathematical Approach

University Of The Witwatersrand
Department Of Computational And Applied Mathematics
Masters' Dissertation

Langton Rogers
389653

Supervised By
Dr Byron Jacobs & Dr Rhameez Herbst

2015

"The great thing in hitting is, not to be half-hearted about it; but when you make up your mind to hit, to do it as if the whole match depended upon that particular stroke."
W. G. Grace

The financial assistance of the National Research Foundation (NRF) towards this research is hereby acknowledged. Opinions expressed and conclusions arrived at, are those of the author and are not necessarily to be attributed to the NRF.

Declaration

I, Langton Rogers, declare that this thesis titled, 'Finding The Sweet-Spot Of A Cricket Bat Using A Mathematical Approach' and the work presented in it are my own. I confirm that:

- This work was done wholly or mainly while in candidature for a research degree at this University.
- Where any part of this thesis has previously been submitted for a degree or any other qualification at this University or any other institution, this has been clearly stated.
- Where I have consulted the published work of others, this is always clearly attributed.
- Where I have quoted from the work of others, the source is always given. With the exception of such quotations, this thesis is entirely my own work.
- I have acknowledged all main sources of help.
- Where the thesis is based on work done by myself jointly with others, I have made clear exactly what was done by others and what I have contributed myself.

Signed: 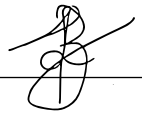

Date: 27 April 2016

Abstract

The ideal hitting location on a cricket bat, the 'sweet-spot', is taken to be defined in two parts: 1) the *Location of Impact* on a cricket bat that transfers the maximum amount of energy into the batted ball and 2) the *Location of Impact* that transfers the least amount of energy to the batsman's hands post-impact with the ball; minimizing the unpleasant stinging sensation felt by the batsman in his hands. An analysis of different hitting locations on a cricket bat is presented with the cricket bat modelled as a one dimensional beam which is approximated by the Euler-Lagrange Beam Equation. The beam is assumed to have uniform density and constant flexural rigidity. These assumptions allow for the Euler-Lagrange Beam Equation to be simplified considerably and hence solved numerically. The solution is presented via both a Central Time, Central Space finite difference scheme and a Crank-Nicolson scheme. Further, the simplified Euler-Lagrange Beam Equation is solved analytically using a Separation of Variables approach. Boundary conditions, initial conditions and the framework of various collision scenarios between the bat and ball are structured in such a way that the model approximates a batsman playing a defensive cricket shot in the first two collision scenarios and an aggressive shot in the third collision scenario. The first collision scenario models a point-like, impulsive, perpendicular collision between the bat and ball. A circular Hertzian pressure distribution is used to model an elastic, perpendicular collision between the bat and ball in the second collision scenario, and an elliptical Hertzian pressure distribution does similarly for an elastic, oblique collision in the third collision scenario. The pressure distributions are converted into initial velocity distributions through the use of the Lagrange Field Equation. The numerical solution via the Crank-Nicolson scheme and the analytical solution via the Separation of Variables approach are analysed. For different *Locations of Impact* along the length on a cricket bat, a post-impact analysis of the displacement of points along the bat and the strain energy in the bat is conducted. Further, through the use of a Fourier Transform, a post-impact frequency analysis of the signals travelling in the cricket bat is performed. Combining the results of these analyses and the two-part definition of a 'sweet-spot' allows for the conclusion to be drawn that a *Location of Impact* as close as possible to the fixed-end of the cricket bat (a point just below the handle of the bat) results in minimum amount of energy transferred to the hands of the batsman. This minimizes the 'stinging' sensation felt by the batsman in his hands and satisfies the second part of the definition of a sweet-spot. Due to the heavy emphasis of the frequency analysis in this study, the conclusion is drawn that bat manufacturers should consider the vibrational properties of bats more thoroughly in bat manufacturing. Further, it is concluded that the solutions from the numerical Crank-Nicolson scheme and the analytical Separation of Variables approach are in close agreement.

Acknowledgments

I would like to extend a note of deep gratitude to Dr Byron Jacobs and Dr Rhameez Herbst for their unending patience, professional conduct, invaluable advice and priceless help over the past two years. The success of this work is owed entirely to their commitment and dedication as supervisors and I am eternally grateful for their efforts.

I trust that you will enjoy reading through this dissertation and that the work done here has provided you with an appreciation of the mathematics behind a collision of cricket bat with a cricket ball; the cornerstone of the great game that is cricket.

Contents

List of Figures

1 Introduction **1**

2 Reviewing The Literature **3**

3 The Model And Relevant Conditions **10**
3.1 The Model 10
3.2 Discussion of the Boundary and Initial Conditions 14
3.2.1 Boundary Conditions 14
3.2.2 Initial Conditions 15
3.3 Discussion Of The Various Collision Scenarios 16
3.3.1 Collision Scenario 1 - Impulsive, Point-Like, Perpendicular Collision 17
3.3.2 Collision Scenario 2 - Elastic, Perpendicular Collision . 18
3.3.3 Collision Scenario 3 - Elastic, Oblique Collision 21
3.4 Parameters and Values Used in the Model 25

4 Numerical Solution To The Equation **28**
4.1 Central-in-Time and Central-in-Space Method 28
4.1.1 CTCS Scheme 28
4.1.2 Boundary Conditions for CTCS Scheme 28
4.1.3 Initial Conditions for CTCS Scheme 29
4.1.4 Discretised Equation via CTCS Scheme 30
4.1.5 Consistency of the CTCS Scheme 34
4.1.6 Stability of the CTCS Scheme 34
4.1.7 Convergence of the CTCS Scheme 37
4.2 Crank-Nicolson Method 38
4.2.1 CN Scheme 38
4.2.2 Boundary Conditions for the CN Scheme 39
4.2.3 The Initial Conditions For The CN Scheme 39
4.2.4 Discretised Equation via the CN Scheme 39
4.2.5 Consistency of the CN Scheme 46
4.2.6 Stability of the CN Scheme 47
4.2.7 Convergence of the CN Scheme 48
4.3 Model Implementation 49

5 Solution Via Separation Of Variables **50**
5.1 The General Solution 50
5.2 Proving Orthogonality of the Spatial Solution 56
5.3 Completing The General Solution 59

6 Analysis Of The Results **63**
6.1 Analyses Used in the Model 63
6.1.1 Initial Velocity Analysis 63
6.1.2 Displacement Analysis And Its Associated Error 64
6.1.3 Strain Energy Analysis And Its Associated Error . . . 65
6.1.4 Analysis Using A Fourier Transform 67
6.1.5 Analyses Of The Pressure Distributions 69
6.1.6 A Note On The `Mathematica` Implementation 69
6.2 Analyzing The Results For An Impulsive, Perpendicular Collision - Scenario 1 70
6.2.1 Analysis for *Location of Impact* Near the Free-End of the Bat (at 0.45m) 71
6.2.2 Analysis for *Location of Impact* at the Middle of the Bat (at 0.25m) 73
6.2.3 Analysis for *Location of Impact* Near the Fixed-End of the Bat (at 0.05m) 76
6.2.4 Discussion for Scenario where Collision is Impulsive and Perpendicular 79
6.3 Analyzing The Results For An Elastic, Perpendicular Collision - Scenario 2 81
6.3.1 Analysis for *Location of Impact* Near the Free-End of the Bat (at 0.45m) 81
6.3.2 Analysis for *Location of Impact* at the Middle of the Bat (at 0.25m) 86
6.3.3 Analysis for *Location of Impact* near the Fixed-End of the Bat (at 0.05m) 89
6.3.4 Discussion for Scenario where Collision is Elastic and Perpendicular 93
6.4 Analyzing The Results For An Elastic, Oblique Collision - Scenario 3 95
6.4.1 Analysis for *Location of Impact* near the Free-End of the Bat (at 0.45m) 95
6.4.2 Analysis for *Location of Impact* at the Middle of the Bat (at 0.25m) 100
6.4.3 Analysis for *Location of Impact* near the Fixed-End of the Bat (at 0.05m) 103
6.4.4 Discussion for Scenario where Collision is Elastic and Oblique 107

7 Discussion of the Results **110**

8 Conclusion **112**

9 References **115**

List of Figures

3.1 *Jacques Kallis illustrating a textbook forward defensive shot. This is the type of shot to be modelled in the first and second collision scenarios.* 10

3.2 *Graeme Smith illustrating a typical aggressive shot. This is the type of shot to be modelled in the third collision scenario. Note the upward motion of the bat through the collision zone with the ball: hitting 'on the up'.* 11

3.3 *Diagram portraying the perpendicular, impulsive collision between bat and ball in the first scenario.* 18

3.4 *Diagram portraying the perpendicular, elastic collision between bat and ball in the second scenario.* 21

3.5 *Diagram portraying the oblique, elastic collision between bat and ball in the third scenario.* 25

5.1 *The graphs of* $y = \cos(x)\cosh(x)$ *and* $y = -1$ *illustrating an infinite number of intersections between the functions.* 53

6.1 *The initial velocity distribution for Location of Impact near the free-end of the bat (0.45m) for an impulsive, perpendicular collision* 71

6.2 *The displacement solution for Location of Impact near the free-end of the bat (at 0.45m) for an impulsive, perpendicular collision* 72

6.3 *The Fourier Transform for Location of Impact near the free-end of the bat (at 0.45m) for an impulsive, perpendicular collision* 72

6.4 *The strain energy for Location Of Impact near the free-end of the bat (at 0.45m) for an impulsive, perpendicular collision* . . 73

6.5 *The initial velocity distribution for Location of Impact at the middle of the bat (0.25m) for an impulsive, perpendicular collision* 74

6.6 *The displacement solution for Location of Impact at the middle of the bat (at 0.25m) for an impulsive, perpendicular collision* 74

6.7 *The Fourier Transform for Location of Impact at the middle of the bat (at 0.25m) for an impulsive, perpendicular collision* 75

6.8 *The strain energy for Location of Impact at the middle of the bat (at 0.25m) for an impulsive, perpendicular collision* 75

6.9 *The initial velocity distribution for Location of Impact near the fixed-end of the bat (0.05m) for an impulsive, perpendicular collision* 76

6.10 *The displacement solution for Location of Impact near the fixed-end of the bat (at 0.05m) for an impulsive, perpendicular collision* 77

6.11 *The Fourier Transform for Location of Impact near the fixed-end of the bat (at 0.05m) for an impulsive, perpendicular collision* 78
6.12 *The strain energy for Location of Impact near the free-end of the bat (at 0.05m) for an impulsive, perpendicular collision* . . 78
6.13 *The presure distribution caused by the ball impacting the bat for Location of Impact near the free-end of the bat (0.45m) for an elastic, perpendicular collision* 81
6.14 *The initial velocity distribution for Location of Impact near the free-end of the bat (0.45m) for an elastic, perpendicular collision* 82
6.15 *The initial velocity distribution as derived from the analytical solution and as used in the numerical solution for Location of Impact near the free-end of the bat (0.45m) for an elastic, perpendicular collision* 82
6.16 *The displacement profile from analytical solution for Location of Impact near the free-end of the bat (at 0.45m) for an elastic, perpendicular collision* 83
6.17 *The displacement profile from numerical solution for Location of Impact near the free-end of the bat (at 0.45m) for an elastic, perpendicular collision* 84
6.18 *The error between the analytical solution and the numerical solution for Location of Impact near the free-end of the bat (at 0.45m) for an elastic, perpendicular collision* 84
6.19 *The Fourier Transform from the numerical solution for Location of Impact near the free-end of the bat (at 0.45m) for an elastic, perpendicular collision* 85
6.20 *The strain energy over the short time period from the analytical solution to be compared to the numerical solution for Location of Impact near the free-end of the bat (at 0.45m) for an elastic, perpendicular collision* 85
6.21 *The strain energy over the short time period from the numerical solution to be compared to the analytical solution for Location of Impact near the free-end of the bat (at 0.45m) for an elastic, perpendicular collision* 86
6.22 *The displacement profile from analytical solution for Location of Impact at the middle of the bat of the bat (at 0.25m) for an elastic, perpendicular collision* 87
6.23 *The displacement profile from numerical solution for Location of Impact at the middle of the bat of the bat (at 0.25m) for an elastic, perpendicular collision* 87

6.24 *The error between the analytical solution and the numerical solution for Location of Impact at the middle of the bat of the bat (at 0.25m) for an elastic, perpendicular collision* 88
6.25 *The Fourier Transform from the numerical solution for Location of Impact at the middle of the bat of the bat (at 0.25m) for an elastic, perpendicular collision* 88
6.26 *The strain energy over the entire time period from the analytical solution for Location of Impact at the middle of the bat of the bat (at 0.25m) for an elastic, perpendicular collision* . . . 89
6.27 *The displacement profile from analytical solution for Location of Impact near the fixed-end of the bat of the bat (at 0.05m) for an elastic, perpendicular collision* 90
6.28 *The displacement profile from numerical solution for Location of Impact near the fixed-end of the bat of the bat (at 0.05m) for an elastic, perpendicular collision* 90
6.29 *The error between the analytical solution and the numerical solution for Location of Impact near the fixed-end of the bat of the bat (at 0.05m) for an elastic, perpendicular collision* . . . 91
6.30 *The Fourier Transform from the numerical solution for Location of Impact near the fixed-end of the bat of the bat (at 0.05m) for an elastic, perpendicular collision* 92
6.31 *The strain energy over the entire time period from the analytical solution for Location of Impact near the fixed-end of the bat of the bat (at 0.05m) for an elastic, perpendicular collision* 92
6.32 *The presure distribution caused by the ball impacting the bat for Location of Impact near the free-end of the bat (0.45m) for an elastic, oblique collision* 95
6.33 *The initial velocity distribution for Location of Impact near the free-end of the bat (0.45m) for an elastic, oblique collision* 96
6.34 *The initial velocity distribution as derived from the analytical solution and as used in the numerical solution for Location of Impact near the free-end of the bat (0.45m) for an elastic, oblique collision* 96
6.35 *The displacement profile from analytical solution for Location of Impact near the free-end of the bat (at 0.45m) for an elastic, oblique collision* 97
6.36 *The displacement profile from numerical solution for Location of Impact near the free-end of the bat (at 0.45m) for an elastic, oblique collision* 97
6.37 *The error between the analytical solution and the numerical solution for Location of Impact near the free-end of the bat (at 0.45m) for an elastic, oblique collision* 98

6.38 *The Fourier Transform from the numerical solution for Location of Impact near the free-end of the bat (at 0.45m) for an elastic, oblique collision* 98
6.39 *The strain energy over the short time period from the analytical solution to be compared to the numerical solution for Location of Impact near the free-end of the bat (at 0.45m) for an elastic, oblique collision* 99
6.40 *The strain energy over the short time period from the numerical solution to be compared to the analytical solution for Location of Impact near the free-end of the bat (at 0.45m) for an elastic, oblique collision* 100
6.41 *The displacement profile from analytical solution for Location of Impact at the middle of the bat of the bat (at 0.25m) for an elastic, oblique collision* 101
6.42 *The displacement profile from numerical solution for Location of Impact at the middle of the bat of the bat (at 0.25m) for an elastic, oblique collision* 101
6.43 *The error between the analytical solution and the numerical solution for Location of Impact at the middle of the bat of the bat (at 0.25m) for an elastic, oblique collision* 102
6.44 *The Fourier Transform from the numerical solution for Location of Impact at the middle of the bat of the bat (at 0.25m) for an elastic, oblique collision* 102
6.45 *The strain energy over the entire time period from the analytical solution for Location of Impact at the middle of the bat of the bat (at 0.25m) for an elastic, oblique collision* 103
6.46 *The displacement profile from analytical solution for Location of Impact near the fixed-end of the bat of the bat (at 0.05m) for an elastic, oblique collision* 104
6.47 *The displacement profile from numerical solution for Location of Impact near the fixed-end of the bat of the bat (at 0.05m) for an elastic, oblique collision* 104
6.48 *The error between the analytical solution and the numerical solution for Location of Impact near the fixed-end of the bat of the bat (at 0.05m) for an elastic, oblique collision* 105
6.49 *The Fourier Transform from the numerical solution for Location of Impact near the fixed-end of the bat of the bat (at 0.05m) for an elastic, oblique collision* 106
6.50 *The strain energy over the entire time period from the analytical solution for Location of Impact near the fixed-end of the bat of the bat (at 0.05m) for an elastic, oblique collision* . . . 107

1 Introduction

There are few better sights in the world of cricket, and indeed in the world of sport, than that of a Virat Kohli cover drive, a AB de Villiers pull over mid-wicket, a Hashim Amla leg-glance through square leg or a David Warner cut behind point. The bowler looks dejected, the batsman looks smug; satisfied that the shot came out of the 'middle' of the bat.

What exactly does that mean; the 'middle' of the bat? Clearly it's where the batsman is striving to hit the ball so he can keep piling runs onto the score and misery onto the bowler. However, ask a batsman to explain what the 'middle' of his bat actually is and he'll shrug his shoulders and point to the general area on the blade of his wooden weapon where he recalls the ball flew off particularly sweetly and say "I don't know mate, but it's somewhere here".

So this begs the question: where on the blade of that bat is the best location to hit a cricket ball? Is it where the impact between bat and ball sounds crisp and sharp? How about where the batsman feels like he was hitting a pat of butter as opposed to a cricket ball? Or is it the location where the ball leaves the bat with maximum possible velocity? Could it be some combination of these?

A fair but rather limited amount of work and research has been conducted into this area in order to determine the location of the 'sweet-spot' on a cricket bat and the location to hit the ball in order to achieve maximum performance of the bat. Of course, the research has not only been limited to cricket but extends to other sports that use a similar idea of hitting a ball with a piece of equipment such as baseball, golf, tennis and squash. In this work, the main focus is on cricket with a number of references to baseball due to the obvious similarities between the two sports when attempting to hit the corresponding balls.

In the work that follows in this project, the results when a moving ball collides with various positions on a cricket bat are analyzed through the use of the presented model. Using a definition taken from the literature and based on the work done in this project, conclusions are drawn for the ideal *Location of Impact* for a moving ball onto a cricket bat; the 'sweet-spot'.

Chapter 2 reviews the literature produced by other authors whose work holds relevance to this project. Chapter 3 introduces the model and the relevant boundary and initial conditions. This Chapter also describes the process of and reasoning behind the analysis of the results of the implementation of the model. Chapter 4 deals with the set-up, structure and solving of

the Central-in-Space, Central-in-Time scheme and Crank-Nicolson scheme as well as the discussions of the stability, consistency and convergence of these schemes. Chapter 5 solves the model that was introduced in Chapter 3 using the Separation Of Variables technique. Chapter 6 presents the results of the implementation of the scheme over various cases. These results are analyzed and conclusions are drawn from these results in Chapters 7 and 8.

Finding The Sweet-Spot Of A Cricket Bat
Using A Mathematical Approach

2 Reviewing The Literature

Before commencing with a discussion of the details of finding the sweet-spot on a bat, it is important to note that the 'sweet-spot' has been defined in numerous ways, but not entirely differently, over time. Russell provides a range of definitions for the sweet-spot in [22]:

- The location which produces the least vibrational sensation (sting) in the batter's hands.
- The location which produces maximum batted ball speed.
- The location where maximum energy is transferred to the ball.
- The location where the coefficient of restitution is maximized.
- The Centre of Percussion.
- The node of the fundamental vibrational mode.
- The region between the nodes of the first two vibrational modes.
- The region between the Centre of Percussion and the node of the first vibrational mode.

An important concept is that of the Centre of Percussion. Russel [22] describes how the Centre of Percussion of a bat can be found. If a bat was pivoted about a point on the handle, say, and one was to measure the time that it the bat takes to swing back and forth through one cycle under the force of gravity, then this will determine the Centre of Percussion using the formula

$$\text{COP} = \frac{T^2 g}{4\pi^2}, \tag{2.1}$$

where T is the period of oscillation and g is acceleration due to gravity. It is interesting to note that Russel immediately rules out the Centre of Percussion as being the sweet-spot on the bat since the Centre of Percussion is dependent on where the bat is pivoted and so is not a fixed point on the bat.

Brearley *et al.* [3] make the assumption that the bat is a rigid object, and this object remains rigid when the bat hits the ball. After constructing a series of experiments using a traditional cricket bat, Brearley *et al.* find that there appears to be a point near the Centre of Percussion where the ball rebounds at maximum speed. Brearley *et al.* consider the Centre of Percussion to be a crucial factor in the determining the location of the sweet-spot, but not going as far to say that the Centre of Percussion is the sweet-spot. However, there

is a distinct difference in their experimental results and the results that their mathematical model predicts with the rigid bat assumption. Brearley *et al.* conclude that although the rigid bat assumption would help in determining the location of the sweet-spot with help from the Centre of Percussion, the maximum ball speed cannot be accurately predicted because the assumption of a rigid bat takes away the 'spring' effect of the bat; that is, the vibrations and flex of the bat during and after impact.

Brody [4] continues the idea of considering a rigid bat, this time by analyzing the dynamics of a baseball bat after collision with a baseball. Brody argues that the point to achieve maximum ball speed off the bat ("maximum power point") is not the Centre of Percussion but another point that is dependent on each individual pitch. This "maximum power point" is dependent on the factors such as the speed of the pitch, the mass of the ball, etc. Brody also mentions a concept that is discussed by Brearley *et al.* [3] too: for balls that approach the bat with higher speed, the "maximum power point" appears to be located closer to the batter's/ batsman's hands and further towards the toe-end (free-end) of the bat for slower pitches. In short, both Brearley *et al.* and Brody, both of whom made the assumption that the bat was rigid, appear to agree that the sweet-spot, as they define it, is the maximum power point that is dependent on the characteristics of each individual delivery/pitch and the location appears to be in the area of, but is not necessarily, the Centre of Percussion.

The idea of a more realistic flexible bat is now introduced. Penrose and Hose [21] use a Finite Element method to model the mechanics of the impact between bat and ball. Penrose and Hose claim that the impact point that provides the greatest velocity to the ball after it has been hit by the bat is dependent on the bat's vibrational properties and is not necessarily at the Centre of Percussion. Penrose and Hose model their bat as a uniform beam. In their experiments and model, Penrose and Hose show that the first flexure mode was of significant importance. This leads to their reasoning that an impact at the node of the first flexure mode will not excite this mode and more energy will be imparted to the ball as kinetic energy as opposed to an impact away from this same node, which will excite this mode and absorb an amount of energy as vibrational energy. Penrose and Hose further reason that it would be desirable to excite as few modes as possible, in order for as few vibrations to take place in the bat as possible and more kinetic energy to be transferred to the ball. They also argue that the flexural and vibrational properties in cricket bat design should be given more consideration than they have been granted in the past.

Knowles *et al.* [17] extend the idea of vibrational analysis in bats. They

also model their bat as a beam and make the simplifying assumption of the ball to be a sphere. Their model uses a combination of vibrational and impact theory through a computer model, a cricket ball impact test as well as a modal analysis. Their results are in agreement with Penrose and Hose [21] with regard to the dominance of the first mode but state that it is difficult to determine the role of higher modes in a real bat due to the cross-section variations in cricket bats. Further, Knowles *et al.* claim that their model comes up short with regards to the the batsman holding the bat. They reason that the batsman's hands cannot be modelled accurately as a clamp and different boundary conditions should be considered. Finally, Knowles *et al.* reason that a stiffer and heavier bat will vibrate less and will hit the ball the furthest.

Hariharan and Srinivasan [14] also make use of a computational Finite Element approach, in order to predict the performance of a cricket bat. Hariharan and Srinivasan use modal analysis to determine the location of the region between the first two modes of vibration. By doing this, they are able to establish the relationship between these two nodes and the area that provides the highest velocity to the ball after an impact has occurred. Hariharan and Srinivasan find that for all the tests that were conducted at various ball speeds and bat angles, this area (or just outside this area) produces the maximum post impact velocity of the ball. So now a new concept can be considered; the idea of not just a sweet-spot but rather that of a sweet-zone on the bat that can produce the highest post impact ball velocity.

Bower [2] builds on the idea of a sweet-zone, saying that an impact at the sweet-zone will provide minimum shock to the hands. In agreement with both Brearley *et al.* [3] and Brody [4] above, Bower claims that the sweet-spot is dependent on the shot being played and the speed of the ball just before impact. Bower, like Brearley *et al.* and Brody, claims that for balls travelling faster before impact the sweet-spot is located about 15-20cm away from the base of the bat. For slower deliveries, the sweet-spot moves towards the toe end of the bat. Bower measures the rebound speeds of balls of a swinging pendulum bat and hence calculated the Apparent Coefficients of Restitution in order to arrive at his results.

Cross [9] also discusses the idea of a sweet-zone. Cross says that the sweet-spot on a baseball bat can be defined in terms of a vibration node or in terms of the Centre of Percussion. Cross attempts to measure the forces that are felt by the hands of the batsman/batter before and during impact. Cross mentions the work done by Brody in [4] and discusses the sweet-zone in terms of the node of the first mode of vibration and the Centre of Percussion. Cross points out that since these two spots are fairly close together, they could lie in a zone that could, in fact, be the sweet-zone on the bat. After his experi-

ments, Cross concludes that there exists a zone of about 3cm in width such that when the ball strikes the bat in this zone, the impulse sent to the hands on the batsman is minimized. Cross measures this force electronically by using two ceramic piezoelectric disks taped to the bat handle. Cross claims that this zone exists because of the Centre of Percussion and the node of the first mode of vibration.

Gutaj [13] uses three different methods to model the dynamics of a cricket bat. Like Penrose and Hose [21] and Hariharan and Srinivasan [14], Gutaj makes use of a Finite Element method. Gutaj makes use of both a tapered and uniform beam model to supplement the Finite Element model. Gutaj argues that the rigid body models introduced would help to model the performance of bats when impact is made near the sweet-spot but don't take into account the energy that is lost to vibrations when impacts are made away from the sweet-spot; a similar argument to that of Brearley *et al.* in [3]. Gutaj, like Brearley *et al.* and Brody [4], questions whether the Centre of Percussion is the sweet-spot of the bat and leans towards the idea that the sweet-spot is some point between the Centre of Percussion and the Centre of Mass. Gutaj's Finite Element model stresses the importance of the first mode, which is consistent to the results found in [21], [17] and [9].

An interesting case in such analyses is that of the *Mongoose* bat, which Bull [5] describes as a bat with a 'short blade and a blade/handle join that does not protrude beyond the neck of the blade'. The *Mongoose* bat was designed to supposedly give batsmen an extra advantage in order to hit the ball further and harder. Bull also likens a cricket bat to a uniform beam and uses a vibrational analysis on traditional and *Mongoose* cricket bats. He attempts to calculate the moment of inertia of the cricket bats by considering them to be a simple pendulum when moving to hit a ball. Bull concludes that the *Mongoose* bats have a stiffer blade than traditional bats. Further, the vibrational properties in both types of bats are similar, resulting in a likely advantage in performance for the *Mongoose* bat, without added discomfort to the batsman in terms of shock to the hands during impact. Bull states that the biggest differences between the *Mongoose* and traditional bats is the fact that the *Mongoose* has a greater moment of inertia, which will allow the bat to swing faster and impart a greater velocity on the ball after the impact.

Jaramillo *et al.* [15] very aptly incorporate many of the ideas presented above. The authors attempt to find peak frequencies and vibrational modes as well as the relation of these to the sweet-spot of the bat. Furthermore, they carry out physical experiments on the bat as well as conducting a modal analysis on the bat which validates the results that are produced by the experiment. As with Penrose and Hose [21], Knowles *et al.* [17], Gutaj [13] and Bull [5],

Jaramillo *et al.* assume that the bat can be modelled as a uniform beam. Further, Jaramillo *et al.* make use of the beam equation of motion, the Euler-Lagrange beam equation given by

$$EI\frac{\partial^4 y}{\partial x^4} + \gamma\frac{\partial^2 y}{\partial t^2} = 0, \tag{2.2}$$

where E is the modulus of elasticity (Young's Modulus), I is the area moment of inertia and γ is the mass per unit length. The product EI is the flexural rigidity of the bat. The solution $y(x,t)$ is displacement of a point x on the beam at time t.

Jaramillo *et al.* agree with Hariharan and Srinivasan [14], Bower [2] and Cross [9] in saying that the sweet-spot on a bat should actually be considered to be a sweet-zone; a zone that should be in the area around the Centre of Percussion and the two nodes of the first two vibration modes.

In order for an elastic collision between a cricket bat and cricket ball to be modelled, it is necessary to determine the force a bat experiences when struck by a ball over an area. This is opposed to the simpler case of an impulsive 'point-collision' where, in the model presented in this work, the contact point on the bat will be have an initial velocity no less than a common speed of a cricket ball when it hits a cricket bat. In the case of elastic collision, the initial velocity of the area of collision will be determined from realistic values and hence the behaviour over time of the bat will be determined.

Pauchard and Rica [20] introduce the important concept of compression of a ping-pong ball when it is being struck by a paddle. The same concepts discussed by Pauchard and Rica will be used in this work in the compression of a cricket ball against a cricket bat. Pauchard and Rica discuss how a ping-pong ball - an elastic spherical body - experiences elastic deformation under a compression force on a plane. Recall that Knowles *et al.* also make the assumption of a the ball being a sphere in [17]. Suppose the sphere is given a radius R, a mass m and that it impacts a rigid plane with an impact velocity of v_0. Pauchard and Rica argue that the kinetic energy in the sphere will transform to elastic energy entirely during contact with the rigid plane. This will halt the motion of the projectile and will cause some deformation to the sphere, which Pauchard and Rica call ϵ_{max}. Pauchard and Rica find ϵ_{max} by solving the following differential equation, which they arrive at through the principle of conservation of energy,

$$\epsilon'(r) + kc^2\left(\frac{\epsilon(r)}{R_b}\right)^{\frac{5}{2}} = {v_0}^2,$$

where k is a dimensionless constant that is dependent on the Poisson Ratio of the sphere, c is the speed of sound in the material of the sphere and

$0 < r \leq R_b$.

This value ϵ_{max} helps in determining the diameter D of the contact zone of the sphere on the plane. Pauchard and Rica provide

$$D = 2(R\epsilon)^{\frac{1}{2}},$$

where the value of ϵ_{max} can then be used in the place of ϵ.

Cross provides a second study which is of use here. In his paper [10], Cross discusses the dynamics of a number of different balls bouncing off an elastic surface, the surface being a 'heavy brass rod'. Cross electronically measures the force acting on the balls when they are dropped on the rod and hence produces dynamic and static hysteresis curves for the balls. Cross is hence able to analyze the compression distances of the balls against the applied forces. Cross concludes that all of the balls - except one - were slightly compressed when they rebounded but is quick to point out that the major loss of energy doesn't occur after the bounce but rather while the ball is in the process of bouncing. Cross writes that the compression of balls is an important feature in some sports (tennis, for example) and that balls with different compression characteristics behave quite differently.

In a similar argument to that of Cross in [10], Carré, James and Haake [6] write that even a cricket ball impacting on a surface with different orientations can produce different results. The authors found that when a cricket ball impacted the surface on the seam, the ball experienced greater deformation than when the ball impacted on the surface perpendicular to the seam.

Adair [1] discusses the collision between a bat and ball in baseball. Of particular importance in this work, Adair writes about the time scale of a collision between a bat and ball as well as the flexibility of the bat during the collision. Essentially, Adair argues that the time that the ball spends in contact with the bat is significantly shorter than the time taken for waves generated in the bat as a result of the collision to propagate back to the point of the collision. Further, and in contrast to Brearley *et al.* [3], Adair notes that the bat is indeed flexible over the time scale of the collision.

Johnson [16] provides a means for determining the pressure distribution of the ball on the cricket bat. This will lead to determining the force of the ball on the bat and eventually the initial velocity of contact area of the ball on the bat. Derived from Hertz Theory, Johnson provides a pressure distribution that arises when two solids of revolution come into contact. Clearly, in the case of a sphere impacting a plane perpendicularly, the contact area will be

circular (in two dimensions). Suppose the radius of the circular contact area is $\hat{R}$. Then Johnson gives the Hertz pressure distribution to be

$$p(\hat{r}) = p_0 \frac{\left(\hat{R}^2 - \hat{r}^2\right)^{\frac{1}{2}}}{\hat{R}},$$

where $0 < \hat{r} \leq \hat{R}$ and p_0 is some initial constant pressure. Also derived from Hertz Theory is the case where the pressure distribution is ellipsoidal in shape, and Johnson [16] gives this pressure distribution as

$$p(x, y) = p_0 \left(1 - \left(\frac{x}{a}\right)^2 - \left(\frac{y}{b}\right)^2\right)^{\frac{1}{2}},$$

where $p_0(v_0)$ is determined from the elastic equations and energy considerations, a is the semi-major axis of the ellipse and b is the semi-minor axis of the ellipse.

The beam equation given by Jaramillo *et al.* in (2.2) can be solved analytically. Meirovitch [18] details a Separation Of Variables approach to solving the beam equation with a variety of boundary conditions.

Fornberg [11] illustrates important finite difference approximations that will be used in this work.

3 The Model And Relevant Conditions

3.1 The Model

The model presented in this work will describe three collision scenarios. The first two collision scenarios will model an initially stationary cricket bat that is struck by a moving ball at some point along the blade of the bat, the *Location of Impact*. This case can be considered as a batsman playing a defensive shot with his bat initially stationary, to simply knock the ball away from himself. Figure 3.1 shows South Africa's now retired Jacques Kallis, formally one of the world's premier batsmen, playing the defensive shot that is to be modelled. As an interesting aside, pundits often referred to Kallis' defensive shot as the 'barn door', as it was seemingly impossible to get past at times.



Figure 3.1: *Jacques Kallis illustrating a textbook forward defensive shot. This is the type of shot to be modelled in the first and second collision scenarios.*

The third collision scenario will model an initially moving cricket bat that is struck by a moving ball at some point along the blade of the bat, the *Location of Impact*. This case can be considered as a batsman playing an aggressive shot with his bat initially moving, with the objective of scoring runs. In this scenario, the ball is taken to be hit 'on-the-up'; that is, the bat is moving through the collision with the ball in an upward motion. This is an important concept for the 'angle of incidence' between the bat and ball that will be discussed later for this collision scenario. Figure 3.2 shows South Africa's recently retired and former captain Graeme Smith playing the shot that is to be modelled.



Figure 3.2: *Graeme Smith illustrating a typical aggressive shot. This is the type of shot to be modelled in the third collision scenario. Note the upward motion of the bat through the collision zone with the ball: hitting 'on the up'.*

Recall from Chapter 2 that the concept of modelling the cricket bat as a uniform beam was was presented by Penrose and Hose [21], Knowles *et al.* [17], Gutaj [13], Bull [5] and Jaramillo *et al.* [15]. In this work, the same assumption is made that the cricket bat is a uniform beam. Further, the beam will be modelled by the Euler-Lagrange Beam Equation in order to conduct the analyses of the sweet-spot or sweet-zone of the cricket bat.

The Euler-Lagrange Beam Equation is given by

$$\frac{\partial^2 y}{\partial t^2} = -\frac{\partial^2}{\partial x^2}\left[\frac{EI}{\gamma}\frac{\partial^2 y}{\partial x^2}\right], \tag{3.1}$$

where E is the modulus of elasticity (Young's Modulus), I is the area moment of inertia and γ is the mass per unit length (density). The product EI is the flexural rigidity of the bat. The solution $y(x,t)$ describes the displacement of point $x \in [0, L]$ at some time $t \geq 0$ where L is the length of the bat.

Recall that the simplifying assumption is made that the beam is uniform. This implies that the elasticity E is uniform throughout the bat and is hence not dependent on x; that is, the elasticity is the for all points on the beam. Also, this assumption implies that the density is constant throughout the beam; that is, the density is equal for all points on the beam. Hence γ is not dependent on x either. Finally, the moment of inertia I will be equal for all points on the beam since it has been assumed that the beam is uniform. Further then, the flexural rigidity of the bat EI will be constant throughout its length. Taking into account these facts, it is possible to arrive at the equation that is used by Jaramillo *et al.* [15]:

$$\frac{\partial^2 y}{\partial t^2} = -\frac{EI}{\gamma}\frac{\partial^4 y}{\partial x^4}. \tag{3.2}$$

This equation is now appropriately scaled by making the following substitutions:

$$x = Lx', t = \Delta t t', \tag{3.3}$$

where Δt is the incremental time step and L is the length of the bat. Then from equation (3.3)

$$dx = Ldx' \tag{3.4}$$

and

$$dt = \Delta t dt'. \tag{3.5}$$

Hence, from the Beam equation (3.2),

$$\begin{aligned} \frac{\partial^2 y}{\partial t^2} &= \left(\frac{\partial}{\partial t}\right)\left(\frac{\partial y}{\partial t}\right) \\ &= \left(\frac{\partial}{\Delta t \partial t'}\right)\left(\frac{\partial y}{\Delta t \partial t'}\right) \\ &= \left(\frac{\partial^2 y}{(\Delta t)^2 \partial t'^2}\right). \end{aligned} \tag{3.6}$$

Similarly, also from equation (3.2),

$$\begin{aligned} \frac{\partial^4 y}{\partial x^4} &= \left(\frac{\partial^3}{\partial x^3}\right)\left(\frac{\partial y}{\partial x}\right) \\ &= \left(\frac{\partial^3}{\partial x^3}\right)\left(\frac{\partial y}{L\partial x'}\right) \\ &\vdots \\ &= \left(\frac{\partial^4 y}{L^4 \partial x'^4}\right). \end{aligned} \tag{3.7}$$

Substituting equations (3.6) and (3.7) into equation (3.2) gives

$$\begin{aligned} \frac{1}{(\Delta t)^2}\left(\frac{\partial^2 y}{\partial t'^2}\right) &= -\frac{EI}{\gamma L^4}\left(\frac{\partial^4 y}{\partial x'^4}\right) \\ \implies \frac{\partial^2 y}{\partial t'^2} &= -Z\frac{\partial^4 y}{\partial x'^4} \end{aligned} \tag{3.8}$$

where

$$Z = \frac{EI\,(\Delta t)^2}{\gamma L^4} \tag{3.9}$$

Z is a dimensionless parameter of the equation. Note that since $(\Delta t)^2$ is measured in squared units of time and L^2 is measured in squared units of distance, it follows that $\frac{EI}{\gamma L^2}$ is measured in the squared units of velocity. Further, the square root of this quantity must represent the wave-speed in the bat. Let

$$\begin{aligned} c_b &= \frac{\sqrt{EI}}{L\sqrt{\gamma}} \\ \implies c_b^2 &= \frac{EI}{\gamma L^2}. \end{aligned} \tag{3.10}$$

Substituting this into equation (3.9) gives

$$\begin{aligned} Z &= {c_b}^2\frac{(\Delta t)^2}{L^2} \\ \implies Z^{\frac{1}{2}} &= c_b\frac{\Delta t}{L} \\ &= \Delta t\frac{c_b}{L} \end{aligned} \tag{3.11}$$

Consider the quantity $\frac{L}{c_b}$. It is clear to see this is a characteristic time scale since L has units of length and c_b has units of velocity. In particular, this quantity represents the time taken for a wave to propagate through the length of the bat L at a velocity c_b. Let

$$\Delta b = \frac{L}{c_b}. \tag{3.12}$$

Substituting equation (3.12) into equation (3.11) gives

$$Z^{\frac{1}{2}} = \frac{\Delta c}{\Delta b} \tag{3.13}$$

where

$$\Delta c = \Delta t \tag{3.14}$$

is the ball contact time with the bat. It is therefore possible to choose $\Delta c = \Delta t << 1$ in such a way to ensure that $Z^{\frac{1}{2}} = \frac{\Delta c}{\Delta b} << 1$.

If the parameter $\frac{\Delta_c}{\Delta_b}$ is much less than 1, then the time that the ball is in contact with the bat is small relative to the time that it takes for a wave to propagate through the length of the bat. This has the implication that the batsman's grip (modelled by the boundary conditions at the fixed-end of the bat $x = 0$) does not affect the velocity of the ball as it leaves the bat. If this were the case, the model presented in this work can be considered to be accurate.

However, if the the ratio $\frac{\Delta_c}{\Delta_b}$ is large (approximately 1 or larger than 1), this has the implication that the waves that are present in the bat as a result of the collision will propagate back to the *Location of Impact* while the ball is still in contact with the bat. This means that the batsman's grip at the fixed-end of the bat will influence the speed of the ball off the bat. If this were the case, the model presented in this work will be considerably inaccurate as the ball propagation problem and the bat flexure problem are then coupled.

The above physical argument informs the choices that are made for the numerical analysis such that the collision between the bat and ball is captured as accurately as possible. It is noted that for the model presented to be considered accurate, there is an implicit requirement that the ball contact time on the bat (Δc) must be considerably smaller than the time taken for a wave to propagate through the length of the bat (Δb). Therefore, it follows that the model presented is limited to only those types of cricket shots where the ball contact time with the bat is extremely short compared to the time taken for the wave to propagate the length of the bat.

3.2 Discussion of the Boundary and Initial Conditions

The bat is modelled as a beam with constant mass, constant elasticity, uniform density and length L using the above beam equation. Equation (3.2) is of fourth order in space and of second order in time and so four boundary conditions and two initial conditions are required to solve this equation completely.

3.2.1 Boundary Conditions

The following boundary conditions are used:

- $y(0,t) = 0 \quad \forall t.$
  This boundary condition ensures that there is no displacement of the cricket bat at the end where the batsman is holding the bat for all time; that is, the displacement of the beam at the fixed end is zero.

- $y_x(0,t) = 0 \quad \forall t.$
  This boundary condition ensures that the end of the bat that is being held by the batsman remains flat; that is, the gradient of the fixed end of the beam is zero.

  It should noted that this clamped boundary condition (at $x = 0$) removes any effect that the batsman's hands have on the ball as it leaves the bat.

- $y_{xx}(L,t) = 0 \quad \forall t.$
  According to [8], a bending moment is a rotational force that occurs within the beam that will cause the beam to bend. This boundary condition ensures that there is no bending moment at the free end of the beam; that is, the toe end of the bat will not experience any sort of bending and the curvature at the free-end of the bat remains 0.

- $y_{xxx}(L,t) = 0 \quad \forall t.$
  Suppose a portion of a beam is being acted upon by a shearing force. According to [8], a shearing force will cause the portion of a beam to either side of this portion to "slide or shear laterally" relative to the portion of the beam that is experiencing the shearing force. This boundary condition ensures that there will be no shearing force at the free-end of the beam.

3.2.2 Initial Conditions

- $y(x,0) = 0 \quad \forall x.$
  This initial condition will ensure that there is initially no displacement of all points along the length of the beam; that is, that the bat has not been displaced at the moment the ball strikes the bat.

- $y_t(x,0) = f(x) \quad \forall x.$
  This initial condition will model the initial velocity of all points on the beam, including the point/s where, when considering the collision of the bat and ball, the velocity of the point/s on the bat that has/have been struck by the ball. $f(x)$ is defined such that the velocity of all points along the bat are initially 0, except for the point/s that has/have been struck by the ball, which has a velocity distribution of $v(x)$. $v(x)$ is defined differently for three different scenarios that will be examined in this work.

The first scenario is that of the ball undergoing a point-like, perpendicular, impulsive collision with the bat. In this scenario, $v(x)$ is defined simply as an impulse function. In this case, $f(x)$ defines the velocity for all points along the bat to be zero, except the single point on the bat that has been struck by the ball (the *Location of Impact*), which is assumed to have an initial velocity no faster than a common speed of a ball hitting the bat.

The second scenario for $v(x)$ models an elastic, perpendicular collision between the bat and the ball. In this scenario, the compression of the ball on the bat is modelled and hence the force distribution of the ball on the contact area of the bat is calculated. From this force distribution, the initial velocity of the area bat that has been struck by the ball can be calculated and modelled by $v(x)$. Hence $f(x)$ models all points on the bat to be zero, except the points on the bat in the contact area of the bat (the *Location of Impact*) which are given a velocity distribution of $v(x)$. Both of these scenarios model a defensive shot played by the batsman - which was discussed earlier in this Chapter - due to the fact that the bat was initially stationary, apart from the point/s on the bat that has/have been struck by the ball.

The third and final scenario to be analyzed in this work will be when the collision between the bat and the ball is non-perpendicular and elastic. This scenario will model an aggressive shot played by the batsman, as opposed to a defensive shot as considered in the previous two cases. Chapter 3.3 discusses the mathematical derivation of these three scenarios.

In general, for all three sceanrios, $f(x)$ is defined as

$$f(x) = \begin{cases} v(x): & x \in LoI, \\ 0: & \text{otherwise}, \end{cases}$$

where $v(x)$ refers to the initial velocity distribution for the LoI.

3.3 Discussion Of The Various Collision Scenarios

The numerical and analytical solutions to the model will be evaluated under three different collision scenarios.

3.3.1 Collision Scenario 1 - Impulsive, Point-Like, Perpendicular Collision

In this scenario, the model will be evaluated in the case where the collision between the bat and the ball is impulsive, point-like and perpendicular. That is, the collision will be modelled as the bat having been struck at a single point. This single point will be considered as the *Location of Impact*.

Further, the ball will strike the bat at a perpendicular angle and so this will model a defensive shot played by the batsman, as discussed in Chapter 3.1. This scenario serves only to demonstrate the beahviour of the model, and is only evaluated using the numerical solution given by the Crank-Nicolson scheme discussed in Chapter 4. This is because the sharp gradient of the initial velocity function $f(x)$ cannot be adequately captured by the eigenvalues of the analytical solution via the Separation of Variables approach discussed in Chapter 5. The results of the implementation of this scenario are discussed in Chapter 6.2.

Figure 3.3 below portrays the inelastic, point-like, perpendicular collision between bat and ball at some *Location of Impact* along the length of the bat. The bat itself forms the vertical x axis and the path of the ball for the perpendicular collision forms the horizontal y axis. For illustrative purposes, it is shown that the 'angle of incidence' θ between the bat and ball is zero, implying that the collision is perpendicular. This models a defensive shot played by the batsman.

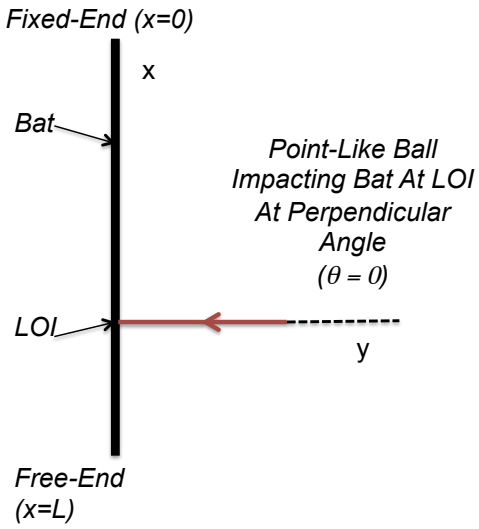

Figure 3.3: *Diagram portraying the perpendicular, impulsive collision between bat and ball in the first scenario.*

3.3.2 Collision Scenario 2 - Elastic, Perpendicular Collision

In this scenario, the approaches will evaluate the model where the collision between the bat and the ball is elastic and perpendicular. Due to the perpendicular collision, this scenario again models a defensive shot played by the batsman. In this scenario, the cricket ball will be modelled as compressing against the cricket bat during the collision. Recall that Carré, James and Haake [6] found that a cricket ball will compress when impacting against a surface. Using the approach of Pauchard and Rica [20], it is possible to determine how much the cricket ball will compress against the bat.

Suppose D_z is the cross-sectional length of the ball in contact with the bat when the compression of the ball is at its maximum. Pauchard and Rica give that

$$D_z = (2R_b\epsilon_{max})^{\frac{1}{2}}, \tag{3.15}$$

where R_b is the radius of the ball and ϵ_{max} is obtained from solving the following differential equation, which is obtained through the conservation of energy:

$$\epsilon'(r) + kc^2 \left(\frac{\epsilon(r)}{R_b}\right)^{\frac{5}{2}} = {v_0}^2. \tag{3.16}$$

Here c is the speed of sound through the material of the ball, k is a dimensionless constant that is dependent on the Poisson Ratio of the ball, v_0 is the velocity of the ball when it first collides with the bat and $0 \leq r \leq R_b$.

Pauchard and Rica give a solution to (3.16) to be

$$\epsilon_{max} \sim R_b \left(\frac{v_0}{c}\right)^{\frac{4}{5}}. \tag{3.17}$$

Substituting this value into (3.15) gives

$$D_z = \sqrt{2} R_b \left(\frac{v_0}{c}\right)^{\frac{2}{5}}, \tag{3.18}$$

which is the cross-sectional length of the ball in contact with the bat when the compression of the ball is at its maximum.

Combining the Hertz Pressure distribution given by Johnson in [16] and the Lagrangian Field Equations, it is possible to use the pressure distribution of the ball on the bat to find the initial velocity distribution of the bat immediately post-collision with the ball. This approach is used in both this collision scenario as well as the next collision scenario.

Recall that in this scenario, the impact between the bat and ball is considered to be elastic and perpendicular. Due to the perpendicular collision, the ball imparts a circular pressure distribution on the bat. Recall from Chapter 2 that the circular Hertz Pressure distribution from Johnson [16] is given by

$$p(r,t) = \frac{p_0 \left(\hat{R}^2 - r^2\right)^{\frac{1}{2}}}{\hat{R}} \delta(t), \tag{3.19}$$

where p_0 is some constant pressure, $0 < r \leq \hat{R} = \frac{D_z}{2}$ and $\delta(t)$ is the dirac delta, which is included because the collision will only be evaluated at one instant in time. In the implementation of the model, p_0 is chosen in such a way as to allow for appropriate initial velocity distributions.

From the Lagrangian Field Equations, the momentum balance equation is given by

$$\rho \frac{D^2 x_i}{Dt^2} = S_{ki,k} + \rho b_i. \tag{3.20}$$

In terms of the cricket bat, $S_{ki,k}$ is a tensor which refers to initial stress forces inside the cricket bat. Hence, by the model, this term is equal to zero. The density of the bat is given by ρ, and from the discussion on parameters in Chapter 3.1: $\rho = \gamma$. Further, $\frac{D^2x_i}{Dt^2}$ is acceleration, so let $\frac{D^2x_i}{Dt^2} = \frac{Dv}{Dt}$ where $v(r,t)$ is the velocity of point r at time t. The applied force on the cricket bat is given by b_i and this will be calculated from the circular Hertz Pressure distribution (3.19) through integration by

$$b_i(r,t) = \frac{\int 2\pi r p(r,t) dr}{\gamma}. \tag{3.21}$$

It is necessary to multiply the Hertz Pressure distribution by $2\pi r$ such that the integration takes place over a circular region, since the collision zone of a cricket ball on a cricket bat is, in general in this scenario, circular. b_i is now the acceleration. Hence, the Momentum Balance Equation (3.20) reduces to

$$\frac{Dv}{Dt} = b_i(r,t). \tag{3.22}$$

Substituting for the body force term gives

$$\begin{aligned} \frac{Dv}{Dt} &= \frac{\int 2\pi r p(r,t) dr}{\gamma} \\ \implies v(r) &= \int_{-\infty}^{\infty} \frac{\int 2\pi r p(r,t) dr}{\gamma} dt \\ \implies v(r) &= -\frac{2\pi p_0 \left(\hat{R}^2 - r^2\right)^{3/2}}{3\hat{R}}, \end{aligned} \tag{3.23}$$

where $\hat{R}$ - the radius of the circular collision zone on the bat - is kept general.

The cricket bat is modelled as a one-dimensional beam and so the radius of the contact zone of the ball on the bat can simply be considered to be a part of the length of the bat. Hence, the initial velocity distribution of the entire bat can be given by

$$f(x) = \begin{cases} v(x) : & x \text{ is LoI} \\ 0 \quad : & \text{otherwise} \end{cases}$$

where $v(x) = v(r)$ as calculated above. Recall from Chapter 3.2.2 that $y_t(x,0) = f(x)$. Figure 3.4 below portrays the elastic, perpendicular collision between bat and ball at some contact zone D_z for some *Location of Impact* along the length of the bat. The bat itself forms the vertical x axis and the

path of the ball for the perpendicular collision forms the horizontal y axis. For illustrative purposes, it is shown that the 'angle of incidence' θ between the bat and ball is zero. The model assumes that the perpendicular collision models a defensive shot played by the batsman. Further, it is illustrated that the ball has compressed against the bat resulting in the contact zone (length D_z) represented by the dashed line.

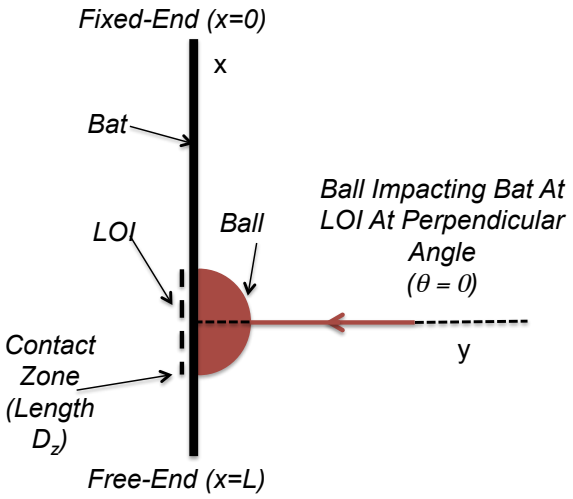

Figure 3.4: *Diagram portraying the perpendicular, elastic collision between bat and ball in the second scenario.*

3.3.3 Collision Scenario 3 - Elastic, Oblique Collision

The third and final collision scenario to be analyzed considers the collision between the bat and the ball to be elastic and oblique. In this scenario, an aggressive cricket shot will be modelled, as opposed to the previous two scenarios that model a defensive cricket shot. In the previous two scenarios, the collision between the bat and ball was assumed to be perpendicular with an initially stationary bat. In this scenario, the oblique collision between the bat and the ball will model an aggressive played by the batsman, using the previously discussed perpendicular collision as a frame of reference to model a defensive shot. Clearly, the velocity distribution of this third scenario will change significantly to that of the second scenario.

With an oblique collision between bat and ball occurring, it is clear that the pressure distribution imparted on the bat by ball will not be circular but will instead be 'egg-shaped', or ellipsoidal. Hence, the elliptical pressure

distribution given by Johnson [16] from Hertz Theory (and discussed briefly in Chapter 2) is used here:

$$p(x,y) = p_0 \left(1 - \left(\frac{x}{a}\right)^2 - \left(\frac{y}{b}\right)^2\right)^{\frac{1}{2}}, \tag{3.24}$$

where p_0 is some initial constant pressure, a is the semi-major axis of the ellipse and b is the semi-minor axis of the ellipse. Again, in the implementation of the model, p_0 is chosen in such a way as to allow for realistic appropriate velocity distributions. Consider the following substitutions:

$$a = x\sin\theta + \hat{R}, \tag{3.25}$$

and

$$b = \frac{r^2}{x\sin\theta + \hat{R}}, \tag{3.26}$$

where $\hat{R}$ is again the radius of the contact zone in the circular case per Chapter 3.3.2 and θ is the 'angle of incidence' of the ball striking the bat, such that in the case of a perpendicular collision between bat and ball, $\theta = 0$. The elliptical Hertz Pressure distribution (3.24) then becomes

$$p(x,y) = p_0 \left(1 - \frac{x^2}{(x\sin\theta + \hat{R})^2} - \frac{y^2(x\sin\theta + \hat{R})^2}{\hat{R}^4}\right)^{\frac{1}{2}}. \tag{3.27}$$

It is clear to see that when $\theta = 0$

$$p(x,y) = p_0 \left(1 - \frac{x^2}{\hat{R}^2} - \frac{y^2}{\hat{R}^2}\right)^{\frac{1}{2}}, \tag{3.28}$$

and converting the Cartesian coordinates to Polar coordinates through

$$x = r\cos\theta \qquad \text{and} \qquad y = r\sin\theta,$$

gives

$$
\begin{aligned}
p(r,\theta) &= p_0\left(1-\frac{r^2\cos^2\theta}{\hat{R}^2}-\frac{r^2\sin^2\theta}{\hat{R}^2}\right)^{\frac{1}{2}} \\
\implies p(r) &= p_0\frac{\left(\hat{R}^2-r^2\right)^{\frac{1}{2}}}{\hat{R}},
\end{aligned}
\tag{3.29}
$$

which is exactly the circular Hertz Pressure distribution given by (3.19), without time dependency.

As was the case in the previous collision scenario, it is possible to use the pressure distribution of the cricket ball impacting the bat to calculate the initial velocity distribution of the bat. A similar process to the previous collision scenario is followed. First, allow the elliptical pressure distribution of the ball on the bat to be

$$
p(x,y,t) = p_0\left(1-\frac{x^2}{(x\sin\theta+\hat{R})^2}-\frac{y^2(x\sin\theta+\hat{R})^2}{\hat{R}^4}\right)^{\frac{1}{2}}\delta(t) \tag{3.30}
$$

where p_0, θ and $\hat{R}$ are as with (3.27) and $\delta(t)$ is the dirac delta which is included because the collision will only be evaluated at one instant in time.

Now, as with the previous collision scenario, the pressure distribution is used to find the force distribution of the ball on the bat. However, a little more insight is required than was the case with the previous collision scenario. Consider the case where both θ and $\hat{R}$ are general. It is not difficult to see that the pressure distribution is symmetric around the x axis and, further, to see that the pressure distribution is equal to zero around the circumference of the ellipse; that is, there is no pressure exerted by the ball on the bat at the edges of the collision zone. By solving the equation

$$
p(x,y,t) = 0 \tag{3.31}
$$

it is possible to find the values for y for which the pressure distribution is zero:

$$
y = \pm\frac{\hat{R}^2\sqrt{\hat{R}^2+2\hat{R}x\sin\theta+x^2\sin^2\theta-x^2}}{(\hat{R}+x\sin\theta)^2}. \tag{3.32}
$$

Now, to find the body force from the elliptical pressure distribution, the pressure distribution is integrated between the bounds formed by the y values of the pressure distribution given by equation (3.32):

$$\begin{aligned} b_i(x,t) &= \frac{1}{\gamma}\int_{-\Phi}^{\Phi} p(x,y,t)dy \\ \implies b_i(x,t) &= 2\int_{0}^{\Phi} p(x,y,t)dy, \end{aligned} \tag{3.33}$$

where $\gamma = \rho$ is the density of the bat and

$$\Phi = \frac{\hat{R}^2\sqrt{\hat{R}^2 + 2\hat{R}x\sin\theta + x^2\sin^2\theta - x^2}}{(\hat{R} + x\sin\theta)^2}. \tag{3.34}$$

Evaluating the integral in equation (3.33) gives

$$b_i(x,t) = \frac{\pi p_0 \hat{R}^2(\hat{R} + x\sin\theta - x)(\hat{R} + x\sin\theta + x)}{2\left|\hat{R} + x\sin\theta\right|^3}\delta(t). \tag{3.35}$$

Recall again the Momentum Balance Equation obtained from the Lagrangian Field Equations, equation (3.20),

$$\rho\frac{D^2x_i}{Dt^2} = S_{ki,k} + \rho b_i.$$

Similarly to before, this reduces to equation (3.22)

$$\frac{Dv}{Dt} = b_i(x,t),$$

where $b_i(x,t)$ is an acceleration. Then, as before, the initial velocity distribution of the contact zone of the ball on the bat $v(x)$ is obtained by evaluating the time integral:

$$\begin{aligned} v(x) &= \int_{-\infty}^{\infty} b_i(x,t)dt \\ &= \frac{\pi p_0 \hat{R}^2(\hat{R} + x\sin\theta - x)(\hat{R} + x\sin\theta + x)}{2\left|\hat{R} + x\sin\theta\right|^3}. \end{aligned} \tag{3.36}$$

Finally then, for this collision scenario, the initial velocity distribution of the bat is given by

$$f(x) = \begin{cases} v(x) : & x \text{ is LoI} \\ 0 \quad : & \text{otherwise} \end{cases}$$

such that $f(x) = y_t(x, 0)$. Figure 3.5 below portrays the elastic, oblique collision between bat and ball at some contact zone D_z for some *Location of Impact* along the length of the bat. The bat itself forms the vertical y axis and the path of the ball for the perpendicular collision forms the horizontal x axis. Here, the 'angle of incidence', θ, between the bat and ball (measured from the y axis) is negative, implying the oblique collision and the corresponding elliptical Hertz pressure distribution given by equation (3.24). Due to the negative 'angle of incidence' between the bat and the ball, the model assumes an aggressive shot is being played by the batsman; the batsman playing the ball 'on the up'. Further, it is illustrated that the ball has compressed against the bat resulting in the contact zone (length D_z) represented by the vertical dashed line along the length of the bat.

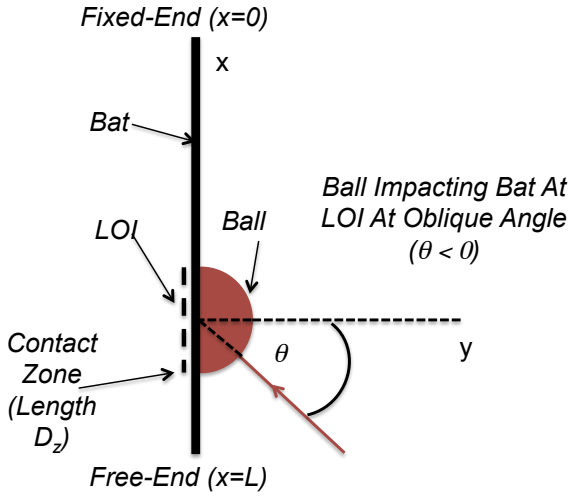

Figure 3.5: *Diagram portraying the oblique, elastic collision between bat and ball in the third scenario.*

All three scenarios discussed above will be analyzed at different *Locations of Impact* along the length of the cricket bat and results will be drawn from these analyses. The three main *Locations of Impact* that will be discussed will be at $x = 0.05$ m (near the fixed-end of the cricket bat), $x = 0.25$ m (at the middle of the cricket bat) and $x = 0.45$ m (near the free-end of the cricket bat).

3.4 Parameters and Values Used in the Model

In order to model the behaviour of a cricket bat as realistically as possible within the scope of this work as discussed throughout Chapter 3, the model is

implemented with realistic values for the various parameters that have been introduced. The following table outlines the parameters used.

Parameter	**Value**	**Unit**	**Description**	**Source**
L	0.5	m	Length of bat.	[17]
Δx	0.005	m	Spatial step in CN scheme.	[17]
Δt	0.000025	s	Time step in CN scheme and chosen ball contact time on bat.	[17]
EI	3300	Nm^2	Flexural rigidity of cricket bat.	[17]
Γ	440	$\frac{\mathrm{kg}}{\mathrm{m}^3}$	Overall blade density of cricket bat.	[17]
A	0.0034	m^2	Blade cross-sectional area.	[17]
γ	1.496	$\frac{\mathrm{kg}}{\mathrm{m}}$	Linear density of cricket bat.	[17]
D_b	0.073	m	Diameter of a cricket ball through its centre.	[7]
R_b	0.0365	m	Radius of a cricket ball from its centre.	[7]
c	442	m/s	Speed of sound through cork - the material inside a cricket ball.	[23]
v_0	27	m/s	Speed of cricket ball hitting a cricket bat - approx. 100 km/h.	[19]
D_z	approx. 0.017	m	Diameter of circular contact zone on cricket bat.	Calculated by model
R_z	approx. 0.01	m	Radius of circular contact zone on cricket bat - rounded up for simplification purposes.	Calculated by model

Recall equation (3.13)

$$Z^{\frac{1}{2}} = \frac{\Delta c}{\Delta b}$$

and the corresponding discussion regarding the parameter $Z^{\frac{1}{2}}$ from Chapter

3.1.

Substituting the relevant values from the above table into equation (3.10) gives the wave-speed in the bat c_b as

$$\begin{aligned} c_b &= \frac{\sqrt{EI}}{L\sqrt{\gamma}} \\ \implies c_b &\approx 93.93 \text{ m/s}. \end{aligned}$$

Then, from equation (3.12), the time taken for a wave to propagate the length of the bat at speed c_b is

$$\begin{aligned} \Delta b &= \frac{L}{c_b} \\ \implies \Delta b &\approx 0.0053 \text{ s}. \end{aligned} \tag{3.37}$$

Then, choosing $\Delta c = \Delta t = 0.000025$ s, gives equation (3.13) as

$$\begin{aligned} Z^{\frac{1}{2}} &= \frac{\Delta c}{\Delta b} \\ \implies Z^{\frac{1}{2}} &\approx 0.0047. \end{aligned} \tag{3.38}$$

Since $Z^{\frac{1}{2}} << 1$, the ball contact time is modelled as being much smaller than the time taken for the wave to propagate through the length of the bat. Therefore, the velocity of the ball as it leaves the bat is not affected by the batsman's grip. This is in agreement with Adair in [1] where he discusses this concept. Under similar circumstances presented in his work, he argues that "the ball will have long have left the bat in [the time taken for the waves to traverse back to the point of the collision] and will never know whether or not hands were holding the bat". It is argued that numerical model presented with this contact time can accurately capture the behaviour of the cricket bat post-collision with a cricket ball.

4 Numerical Solution To The Equation

Two numerical approaches are presented to solve the beam equation with initial and boundary conditions presented in Chapter 3. Firstly, a Central-in-Time and Central-in-Space finite difference method is presented and discussed in Chapter 4.1. Secondly, a Crank-Nicolson finite difference method is presented and discussed in Chapter 4.2. The solution of both these schemes are presented and their stability analysed.

4.1 Central-in-Time and Central-in-Space Method

To solve the above beam equation (3.2), a Central-in-Time and Central-in-Space (CTCS) finite difference scheme is used. The various difference approximations that are used to solve the above equation are shown below. The solution $y(x,t)$ is approximated as $y_n^m = y(x_n, t_m)$ where $x_n = n\Delta x$ for $n = 0, 1, 2, \ldots, N$ so that $N\Delta x = L$ and $t_m = m\Delta t$ for $m = 0, 1, 2, \ldots, M$ so that $M\Delta t$ is the final time. Δx and Δt are the incremental space and time steps respectively. All the approximations are central difference approximations and are accurate to the second order.

4.1.1 CTCS Scheme

Per Fornberg [11], the fourth-order spatial derivative is discretized by the central difference formula given by

$$\frac{\partial^4 y}{\partial x^4} = \frac{y_{n+2}^m - 4y_{n+1}^m + 6y_n^m - 4y_{n-1}^m + y_{n-2}^m}{(\Delta x)^4} + O(\Delta x^2), \quad \forall n \in [0, N], m \in [0, M]. \tag{4.1}$$

Also, per Fornberg [11], the second-order time derivative is discretized by the central difference formula given by

$$\frac{\partial^2 y}{\partial t^2} = \frac{y_n^{m+1} - 2y_n^m + y_n^{m-1}}{(\Delta t)^2} + O(\Delta t^2) \quad \forall n \in [0, N], m \in [0, M]. \tag{4.2}$$

4.1.2 Boundary Conditions for CTCS Scheme

- For $y(0,t) = 0$ the approximation is given by

$$y_0^m = 0 \qquad \forall m \in [0, M]. \tag{4.3}$$

- For $y_x(0,t) = 0$ the approximation is given by

$$\begin{aligned} &\frac{y_1^m - y_{-1}^m}{2\Delta x} = 0 \\ &\implies y_{-1}^m = y_1^m \qquad \forall m \in [0, M]. \end{aligned} \tag{4.4}$$

- For $y_{xx}(L,t) = 0$ the approximation is given by

$$\begin{aligned} &\frac{y_{N+1}^m - 2y_N^m + y_{N-1}^m}{(\Delta x)^2} = 0 \\ &\implies y_{N+1}^m = 2y_N^m - y_{N-1}^m \qquad \forall m \in [0, M]. \end{aligned} \tag{4.5}$$

  where N is defined above.

- For $y_{xxx}(L,t) = 0$ the approximation is given by

$$\begin{aligned} &\frac{y_{N+2}^m - 2y_{N+1}^m + 2y_{N-1}^m - y_{N-2}^m}{2(\Delta x)^3} = 0 \\ &\implies y_{N+2}^m = y_{N-2}^m - 4y_{N-1}^m + 4y_N^m \qquad \forall m \in [0, M]. \end{aligned} \tag{4.6}$$

  where N is defined above.

4.1.3 Initial Conditions for CTCS Scheme

- For $y(x,0) = 0$ the approximation is given by

$$y_n^0 = 0 \qquad \forall n \in [0, N]. \tag{4.7}$$

- For $y_t(x,0) = 0$ the approximation is given by

$$\begin{aligned} &\frac{y_n^1 - y_n^{-1}}{2\Delta t} = f(x_n) \\ &\implies y_n^{-1} = y_n^1 - 2\Delta t f(x_n) \qquad \forall n \in [0, N]. \end{aligned} \tag{4.8}$$

  and $f(x_n)$ is as discussed in Chapter 3.2.2.

4.1.4 Discretised Equation via CTCS Scheme

Recall the beam equation given by equation (3.2),

$$\frac{\partial^2 y}{\partial t^2} = -\frac{EI}{\gamma}\frac{\partial^4 y}{\partial x^4},$$

where E is the modulus of elasticity (Young's Modulus), I is the area moment of inertia and γ is the mass per unit length (density). EI is the flexural rigidity of the bat. $x \in [0, L]$ denotes the length along the beam and $t > 0$ denotes time and $y(x, t)$ is the solution to the equation; the displacement of point x at time t.

Then making the approximations (4.1) and (4.2) for the terms in the beam equation (3.2), the equation becomes

$$\begin{aligned}
0 &= EI\left[\frac{y_{n+2}^m - 4y_{n+1}^m + 6y_n^m - 4y_{n-1}^m + y_{n-2}^m}{(\Delta x)^4}\right] + \gamma\left[\frac{y_n^{m+1} - 2y_n^m + y_n^{m-1}}{(\Delta t)^2)}\right] \\
\implies y_n^{m+1} - 2y_n^m + y_n^{m-1} &= \frac{-EI(\Delta t)^2}{\gamma(\Delta x)^4}\left[y_{n+2}^m - 4y_{n+1}^m + 6y_n^m - 4y_{n-1}^m + y_{n-2}^m\right] \\
\implies y_n^{m+1} &= \alpha y_{n-2}^m - 4\alpha y_{n-1}^m + (6\alpha + 2)y_n^m - 4\alpha y_{n+1}^m + \alpha y_{n+2}^m - y_n^{m-1}
\end{aligned} \tag{4.9}$$

where

$$\alpha = \frac{-EI(\Delta t)^2}{\gamma(\Delta x)^4}. \tag{4.10}$$

The cases for

$n = \{0, 1, 2, \ldots, N\}$

at the $(m+1)^{\text{th}}$ time step are now considered.

<u>When $n = 0$</u>:

$$y_0^{m+1} = 0 \tag{4.11}$$

from the boundary condition (4.3).

When $n = 1$:

$$\begin{aligned} y_1^{m+1} &= \alpha y_{-1}^m - 4\alpha y_0^m + (6\alpha + 2)y_1^m - 4\alpha y_2^m + \alpha y_3^m - y_1^{m-1} \\ \implies y_1^{m+1} &= (7\alpha + 2)y_1^m - 4\alpha y_2^m + \alpha y_3^m - y_1^{m-1} \end{aligned} \tag{4.12}$$

since $y_{-1}^m = y_1^m$ from equation (4.3) and $y_0^m = 0$ from equation (4.4).

When $n = 2$:

$$\begin{aligned} y_2^{m+1} &= \alpha y_0^m - 4\alpha y_1^m + (6\alpha + 2)y_2^m - 4\alpha y_3^m + \alpha y_4^m - y_2^{m-1} \\ \implies y_2^{m+1} &= -4\alpha y_1^m + (6\alpha + 2)y_2^m - 4\alpha y_3^m + \alpha y_4^m - y_2^{m-1} \end{aligned} \tag{4.13}$$

since $y_0^m = 0$.

When $n = 3$:

$$y_3^{m+1} = \alpha y_1^m - 4\alpha y_2^m + (6\alpha + 2)y_3^m - 4\alpha y_4^m + \alpha y_5^m - y_3^{m-1} \tag{4.14}$$

$\vdots$

When $n = N - 2$:

$$y_{N-2}^{m+1} = \alpha y_{N-4}^m - 4\alpha y_{N-3}^m + (6\alpha + 2)y_{N-2}^m - 4\alpha y_{N-1}^m + \alpha y_N^m - y_{N-2}^{m-1} \tag{4.15}$$

When $n = N - 1$:

$$\begin{aligned} y_{N-1}^{m+1} &= \alpha y_{N-3}^m - 4\alpha y_{N-2}^m + (6\alpha + 2)y_{N-1}^m - 4\alpha y_N^m + \alpha y_{N+1}^m - y_{N-1}^{m-1} \\ &= \alpha y_{N-3}^m - 4\alpha y_{N-2}^m + (6\alpha + 2)y_{N-1}^m - 4\alpha y_N^m + 2\alpha y_N^m - \alpha y_{N-1}^m - y_{N-1}^{m-1} \\ &= \alpha y_{N-3}^m - 4\alpha y_{N-2}^m + (5\alpha + 2)y_{N-1}^m - 2\alpha y_N^m - y_{N-1}^{m-1} \end{aligned} \tag{4.16}$$

since $y_{N+1}^m = 2y_N^m - y_{N-1}^m$ from equation (4.5).

When $n = N$:

$$\begin{aligned} y_N^{m+1} &= \alpha y_{N-2}^m - 4\alpha y_{N-1}^m + (6\alpha + 2)y_N^m - 4\alpha y_{N+1}^m + \alpha y_{N+2}^m - y_N^{m-1} \\ &= \alpha y_{N-2}^m - 4\alpha y_{N-1}^m + (6\alpha + 2)y_N^m - 8\alpha y_N^m + 4\alpha y_{N-1}^m + \alpha y_{N-2}^m - 4\alpha y_{N-1}^m + 4\alpha y_N^m - y_N^{m-1} \\ &= 2\alpha y_{N-2}^m - 4\alpha y_{N-1}^m + (2\alpha + 2)y_N^m - y_N^{m-1} \end{aligned} \tag{4.17}$$

since $y_{N+1}^m = 2y_N^m - y_{N-1}^m$ from equation (4.5) and $y_{N+2}^m = y_{N-2}^m - 4y_{N-1}^m + 4y_N^m$ from equation (4.6).

Hence the system can be written out in matrix form as follows:

$$\begin{bmatrix} y_1^{m+1} \\ y_2^{m+1} \\ y_3^{m+1} \\ y_4^{m+1} \\ \vdots \\ \vdots \\ y_{N-3}^{m+1} \\ y_{N-2}^{m+1} \\ y_{N-1}^{m+1} \\ y_N^{m+1} \end{bmatrix} = \begin{bmatrix} (7\alpha+2) & -4\alpha & \alpha & 0 & 0 & 0 & 0 & \dots & 0 \\ -4\alpha & (6\alpha+2) & -4\alpha & \alpha & 0 & 0 & 0 & \dots & 0 \\ \alpha & -4\alpha & (6\alpha+2) & -4\alpha & \alpha & 0 & 0 & \dots & 0 \\ 0 & \alpha & -4\alpha & (6\alpha+2) & -4\alpha & \alpha & 0 & \dots & 0 \\ \vdots & \ddots & \ddots & \ddots & \ddots & \ddots & \ddots & \dots & \vdots \\ \vdots & \ddots & \ddots & \ddots & \ddots & \ddots & \ddots & \dots & \vdots \\ 0 & \dots & 0 & \alpha & -4\alpha & (6\alpha+2) & -4\alpha & \alpha & 0 \\ 0 & \dots & 0 & 0 & \alpha & -4\alpha & (6\alpha+2) & -4\alpha & \alpha \\ 0 & \dots & 0 & 0 & 0 & \alpha & -4\alpha & (5\alpha+2) & -2\alpha \\ 0 & \dots & 0 & 0 & 0 & 0 & 2\alpha & -4\alpha & (2\alpha+2) \end{bmatrix} \begin{bmatrix} y_1^m \\ y_2^m \\ y_3^m \\ y_4^m \\ \vdots \\ \vdots \\ y_{N-3}^m \\ y_{N-2}^m \\ y_{N-1}^m \\ y_N^m \end{bmatrix} - \begin{bmatrix} y_1^{m-1} \\ y_2^{m-1} \\ y_3^{m-1} \\ y_4^{m-1} \\ \vdots \\ \vdots \\ y_{N-3}^{m-1} \\ y_{N-2}^{m-1} \\ y_{N-1}^{m-1} \\ y_N^{m-1} \end{bmatrix}$$

Equivalently the system can be written in vector form as:

$$\boldsymbol{y}^{m+1} = \boldsymbol{A}\boldsymbol{y}^m - \boldsymbol{y}^{m-1} \tag{4.18}$$

where $\boldsymbol{y}^m$ is the vector of displacements at time m and $\boldsymbol{A}$ is the quint-diagonal matrix defined in the scheme above.

The matrix system described by the matrix equation (4.18) will calculate the values for all points in space $n = 1, \ldots, N$ and the boundary condition (4.3) at $n = 0$ is enforced. This vector of $N + 1$ points is then stored (in a *displacement* matrix) for the $(m+1)^{\text{th}}$ time step. Clearly, though, the vectors at the first two time steps must be defined independently of this system since for the system to calculate its first vector ($m = 2$) it requires the two initial time steps. Clearly, from then on, the matrix system can simply recall the previously calculated time steps to calculate the next vector.

From the initial condition for $y(x, 0) = 0$ given by (4.7): $y_n^0 = 0 \ \forall n$. Hence the first column (the first vector, $\boldsymbol{y}^0$) in the *displacement* matrix is a full of zeros. This column corresponds to $m = 0$.

Now, to calculate $\boldsymbol{y}^1$, consider matrix equation (4.18):

$$\begin{aligned} \boldsymbol{y}^1 &= \boldsymbol{A}\boldsymbol{y}^0 - \boldsymbol{y}^{-1} \\ \implies \boldsymbol{y}^1 &= -\boldsymbol{y}^{-1}, \end{aligned} \tag{4.19}$$

since $\boldsymbol{y}^0 = \boldsymbol{0}$.

Also recall from initial condition (4.8) that

$$\boldsymbol{y}^{-1} = \boldsymbol{y}^1 - 2\Delta t f(\boldsymbol{x}). \tag{4.20}$$

So substituting into (4.19) gives

$$\begin{aligned} \boldsymbol{y}^1 &= -\boldsymbol{y}^1 + 2\Delta t f(\boldsymbol{x}) \\ \implies \boldsymbol{y}^1 &= \Delta t f(\boldsymbol{x}). \end{aligned} \tag{4.21}$$

It is noted here that if a backward difference discretization of the initial velocity condition had been used, the same result would have been achieved.

$\boldsymbol{y}^0$ and $\boldsymbol{y}^1$ describe the first two columns in the displacement matrix, from rows $n = 1$ to $n = N$. Clearly the boundary condition at $n = 0$ will be enforced in the top row of each column as described earlier. The system described by (4.18) will then calculate the vectors corresponding to the remaining time steps and will hence construct the entire *displacement* matrix. In summary, the columns in the *displacement* matrix describe the displacement at each point along the bat and these columns progress through time.

4.1.5 Consistency of the CTCS Scheme

Recall from equation (4.9) that the CTCS scheme can be written as

$$0 = EI\left[\frac{y_{n+2}^m - 4y_{n+1}^m + 6y_n^m - 4y_{n-1}^m + y_{n-2}^m}{(\Delta x)^4}\right] + \gamma\left[\frac{y_n^{m+1} - 2y_n^m + y_n^{m-1}}{(\Delta t)^2)}\right]. \tag{4.22}$$

In order to show the consistency of the CTCS scheme, let

$$y_{n+j}^{m+i} = u(x + i\Delta x, t + j\Delta t) \quad i, j \in \mathbb{Z}. \tag{4.23}$$

Substituting equation (4.23) into equation (4.22) gives

$$\begin{aligned} 0 =& \vartheta\left[\frac{u(x+2\Delta x,t) - 4u(x+\Delta x,t) + 6u(x,t) - 4u(x-\Delta x,t) + u(x-2\Delta x,t)}{(\Delta x)^4}\right] \\ &+ \frac{u(x,t+\Delta t) - 2u(x,t) + u(x,t-\Delta t)}{(\Delta t)^2} \end{aligned} \tag{4.24}$$

where $\vartheta = \frac{EI}{\gamma}$. Expanding (4.24) in a Taylor series around $\Delta x = 0$ and $\Delta t = 0$ and performing some algebraic manipulation gives

$$\left(\left(\vartheta\frac{\partial^4 u}{\partial x^4} + \frac{\partial^2 u}{\partial t^2}\right) + O(\Delta t)^2\right) + O(\Delta x)^2 = 0. \tag{4.25}$$

As Δx and Δt tend to zero, the original Beam equation is recovered:

$$\vartheta\frac{\partial^4 u}{\partial x^4} + \frac{\partial^2 u}{\partial t^2} = 0. \tag{4.26}$$

Therefore, the CTCS scheme described by equation (4.9) is consistent with the beam equation described by equation (3.2).

4.1.6 Stability of the CTCS Scheme

Recall that the general CTCS scheme is given by equation (4.9):

$$0 = EI\left[\frac{y_{n+2}^m - 4y_{n+1}^m + 6y_n^m - 4y_{n-1}^m + y_{n-2}^m}{(\Delta x)^4}\right] + \gamma\left[\frac{y_n^{m+1} - 2y_n^m + y_n^{m-1}}{(\Delta t)^2)}\right].$$

The Beam equation given by equation (3.2) is linear. However, it is not diffusive. The underlying assumption of the von Neumann stability analysis is that any general Fourier mode must decay as time progresses. Since the Beam equation (3.2) is not diffusive, this will not occur in general. Therefore, a standard von Neumann stability analysis will not suffice to analyse the stability of the scheme given by equation (4.9). A more intuitive definition of error and stability is required.

Due to the linearity of the Beam equation (3.2), the error between the exact solution and numerical solution must behave in a similar way to these solutions themselves. Furthermore, if the error between these two solutions is bounded over all time, then the scheme itself must be stable.

Suppose that the error of the scheme at time-step m and spatial-step n is given by

$$\Lambda(m,n) = e(m)\text{Exp}(i\omega n\Delta x) \tag{4.27}$$

where $i = \sqrt{-1}$ and ω is the wave number.

Substituting equation (4.27) into equation (4.9) gives

$$\begin{aligned}&\frac{\Lambda(m+1,n) - 2\Lambda(m,n) + \Lambda(m-1,n)}{\Delta t^2}\\ &+\vartheta\left(\frac{\Lambda(m,n+2) - 4\Lambda(m,n+1) + 6\Lambda(m,n) - 4\Lambda(m,n-1) + \Lambda(m,n+2)}{\Delta x^4}\right) = 0\end{aligned} \tag{4.28}$$

where $\vartheta = \frac{EI}{\gamma}$. Further, recall from equation (4.10) that

$$\begin{aligned}\alpha &= \frac{-EI(\Delta t)^2}{\gamma(\Delta x)^4} < 0\\ \implies \alpha &= -\vartheta\frac{(\Delta t)^2}{(\Delta x)^4}\\ \implies \Delta t &= \frac{\tau}{\sqrt{\vartheta}}(\Delta x)^2\end{aligned}$$

where

$$\tau = \sqrt{-\alpha}. \tag{4.29}$$

Also, for simplification purposes, let

$$\sigma = \omega \Delta x. \tag{4.30}$$

Making the above substitutions and simplifying equation (4.28) gives

$$\vartheta \left[2e(m) \left(\tau^2 \left(2\cos^2(\sigma) - 4\cos(\sigma) - 1 \right) + 3\tau^2 - 1 \right) + e(m-1) + e(m+1) \right] = 0. \tag{4.31}$$

This is a difference equation with an initial condition $e(0) = 0$. Solving this equation with the aforementioned initial condition gives the solution as

$$\begin{aligned} e(m) = c_1 \left(-2^{-m}\right) \Big[& \left(2 - 4(\varphi - 1)\tau \left(\sqrt{(\varphi-1)^2\tau^2 - 1} + (\varphi - 1)\tau \right) \right)^m \\ & - \left(4(\varphi - 1)\tau \left(\sqrt{(\varphi-1)^2\tau^2 - 1} - \varphi\tau + \tau \right) + 2 \right)^m \Big], \end{aligned} \tag{4.32}$$

where c_1 is an arbitary constant and $\varphi = \cos(\sigma)$. Clearly $-1 \leq \varphi \leq 1$. In order to analyse the temporal error $e(m)$, its solution (4.32) is evaluated at the bounds of φ. When $\varphi = 1$ then

$$e(m) = 0 \quad \forall m \in \mathbb{Z} \geq 0 \tag{4.33}$$

and the error $e(m)$ is bounded. When $\varphi = -1$ then

$$e(m) = c_1 \Big[\left(1 - 4\tau \left(\sqrt{4\tau^2 - 1} + 2\tau \right) \right)^m - \left(4\tau \left(\sqrt{4\tau^2 - 1} - 2\tau \right) + 1 \right)^m \Big] \quad \forall m \in \mathbb{Z} \geq 0 \tag{4.34}$$

Making the substitution $\tau = \frac{\sin(\theta)}{2}$ simplifies equation (4.34) to

$$e(m) = -2c_1 i \sin(2m\theta). \tag{4.35}$$

Given $-1 \leq \sin(2m\theta) \leq 1 \quad \forall \theta \in \mathbb{R}$, then $e(m)$ is bounded for all m.

Recall that $\tau = \frac{\sin(\theta)}{2}$. Therefore, if $\theta \in \mathbb{R}$, then $e(m)$ will be bounded when

$$-\frac{1}{2} \leq \tau \leq \frac{1}{2} \tag{4.36}$$

Since $\tau = \sqrt{-\alpha} > 0$ from equation (4.29), then the inequality (4.36) reduces to

$$0 < \tau \leq \frac{1}{2}. \tag{4.37}$$

For the temporal error $e(m)$ and, therefore, the error between the exact and numerical solution $\Lambda(m, n)$ to remain bounded for all m when $\theta \in \mathbb{R}$, it is required that

$$-\frac{1}{4} \leq \alpha < 0. \tag{4.38}$$

Now suppose that θ is a complex number with a non-zero imaginary part. That is, without loss of generality, suppose $\theta = i\phi$ where $\phi \in \mathbb{R}$. Then equation (4.35) reduces to

$$\begin{aligned} e(m) &= -2c_1 i \sin(2m\theta) \\ \implies e(m) &= 2c_1 \sinh(2m\phi). \end{aligned}$$

Clearly the error described in (4.35) is unbounded for all values of ϕ and therefore for all values of θ that are imaginary.

The temporal error $e(m)$ and therefore the error between the exact and numerical solutions $\Lambda(m, n)$ remain bounded for all m if and only if expression (4.38) holds. Hence, the CTCS scheme described by (4.9) is conditionally stable.

4.1.7 Convergence of the CTCS Scheme

Recall that the Beam equation (3.2) is linear. Further, the CTCS scheme described by (4.9) is consistent - as proved in Section 4.1.5 - and (conditionally) stable - as proved in Section 4.1.6. Therefore, by the Lax Thereom, the CTCS scheme described by equation (4.9) is convergent.

4.2 Crank-Nicolson Method

Due to the fact that the Central Time, Central Space method discussed in Chapter 4.1 is only stable for

$$-\frac{1}{4} \leq \alpha \leq 0,$$

where $\alpha = \frac{-EI(\Delta t)^2}{\gamma(\Delta x)^4}$, it is possible and advantageous to introduce a more sophisticated Crank-Nicolson finite difference scheme to solve the model presented in Chapter 3. The Crank-Nicolson scheme has a higher order of accuracy than the CTCS scheme and is unconditionally stable (as will be shown in Chapter 4.2.6). Once again, the solution $y(x,t)$ is approximated as $y_n^m = y(x_n, t_m)$ where $x_n = n\Delta x$ for $n = 0, 1, 2, \ldots, N$ so that $N\Delta x = L$ and $t_m = m\Delta t$ for $m = 0, 1, 2, \ldots, M$ so that $M\Delta t$ is the final time. Δx and Δt are the incremental space and time steps respectively. All the approximations are central difference approximations. Per Fornberg [11], the central difference approximation for the fourth derivative in space is accurate to the second order. Further, the time central difference approximation for the second derivative in time is accurate to the first order.

4.2.1 CN Scheme

Due to the implicit nature of a Crank-Nicolson scheme, the fourth-order spatial derivative is discretized by the central difference formula given by

$$\begin{aligned}\frac{\partial^4 y}{\partial x^4} = \frac{1}{3(\Delta x)^4} \big[& y_{n+2}^{m+1} - 4y_{n+1}^{m+1} + 6y_n^{m+1} - 4y_{n-1}^{m+1} + y_{n-2}^{m+1} \\ & + y_{n+2}^{m} - 4y_{n+1}^{m} + 6y_n^{m} - 4y_{n-1}^{m} + y_{n-2}^{m} \\ & + y_{n+2}^{m-1} - 4y_{n+1}^{m-1} + 6y_n^{m-1} - 4y_{n-1}^{m-1} + y_{n-2}^{m-1} \big] \\ & + O(\Delta x^2), \ \forall n \in [0, N], m \in [0, M],\end{aligned} \tag{4.39}$$

and the second-order time derivative is discretized by the central difference formula given by

$$\frac{\partial^2 y}{\partial t^2} = \frac{y_n^{m+1} - 2y_n^m + y_n^{m-1}}{(\Delta t)^2} + O(\Delta t) \quad \forall n \in [0, N], m \in [0, M]. \tag{4.40}$$

4.2.2 Boundary Conditions for the CN Scheme

The boundary condition approximations for the Crank-Nicolson scheme are exactly the same as those for the Central-in-Time and Central-in-Space scheme as discussed in Chapter 4.1.2. So equations (4.3) through (4.6) are also used for the CN scheme.

4.2.3 The Initial Conditions For The CN Scheme

Similarly to the boundary conditions, the initial condition approximations for the Crank-Nicolson scheme are exactly the same as those for the CTCS scheme as discussed in Chapter 4.1.3. So equations (4.7) and (4.8) are also used for the CN scheme.

4.2.4 Discretised Equation via the CN Scheme

Recall the beam equation given by (3.2),

$$\frac{\partial^2 y}{\partial t^2} = -\frac{EI}{\gamma}\frac{\partial^4 y}{\partial x^4},$$

where E is the modulus of elasticity (Young's Modulus), I is the area moment of inertia and γ is the mass per unit length (density). EI is the flexural rigidity of the bat. $x \in [0, L]$ denotes the length along the beam and $t > 0$ denotes time and $y(x, t)$ is the solution to the equation; the displacement of point x at time t.

Recall that the initial and boundary conditions imposed on the equation are given by

$$\begin{aligned} &y(x,0) = 0, && y_t(x,0) = f(x), \\ &y(0,t) = 0, && y_x(0,t) = 0, \\ &y_{xx}(L,t) = 0, && y_{xxx}(L,t) = 0. \end{aligned}$$

Then making the approximations (4.39) and (4.40) for the terms in the beam equation (3.2), the equation becomes

$$\begin{aligned}\frac{EI}{3\Delta x^4}\big[&y_{n+2}^{m+1} - 4y_{n+1}^{m+1} + 6y_n^{m+1} - 4y_{n-1}^{m+1} + y_{n-2}^{m+1} \\ &+ y_{n+2}^{m} - 4y_{n+1}^{m} + 6y_n^{m} - 4y_{n-1}^{m} + y_{n-2}^{m} \\ &+ y_{n+2}^{m-1} - 4y_{n+1}^{m-1} + 6y_n^{m-1} - 4y_{n-1}^{m-1} + y_{n-2}^{m-1}\big] = \frac{-\gamma}{\Delta t^2}\left[y_n^{m+1} - 2y_n^m + y_n^{m-1}\right].\end{aligned} \tag{4.41}$$

Setting

$$\chi = -\frac{EI\Delta t^2}{3\gamma\Delta x^4}, \tag{4.42}$$

and rearranging terms gives

$$\begin{aligned}&-\chi y_{n+2}^{m+1} + 4\chi y_{n+1}^{m+1} + (1-6\chi)y_n^{m+1} + 4\chi y_{n-1}^{m+1} - \chi y_{n-2}^{m+1} \\ = \;& \chi y_{n+2}^{m} - 4\chi y_{n+1}^{m} + (2+6\chi)y_n^{m} - 4\chi y_{n-1}^{m} + \chi y_{n-2}^{m} \\ &+\chi y_{n+2}^{m-1} - 4\chi y_{n+1}^{m-1} + (6\chi-1)y_n^{m-1} - 4\chi y_{n-1}^{m-1} + \chi y_{n-2}^{m-1}.\end{aligned} \tag{4.43}$$

Now, due to the fact that the boundary and initial conditions are identical for both the CTCS scheme and the CN scheme, it follows that equations (4.3) through (4.6) for the boundary conditions and equations (4.7) and (4.8) for the initial conditions hold true for both schemes.

Then returning to the scheme given by (4.43), the cases for $n = \{0, 1, 2, \ldots, N\}$ at the $(m+1)^{\text{th}}$ time step are considered.

<u>When $n = 0$</u>:

$$y_0^{m+1} = 0 \tag{4.44}$$

from the boundary condition (4.3).

<u>When $n = 1$</u>:

$$\begin{aligned}&-\chi y_3^{m+1} + 4\chi y_2^{m+1} + (1-6\chi)y_1^{m+1} + 4\chi y_0^{m+1} - \chi y_{-1}^{m+1} \\ = \;& \chi y_3^{m} - 4\chi y_2^{m} + (2+6\chi)y_1^{m} - 4\chi y_0^{m} + \chi y_{-1}^{m} \\ &+\chi y_3^{m-1} - 4\chi y_2^{m-1} + (6\chi-1)y_1^{m-1} - 4\chi y_0^{m-1} + \chi y_{-1}^{m-1} \\ \Longrightarrow\; & -\chi y_3^{m+1} + 4\chi y_2^{m+1} + (1-7\chi)y_1^{m+1} \\ = \;& \chi y_3^{m} - 4\chi y_2^{m} + (2+7\chi)y_1^{m} \\ &+\chi y_3^{m-1} - 4\chi y_2^{m-1} + (7\chi-1)y_1^{m-1}\end{aligned} \tag{4.45}$$

since $y_{-1}^m = y_1^m$ from (4.3) and $y_0^m = 0$ from (4.4).

When $n = 2$:

$$\begin{aligned} & -\chi y_4^{m+1} + 4\chi y_3^{m+1} + (1-6\chi) y_2^{m+1} + 4\chi y_1^{m+1} - \chi y_0^{m+1} \\ = \;& \chi y_4^m - 4\chi y_3^m + (2+6\chi) y_2^m - 4\chi y_1^m + \chi y_0^m \\ & + \chi y_4^{m-1} - 4\chi y_3^{m-1} + (6\chi - 1) y_2^{m-1} - 4\chi y_1^{m-1} + \chi y_0^{m-1} \end{aligned} \tag{4.46}$$

$$\begin{aligned} \Longrightarrow \; & -\chi y_4^{m+1} + 4\chi y_3^{m+1} + (1-6\chi) y_2^{m+1} + 4\chi y_1^{m+1} \\ = \;& \chi y_4^m - 4\chi y_3^m + (2+6\chi) y_2^m - 4\chi y_1^m \\ & + \chi y_4^{m-1} - 4\chi y_3^{m-1} + (6\chi - 1) y_2^{m-1} - 4\chi y_1^{m-1} \end{aligned}$$

since $y_0^m = 0$.

When $n = 3$:

$$\begin{aligned} & -\chi y_5^{m+1} + 4\chi y_4^{m+1} + (1-6\chi) y_3^{m+1} + 4\chi y_2^{m+1} - \chi y_1^{m+1} \\ = \;& \chi y_5^m - 4\chi y_4^m + (2+6\chi) y_3^m - 4\chi y_2^m + \chi y_1^m \\ & + \chi y_5^{m-1} - 4\chi y_4^{m-1} + (6\chi - 1) y_3^{m-1} - 4\chi y_2^{m-1} + \chi y_1^{m-1} \end{aligned} \tag{4.47}$$

$\vdots$

When $n = N - 2$:

$$\begin{aligned} & -\chi y_N^{m+1} + 4\chi y_{N-1}^{m+1} + (1-6\chi) y_{N-2}^{m+1} + 4\chi y_{N-3}^{m+1} - \chi y_{N-4}^{m+1} \\ = \;& \chi y_N^m - 4\chi y_{N-1}^m + (2+6\chi) y_{N-2}^m - 4\chi y_{N-3}^m + \chi y_{N-4}^m \\ & + \chi y_N^{m-1} - 4\chi y_{N-1}^{m-1} + (6\chi - 1) y_{N-2}^{m-1} - 4\chi y_{N-3}^{m-1} + \chi y_{N-4}^{m-1} \end{aligned} \tag{4.48}$$

When $n = N - 1$:

$$\begin{aligned} & -\chi y_{N+1}^{m+1} + 4\chi y_N^{m+1} + (1-6\chi) y_{N-1}^{m+1} + 4\chi y_{N-2}^{m+1} - \chi y_{N-3}^{m+1} \\ = \;& \chi y_{N+1}^m - 4\chi y_N^m + (2+6\chi) y_{N-1}^m - 4\chi y_{N-2}^m + \chi y_{N-3}^m \\ & + \chi y_{N+1}^{m-1} - 4\chi y_N^{m-1} + (6\chi - 1) y_{N-1}^{m-1} - 4\chi y_{N-2}^{m-1} + \chi y_{N-3}^{m-1} \end{aligned} \tag{4.49}$$

$$\begin{aligned} \Longrightarrow \; & 2\chi y_N^{m+1} + (1-5\chi) y_{N-1}^{m+1} + 4\chi y_{N-2}^{m+1} - \chi y_{N-3}^{m+1} \\ = \;& -2\chi y_N^m + (2+5\chi) y_{N-1}^m - 4\chi y_{N-2}^m + \chi y_{N-3}^m \\ & - 2\chi y_N^{m-1} + (5\chi - 1) y_{N-1}^{m-1} - 4\chi y_{N-2}^{m-1} + \chi y_{N-3}^{m-1} \end{aligned}$$

since $y_{N+1}^m = 2y_N^m - y_{N-1}^m$ from equation (4.5).

When $n = N$:

$$\begin{aligned} & -\chi y_{N+2}^{m+1} + 4\chi y_{N+1}^{m+1} + (1-6\chi) y_N^{m+1} + 4\chi y_{N-1}^{m+1} - \chi y_{N-2}^{m+1} \\ = \quad & \chi y_{N+2}^{m} - 4\chi y_{N+1}^{m} + (2+6\chi) y_N^{m} - 4\chi y_{N-1}^{m} + \chi y_{N-2}^{m} \\ & + \chi y_{N+2}^{m-1} - 4\chi y_{N+1}^{m-1} + (6\chi - 1) y_N^{m-1} - 4\chi y_{N-1}^{m-1} + \chi y_{N-2}^{m-1} \end{aligned} \tag{4.50}$$

$$\begin{aligned} \Longrightarrow & (1-2\chi) y_N^{m+1} + 4\chi y_{N-1}^{m+1} - 2\chi y_{N-2}^{m+1} \\ = \quad & (2+2\chi) y_N^{m} - 4\chi y_{N-1}^{m} + 2\chi y_{N-2}^{m} \\ & + (2\chi - 1) y_N^{m-1} - 4\chi y_{N-1}^{m-1} + 2\chi y_{N-2}^{m-1} \end{aligned}$$

since $y_{N+1}^m = 2y_N^m - y_{N-1}^m$ from (4.5) and $y_{N+2}^m = y_{N-2}^m - 4y_{N-1}^m + 4y_N^m$ from (4.6).

Hence,the system can be written in vector form as

$$\boldsymbol{P}\boldsymbol{y}^{m+1} = \boldsymbol{Q}\boldsymbol{y}^{m} + \boldsymbol{R}\boldsymbol{y}^{m-1}, \tag{4.51}$$

where

$$\boldsymbol{P} = \begin{bmatrix} (1-7\chi) & 4\chi & -\chi & 0 & 0 & 0 & 0 & \dots & 0 \\ 4\chi & (1-6\chi) & 4\chi & -\chi & 0 & 0 & 0 & \dots & 0 \\ -\chi & 4\chi & (1-6\chi) & 4\chi & -\chi & 0 & 0 & \dots & 0 \\ 0 & -\chi & 4\chi & (1-6\chi) & 4\chi & -\chi & 0 & \dots & 0 \\ \vdots & \ddots & \ddots & \ddots & \ddots & \ddots & \ddots & \dots & \vdots \\ \vdots & \ddots & \ddots & \ddots & \ddots & \ddots & \ddots & \dots & \vdots \\ 0 & \dots & 0 & -\chi & 4\chi & (1-6\chi) & 4\chi & -\chi & 0 \\ 0 & \dots & 0 & 0 & -\chi & 4\chi & (1-6\chi) & 4\chi & -\chi \\ 0 & \dots & 0 & 0 & 0 & -\chi & 4\chi & (1-5\chi) & 2\chi \\ 0 & \dots & 0 & 0 & 0 & 0 & -2\chi & 4\chi & (1-2\chi) \end{bmatrix}$$

and

$$\boldsymbol{Q} = \begin{bmatrix} (2+7\chi) & -4\chi & \chi & 0 & 0 & 0 & 0 & \dots & 0 \\ -4\chi & (2+6\chi) & -4\chi & \chi & 0 & 0 & 0 & \dots & 0 \\ \chi & -4\chi & (2+6\chi) & -4\chi & \chi & 0 & 0 & \dots & 0 \\ 0 & \chi & -4\chi & (2+6\chi) & -4\chi & \chi & 0 & \dots & 0 \\ \vdots & \ddots & \ddots & \ddots & \ddots & \ddots & \ddots & \dots & \vdots \\ \vdots & \ddots & \ddots & \ddots & \ddots & \ddots & \ddots & \dots & \vdots \\ 0 & \dots & 0 & \chi & -4\chi & (2+6\chi) & -4\chi & \chi & 0 \\ 0 & \dots & 0 & 0 & \chi & -4\chi & (2+6\chi) & -4\chi & \chi \\ 0 & \dots & 0 & 0 & 0 & \chi & -4\chi & (2+5\chi) & -2\chi \\ 0 & \dots & 0 & 0 & 0 & 0 & 2\chi & -4\chi & (2+2\chi) \end{bmatrix}$$

and

$$\boldsymbol{R} = \begin{bmatrix} (7\chi-1) & -4\chi & \chi & 0 & 0 & 0 & 0 & \dots & 0 \\ -4\chi & (6\chi-1) & -4\chi & \chi & 0 & 0 & 0 & \dots & 0 \\ \chi & -4\chi & (6\chi-1) & -4\chi & \chi & 0 & 0 & \dots & 0 \\ 0 & \chi & -4\chi & (6\chi-1) & -4\chi & \chi & 0 & \dots & 0 \\ \vdots & \ddots & \ddots & \ddots & \ddots & \ddots & \ddots & \dots & \vdots \\ \vdots & \ddots & \ddots & \ddots & \ddots & \ddots & \ddots & \dots & \vdots \\ 0 & \dots & 0 & \chi & -4\chi & (6\chi-1) & -4\chi & \chi & 0 \\ 0 & \dots & 0 & 0 & \chi & -4\chi & (6\chi-1) & -4\chi & \chi \\ 0 & \dots & 0 & 0 & 0 & \chi & -4\chi & (5\chi-1) & -2\chi \\ 0 & \dots & 0 & 0 & 0 & 0 & 2\chi & -4\chi & (2\chi-1) \end{bmatrix}$$

As before for the CTCS scheme, the matrix system described by (4.51) will calculate the values for all points in space $n = 1, \dots, N$ and the boundary condition (4.3) at $n = 0$ is enforced. This vector of $N + 1$ points is then stored (in a *displacement* matrix) for the $(m + 1)^{\text{th}}$ time step. Clearly, though, the vectors at the first two time steps must be defined independently of this system since for the system to calculate its first vector ($m = 2$) it requires the two initial time steps. Clearly, from then on, the matrix system can simply recall the previously calculated time steps to calculate the next vector.

As with the CTCS scheme, from the initial condition for $y(x,0) = 0$ given by (4.7): $y_n^0 = 0 \ \forall n$. Hence the first column (the first vector, $\boldsymbol{y}^0$) in the *displacement* matrix is a full of zeros. This column corresponds to $m = 0$.

Now, to calculate $\boldsymbol{y}^1$, consider (4.51)

$$\begin{aligned} \boldsymbol{P}\boldsymbol{y}^1 &= \boldsymbol{Q}\boldsymbol{y}^0 + \boldsymbol{R}\boldsymbol{y}^{-1} \\ \implies \boldsymbol{P}\boldsymbol{y}^1 &= \boldsymbol{R}\boldsymbol{y}^{-1}. \end{aligned} \tag{4.52}$$

Now recall from (4.8)

$$\boldsymbol{y}^{-1} = \boldsymbol{y}^1 - 2\Delta t f(\boldsymbol{x}).$$

Substituting this into (4.52) gives

$$\begin{aligned} \boldsymbol{P}\boldsymbol{y}^1 &= \boldsymbol{R}\left(\boldsymbol{y}^1 - 2\Delta t f(\boldsymbol{x})\right) \\ \implies (\boldsymbol{P} - \boldsymbol{R})\,\boldsymbol{y}^1 &= -2\Delta t \boldsymbol{R} f(\boldsymbol{x}) \\ \implies \boldsymbol{y}^1 &= -2\Delta t (\boldsymbol{P} - \boldsymbol{R})^{-1} \boldsymbol{R} f(\boldsymbol{x}). \end{aligned} \tag{4.53}$$

It is noted here that the above is a linear system and can be solved with methods that are more computationally efficient than the inversion of the matrix. `Mathematica`'s `LinearSolve` function was used to solve this system as it is state-of-the-art.

As before with the CTCS scheme, $\boldsymbol{y}^0$ and $\boldsymbol{y}^1$ describe the first two columns in the displacement matrix, from rows $n = 1$ to $n = N$. Clearly the boundary condition at $n = 0$ will be enforced in the top row of each column as described earlier. The system described by (4.51) will then calculate the vectors corresponding to the remaining time steps and will hence construct the entire *displacement* matrix. In summary, the columns in the *displacement* matrix describe the displacement at each point along the bat and these columns progress through time.

4.2.5 Consistency of the CN Scheme

Recall from equation (4.41) that the Crank-Nicolson scheme can be written as

$$\begin{aligned}\frac{EI}{3\Delta x^4}\big[&y_{n+2}^{m+1}-4y_{n+1}^{m+1}+6y_n^{m+1}-4y_{n-1}^{m+1}+y_{n-2}^{m+1}\\ &+y_{n+2}^{m}-4y_{n+1}^{m}+6y_n^{m}-4y_{n-1}^{m}+y_{n-2}^{m} \qquad = \frac{-\gamma}{\Delta t^2}\left[y_n^{m+1}-2y_n^{m}+y_n^{m-1}\right].\\ &+y_{n+2}^{m-1}-4y_{n+1}^{m-1}+6y_n^{m-1}-4y_{n-1}^{m-1}+y_{n-2}^{m-1}\big]\end{aligned}$$

In order to show the consistency of the CN scheme, let

$$y_{n+j}^{m+i} = u(x+i\Delta x, t+j\Delta t) \quad i,j \in \mathbb{Z}. \tag{4.54}$$

Substituting equation (4.54) into equation (4.41) gives

$$\begin{aligned}\frac{\vartheta}{3\Delta x^4}[&u(x+2\Delta x,t+\Delta t)-4u(x+dx,t+\Delta t)+6u(x,t+\Delta t)\\ &-4u(x-\Delta x,t+\Delta t)+u(x-2\Delta x,t+\Delta t)\\ &+u(x+2\Delta x,t)-4u(x+dx,t)+6u(x,t) \qquad = \frac{-1}{\Delta t^2}[u(x,t+\Delta t)-2u(x,t)\\ &-4u(x-\Delta x,t)+u(x-2\Delta x,t) \qquad + u(x,t-\Delta t)]\\ &u(x+2\Delta x,t-\Delta t)-4u(x+dx,t-\Delta t)+6u(x,t-\Delta t)\\ &-4u(x-\Delta x,t-\Delta t)+u(x-2\Delta x,t-\Delta t)]\end{aligned} \tag{4.55}$$

where $\vartheta = \frac{EI}{\gamma}$. By expanding equation (4.55) in a Taylor series around $\Delta x = 0$ and $\Delta t = 0$ and performing some algebraic manipulation gives

$$\left(\left(\vartheta\frac{\partial^4 u}{\partial x^4}+\frac{\partial^2 u}{\partial t^2}\right)+O(\Delta t)^2\right)+O(\Delta x)^2 = 0. \tag{4.56}$$

As Δx and Δt tend to zero, the original Beam equation is recovered:

$$\vartheta\frac{\partial^4 u}{\partial x^4}+\frac{\partial^2 u}{\partial t^2} = 0. \tag{4.57}$$

Therefore, the CN scheme described by equation (4.41) is consistent with the Beam equation as described by equation (3.2).

4.2.6 Stability of the CN Scheme

Recall that the general CN scheme for the is given by equation (4.41):

$$\begin{aligned}\frac{EI}{3\Delta x^4}\left[y_{n+2}^{m+1}-4y_{n+1}^{m+1}+6y_n^{m+1}-4y_{n-1}^{m+1}+y_{n-2}^{m+1}\right.&\\ +y_{n+2}^{m}-4y_{n+1}^{m}+6y_n^{m}-4y_{n-1}^{m}+y_{n-2}^{m} &= \frac{-\gamma}{\Delta t^2}\left[y_n^{m+1}-2y_n^m+y_n^{m-1}\right]\\ \left.+y_{n+2}^{m-1}-4y_{n+1}^{m-1}+6y_n^{m-1}-4y_{n-1}^{m-1}+y_{n-2}^{m-1}\right]&.\end{aligned}$$

Suppose that the error of the scheme at time-step m and spatial-step n is given by

$$\Lambda(m,n) = e(m)\text{Exp}(i\omega n\Delta x) \tag{4.58}$$

where $i=\sqrt{-1}$ and ω is the wave number.

In order for stability of the CN scheme to be determined, a similar process to Chapter 4.1.6 is followed. The solution to the resulting difference equation that models the temporal error between the exact and numerical solutions is given by

$$\begin{aligned}e(m) = c_2\Bigg[&\left(\frac{3+2\tau(\varphi-1)\left(i\sqrt{3}\sqrt{\tau^2(\phi-1)^2+3}-\tau\phi+\tau\right)}{4\tau^2(\varphi-1)^2+3}\right)^m\\ &-\left(\frac{3+2\tau(\varphi-1)\left(-i\sqrt{3}\sqrt{\tau^2(\varphi-1)^2+3}-\tau\varphi+\tau\right)}{4\tau^2(\varphi-1)^2+3}\right)^m\Bigg]\end{aligned} \tag{4.59}$$

where c_2 is an arbitrary constant. Further, in this case, $\tau=\sqrt{-3\chi}$ where, from equation (4.42),

$$\begin{aligned}\chi &= -\frac{EI\Delta t^2}{3\gamma\Delta x^4}\\ \implies \Delta t &= \frac{\tau}{\sqrt{\vartheta}}\Delta x^2.\end{aligned} \tag{4.60}$$

where $\vartheta=\frac{EI}{\gamma}$. Also, similar to Section 4.1.6, $\varphi=\cos(\sigma)$ and $\sigma=n\Delta x$.

Note that $-1 \leq \varphi \leq 1$. In order for stability to be analysed, $e(m)$ must be evaluated at the bounds of φ. When $\varphi = 1$, then $e(m) = 0 \ \forall m$ and the error is bounded. When $\varphi = -1$ and the substitution

$$\tau = \frac{\sqrt{3}}{2} \tan(\theta) \tag{4.61}$$

is made, then (4.60) reduces to

$$c_2 \left(\left(\left(\sqrt{3} - 3i\zeta \right)^2 \right)^m - \left(\left(\sqrt{3} + 3i\zeta \right)^2 \right)^m \right) \left(9\zeta^2 + 3 \right)^{-m} \tag{4.62}$$

where

$$\zeta = \sin(\theta). \tag{4.63}$$

Note that $-1 \leq \zeta \leq 1$. Evaluating (4.62) at the bounds of ζ gives

$$e(m) = 2ic_2 \sin\left(\frac{2\pi m}{3} \right) \quad \forall m \tag{4.64}$$

when $\zeta = -1$ and

$$e(m) = -2ic_2 \sin\left(\frac{2\pi m}{3} \right) \quad \forall m \tag{4.65}$$

when $\zeta = 1$. Therefore, the temporal error $e(m)$ is bounded for all values of m and, furthermore, the error between the exact and numerical solutions $\Lambda(m, n)$ remains bounded for all values of m. Therefore, the CN scheme described by equation (4.41) is unconditionally stable.

4.2.7 Convergence of the CN Scheme

Recall that the Beam equation (3.2) is linear. Further, the CN scheme described by (4.41) is consistent - as proved in Section 4.2.5 - and (unconditionally) stable - as proved in Section 4.2.6. Therefore, by the Lax Thereom, the CN scheme described by equation (4.41) is convergent.

4.3 Model Implementation

The Crank-Nicolson approach to solve the model (discussed in Chapter 4.2) is the preferred numerical approach over the CSCT approach (discussed in Chapter 4.1) due to the fact that the CN scheme has a higher order of accuracy and is unconditionally stable, as was shown in Chapter 4.2.6.

In the Crank-Nicolson approach, the number of spatial steps along the bat (N) is set to be 100 and the number of time steps (M) to be 6000. This allows for a sufficiently long characteristic time interval to analyze the results. Recall from equation (4.42) in Chapter 4.2.4 that

$$\chi = -\frac{EI\Delta t^2}{3\gamma\Delta x^4}.$$

Now, with EI, γ, Δx and Δt all as described in Chapter 3.4, it follows that $\chi = -735.3$. Recall from Chapter 4.2.6 that the Crank-Nicolson scheme is unconditionally stable. The matrix scheme described in Chapter 4.2.4 will calculate the bat's displacement at all $N + 1$ points along the length of the bat for all $M + 1$ time steps. After each time iteration, information regarding the displacement of each point along the edge of the bat is stored in a *displacement* matrix. That is, once the entire *displacement* matrix has been constructed through the scheme described in Chapter 4.2.4, there remains a $(N+1) \times (M+1)$ matrix where the entry (n, m) describes the displacement of point n at the time step m where $n \in [0, N]$ and $m \in [0, M]$.

5 Solution Via Separation Of Variables

5.1 The General Solution

The model introduced in Chapter 3 can be solved analytically using the technique of Separation of Variables. This was the approach used by Meirovitch in [18].

Recall the Beam Equation given by (3.2)

$$\frac{EI}{\gamma}\frac{\partial^4 y}{\partial x^4} + \frac{\partial^2 y}{\partial t^2} = 0,$$

where E is the modulus of elasticity (Young's Modulus), I is the area moment of inertia and γ is the mass per unit length (density). EI is the flexural rigidity of the bat. The solution $y(x,t)$ denotes the displacement of a point $x \in [0, L]$ at a time $t \geq 0$.

Recall that the initial and boundary conditions imposed on the equation:

$$\begin{aligned} &y(x,0) = 0, && y_t(x,0) = f(x), \\ &y(0,t) = 0, && y_x(0,t) = 0, \\ &y_{xx}(L,t) = 0, && y_{xxx}(L,t) = 0. \end{aligned}$$

To begin the Separation Of Variables approach, the assumption is made that the solution to (3.2) can be written as the product of two univariate functions, that is

$$y(x,t) = X(x)T(t). \tag{5.1}$$

Hence, (3.2) reduces to

$$\eta^2 X''''T + XT'' = 0, \tag{5.2}$$

where the 'dashes' ($'$) denote differentiation with respect to the appropriate variable and $\eta^2 = \frac{EI}{\gamma}$. Then, through simple rearrangement

$$\frac{\eta^2 X''''}{X} = \frac{-T''}{T} = k^2, \tag{5.3}$$

where k^2 is the constant of separation. The left-hand term in (5.3) is dependent on x only and the middle term is dependent on t only. Then, because

these two terms are equal, it follows that both the left-hand term and the middle term are actually both constant. This is the reason that it can be assumed that k is constant and, further, it is noted that the sign k is irrelevant due to the presence of trigonometric and hyperbolic functions in the spatial part of the solution . Equation (5.3) hence reduces to the two differential equations

$$X'''' - \frac{k^2}{\eta^2}X = 0, \tag{5.4}$$

and

$$T'' + k^2 T = 0. \tag{5.5}$$

Equation (5.4) can be solved to give

$$X(x) = A\sin\left(\sqrt{\frac{k}{\eta}}x\right) + B\cos\left(\sqrt{\frac{k}{\eta}}x\right) + C\sinh\left(\sqrt{\frac{k}{\eta}}x\right) + D\cosh\left(\sqrt{\frac{k}{\eta}}x\right), \tag{5.6}$$

where A, B, C and D are arbitrary constants that will be determined from the boundary conditions discussed in Chapter 3.2.1.

Equation (5.5) can be solved to give

$$T(t) = E\sin(kt) + F\cos(kt), \tag{5.7}$$

where E and F are arbitrary constants.

Applying the first two boundary conditions to equation (5.6) gives

$$\begin{aligned} & y(0,t) = 0 \\ \implies & X(0) = 0 \\ \implies & B + D = 0 \\ \implies & D = -B, \end{aligned}$$

and

$$\begin{aligned} & y_x(0,t) = 0 \\ \implies & X'(0) = 0 \\ \implies & A + C = 0 \\ \implies & C = -A. \end{aligned}$$

Hence, equation (5.6) reduces to

$$X(x) = A\sin\left(\sqrt{\frac{k}{\eta}}x\right) + B\cos\left(\sqrt{\frac{k}{\eta}}x\right) - A\sinh\left(\sqrt{\frac{k}{\eta}}x\right) - B\cosh\left(\sqrt{\frac{k}{\eta}}x\right). \tag{5.8}$$

Applying the third boundary condition to equation (5.8) gives

$$\begin{aligned}
& y_{xx}(L,t) = 0 \\
\implies & X''(L) = 0 \\
\implies & \frac{Bk\cos\left(\sqrt{\frac{k}{\eta}}L\right)}{\eta} + \frac{Bk\cosh\left(\sqrt{\frac{k}{\eta}}L\right)}{\eta} + \frac{Ak\sin\left(\sqrt{\frac{k}{\eta}}L\right)}{\eta} + \frac{Ak\sinh\left(\sqrt{\frac{k}{\eta}}L\right)}{\eta} = 0 \\
\implies & B\left[\cos\left(\sqrt{\frac{k}{\eta}}L\right) + \cosh\left(\sqrt{\frac{k}{\eta}}L\right)\right] + A\left[\sin\left(\sqrt{\frac{k}{\eta}}L\right) + \sinh\left(\sqrt{\frac{k}{\eta}}L\right)\right] = 0,
\end{aligned} \tag{5.9}$$

and similarly applying the fourth boundary condition to equation (5.8) gives

$$\begin{aligned}
& y_{xxx}(L,t) = 0 \\
\implies & X'''(L) = 0 \\
\implies & \frac{Bk\sqrt{\frac{k}{\eta}}\sin\left(\sqrt{\frac{k}{\eta}}L\right)}{\eta} - \frac{Bk\sqrt{\frac{k}{\eta}}\sinh\left(\sqrt{\frac{k}{\eta}}L\right)}{\eta} \\
& - \frac{Ak\sqrt{\frac{k}{\eta}}\cos\left(\sqrt{\frac{k}{\eta}}L\right)}{\eta} - \frac{Ak\sqrt{\frac{k}{\eta}}\cosh\left(\sqrt{\frac{k}{\eta}}L\right)}{\eta} = 0 \\
\implies & B\left[\sin\left(\sqrt{\frac{k}{\eta}}L\right) - \sinh\left(\sqrt{\frac{k}{\eta}}L\right)\right] - A\left[\cos\left(\sqrt{\frac{k}{\eta}}L\right) + \cosh\left(\sqrt{\frac{k}{\eta}}L\right)\right] = 0.
\end{aligned} \tag{5.10}$$

For simplicity, let $\xi = \sqrt{\frac{k}{\eta}}L$. Then equations (5.9) and (5.10) reduce to

$$B\left[\cos\xi + \cosh\xi\right] + A\left[\sin\xi + \sinh\xi\right] = 0,$$

and

$$B\left[\sin\xi - \sinh\xi\right] - A\left[\cos\xi + \cosh\xi\right] = 0,$$

respectively. This system of equations can be written in matrix form as

$$\begin{bmatrix} \sin\xi + \sinh\xi & \cos\xi + \cosh\xi \\ -(\cos\xi + \cosh) & \sin\xi - \sinh\xi \end{bmatrix} \begin{bmatrix} A \\ B \end{bmatrix} = \begin{bmatrix} 0 \\ 0 \end{bmatrix}. \tag{5.11}$$

Since A and B are not equal to zero, it follows that the determinant of the matrix in equation (5.11) must equal zero. Hence

$$\begin{aligned}&(\sin\xi+\sinh\xi)(\sin\xi-\sinh\xi)+(\cos\xi+\cosh\xi)^2=0\\ \implies &\sin^2\xi-\sinh^2\xi+\cos^2\xi+2\cos\xi\cosh\xi+\cosh^2\xi=0.\end{aligned}$$

Noticing that $\cos^2\xi+sin^2\xi=1$ and $\cosh^2\xi-\sinh^2\xi=1$, performing some rearrangements and substituting back $\xi=\sqrt{\frac{k}{\eta}}L$ gives

$$\cos\left(\sqrt{\frac{k}{\eta}}L\right)\cosh\left(\sqrt{\frac{k}{\eta}}L\right)=-1. \tag{5.12}$$

From Figure 5.1 below which uses the functions $y=\cos(x)\cosh(x)$ and $y=-1$, it is clear to see that there are an infinite number of points of intersection between the two functions, indicating that there exists an infinite number of solutions for k to satisfy equation (5.12).

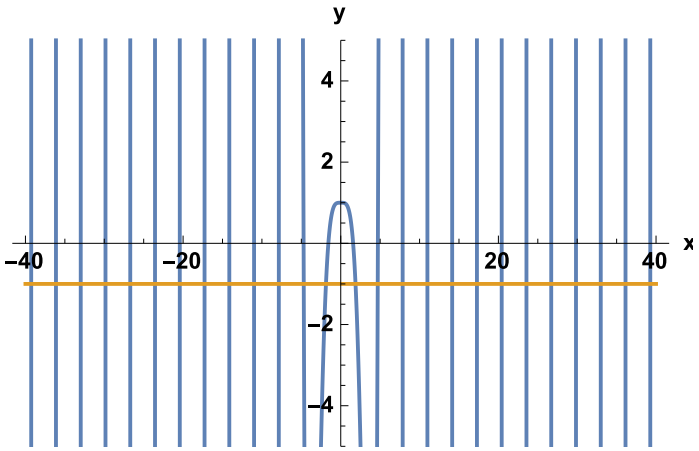

Figure 5.1: *The graphs of* $y=\cos(x)\cosh(x)$ *and* $y=-1$ *illustrating an infinite number of intersections between the functions.*

Using `Mathematica`'s `FindRoot` function, which implements Newton's Method, it is possible to solve for k_n, the nth eigenvalue. The `FindRoot` function gives the following list of solutions to equation (5.12), correct to 3 decimal places:

$$\sqrt{\frac{k_n}{\eta}}L = \{\pm 1.875, \pm 4.694, \pm 7.854, \dots\}$$
$$\implies k_n = \frac{\eta}{L^2}\left\{(1.875)^2, (4.694)^2, (7.854)^2, \dots\right\} \tag{5.13}$$
$$\implies k_n = \sqrt{\frac{EI}{\gamma L^4}}\left\{(1.875)^2, (4.694)^2, (7.854)^2, \dots\right\}$$

Hence, the nth element in the list in (5.13) is the nth eigenvalue in the solution of (5.8).

Note that because there are now an infinite number of eigenvalues k_n and because the arbitrary constants depend on the eigenvalues, there must be an infinite number of arbitrary constants too. Using equation (5.9), it is possible to write one of the arbitrary constants B_n in terms of the other A_n:

$$B_n\left[\cos\left(\sqrt{\frac{k_n}{\eta}}L\right) + \cosh\left(\sqrt{\frac{k_n}{\eta}}L\right)\right] + A_n\left[\sin\left(\sqrt{\frac{k_n}{\eta}}L\right) + \sinh\left(\sqrt{\frac{k_n}{\eta}}L\right)\right] = 0$$
$$\implies B_n = -\frac{A_n\left[\sin\left(\sqrt{\frac{k_n}{\eta}}L\right) + \sinh\left(\sqrt{\frac{k_n}{\eta}}L\right)\right]}{\left[\cos\left(\sqrt{\frac{k_n}{\eta}}L\right) + \cosh\left(\sqrt{\frac{k_n}{\eta}}L\right)\right]}. \tag{5.14}$$

Hence, equation (5.8) reduces as

$$\begin{aligned} X_n(x) &= A_n \sin\left(\sqrt{\frac{k_n}{\eta}}x\right) + B_n \cos\left(\sqrt{\frac{k_n}{\eta}}x\right) - A_n \sinh\left(\sqrt{\frac{k_n}{\eta}}x\right) - B_n \cosh\left(\sqrt{\frac{k_n}{\eta}}x\right) \\ &= A_n \bar{X}_n(x), \end{aligned} \tag{5.15}$$

where

$$\begin{aligned} \bar{X}_n(x) &= \sin\left(\sqrt{\frac{k_n}{\eta}}x\right) - \sinh\left(\sqrt{\frac{k_n}{\eta}}x\right) \\ &- \left[\frac{\sin\left(\sqrt{\frac{k_n}{\eta}}L\right) + \sinh\left(\sqrt{\frac{k_n}{\eta}}L\right)}{\cos\left(\sqrt{\frac{k_n}{\eta}}L\right) + \cosh\left(\sqrt{\frac{k_n}{\eta}}L\right)}\right]\left[\cos\left(\sqrt{\frac{k_n}{\eta}}x\right) - \cosh\left(\sqrt{\frac{k_n}{\eta}}x\right)\right]. \end{aligned} \tag{5.16}$$

Recall equation (5.7), the general solution to the temporal differential equation (5.5)

$$T(t) = E\sin(kt) + F\cos(kt).$$

Applying the first initial condition of the model to equation (5.7) gives

$$\begin{aligned} y(x,0) &= 0 \\ &\implies T(0) = 0 \\ &\implies F = 0. \end{aligned} \tag{5.17}$$

Hence,

$$T_n(t) = E_n \sin(k_n t). \tag{5.18}$$

Thus, the general solution to the Beam Equation (3.2), using the Separation of Variables technique is given by

$$\begin{aligned} y(x,t) &= \sum_{n=1}^{\infty} X_n(x)T_n(t) \\ &= \sum_{n=1}^{\infty} G_n \bar{X}_n(x)\sin(k_n t), \end{aligned} \tag{5.19}$$

where, from equation (5.16),

$$\begin{aligned} \bar{X}_n(x) &= \sin\left(\sqrt{\frac{k_n}{\eta}}x\right) - \sinh\left(\sqrt{\frac{k_n}{\eta}}x\right) \\ &- \left[\frac{\sin\left(\sqrt{\frac{k_n}{\eta}}L\right) + \sinh\left(\sqrt{\frac{k_n}{\eta}}L\right)}{\cos\left(\sqrt{\frac{k_n}{\eta}}L\right) + \cosh\left(\sqrt{\frac{k_n}{\eta}}L\right)}\right]\left[\cos\left(\sqrt{\frac{k_n}{\eta}}x\right) - \cosh\left(\sqrt{\frac{k_n}{\eta}}x\right)\right], \end{aligned}$$

and the coefficients $G_n = A_n E_n$ are to be determined from the remaining initial condition and the orthogonality which will be discussed below.

5.2 Proving Orthogonality of the Spatial Solution

For the general solution (5.19), it remains to solve for the arbitrary constant G_n. To do this, it is useful to make use of the fact that $X_n(x)$ is orthogonal with respect to $X_s(x)$ where $n \neq s$:

$$\int_0^L X_n(x)X_s(x)\mathrm{d}x = \begin{cases} 0 & : n \neq s \\ \omega_n & : n = s \end{cases}$$

where ω_n is a arbitrary constant.

To show that this is indeed the case, recall equation (5.15),

$$X_n(x) = A_n\bar{X}_n(x),$$

where, from equation (5.16),

$$\begin{aligned}\bar{X}_n(x) &= \sin\left(\sqrt{\frac{k_n}{\eta}}x\right) - \sinh\left(\sqrt{\frac{k_n}{\eta}}x\right) \\ &- \left[\frac{\sin\left(\sqrt{\frac{k_n}{\eta}}L\right) + \sinh\left(\sqrt{\frac{k_n}{\eta}}L\right)}{\cos\left(\sqrt{\frac{k_n}{\eta}}L\right) + \cosh\left(\sqrt{\frac{k_n}{\eta}}L\right)}\right]\left[\cos\left(\sqrt{\frac{k_n}{\eta}}x\right) - \cosh\left(\sqrt{\frac{k_n}{\eta}}x\right)\right].\end{aligned}$$

Since $X(x)$ was derived using the boundary conditions from the model, it is clear then that the following all hold:

$$\begin{aligned} X(0) &= 0, \\ X'(0) &= 0, \\ X''(L) &= 0, \\ X'''(L) &= 0, \end{aligned} \tag{5.20}$$

where the dashes (') denote differentiation with respect to x.

Recall the spatial differential equation (5.15)

$$\begin{aligned} X_n'''' - \frac{{k_n}^2}{\eta^2}X_n &= 0 \\ \implies X_n'''' &= \frac{k_n^2}{\eta^2}X_n. \end{aligned}$$

Left multiplying both sides by $X_s(x)$ $(n \neq s)$ and integrating with respect to x over the length of the bat (L) gives

$$\int_0^L X_s X_n'''' \mathrm{d}x = \frac{{k_n}^2}{\eta^2} \int_0^L X_s X_n \mathrm{d}x \tag{5.21}$$

Consider the left hand side of equation (5.21). It is possible to expand this integral using Integration by Parts:

$$\begin{aligned} \int_0^L X_s X_n'''' \mathrm{d}x &= X_s X_n''' \Big|_0^L - \int_0^L X_n''' X_s' \mathrm{d}x \\ &= [X_s(L) X_n'''(L) - X_s(0) X_n'''(0)] - \int_0^L X_n''' X_s' \mathrm{d}x \\ &= - \int_0^L X_n''' X_s' \mathrm{d}x, \end{aligned} \tag{5.22}$$

since $X_n'''(L) = 0 = X_s(0)$ by equation (5.20). Using Integration by Parts again gives

$$\begin{aligned} \int_0^L X_s X_n'''' \mathrm{d}x &= - \int_0^L X_n''' X_s' \mathrm{d}x \\ &= - \left[X_s' X_n'' \Big|_0^L - \int_0^L X_n'' X_s'' \mathrm{d}x \right] \\ &= - \left[X_s'(L) X_n''(L) - X_s'(0) X_n''(0) - \int_0^L X_n'' X_s'' \mathrm{d}x \right] \\ &= \int_0^L X_n'' X_s'' \mathrm{d}x, \end{aligned} \tag{5.23}$$

since $X_n''(L) = 0 = X_s'(0)$ by (5.20).

Hence, equation (5.21) becomes

$$\int_0^L X_s'' X_n'' \mathrm{d}x = \frac{{k_n}^2}{\eta^2} \int_0^L X_s X_n \mathrm{d}x, \tag{5.24}$$

and by a similar argument

$$\int_0^L X_n'' X_s'' \mathrm{d}x = \frac{{k_s}^2}{\eta^2} \int_0^L X_n X_s \mathrm{d}x. \tag{5.25}$$

Continuing with the process of Integration by Parts shows that

$$\int_0^L X_s X_n'''' \mathrm{d}x = \int_0^L X_n X_s'''' \mathrm{d}x. \tag{5.26}$$

Now from equation (5.23), since

$$\int_0^L X_s X_n'''' \mathrm{d}x = \int_0^L X_n'' X_s'' \mathrm{d}x,$$

and, therefore,

$$\int_0^L X_n X_s'''' \mathrm{d}x = \int_0^L X_s'' X_n'' \mathrm{d}x, \tag{5.27}$$

it follows from equation (5.26) that

$$\int_0^L X_n'' X_s'' \mathrm{d}x = \int_0^L X_s'' X_n'' \mathrm{d}x. \tag{5.28}$$

Then, with the use of equation (5.28), subtracting equation (5.25) from equation (5.24) gives

$$0 = \frac{({k_n}^2 - {k_s}^2)}{\eta^2} \int_0^L X_n X_s \mathrm{d}x. \tag{5.29}$$

Clearly $\frac{({k_n}^2 - {k_s}^2)}{\eta^2} \neq 0$ if $n \neq s$ and so

$$\int_0^L X_n(x) X_s(x) \mathrm{d}x = 0, \tag{5.30}$$

as required. Hence $X_n(x)$ is orthogonal with respect to $X_s(x)$. That is

$$\int_0^L X_n(x) X_s(x) \mathrm{d}x = \begin{cases} 0 & : n \neq s \\ \omega_n & : n = s \end{cases} \tag{5.31}$$

where ω_n is a arbitrary constant.

5.3 Completing The General Solution

To fully complete the general solution to the Beam Equation (3.2), the arbitrary constants ω_n and G_n must be found. Recall equation (5.31)

$$\int_0^L X_n(x)X_s(x)\mathrm{d}x = \begin{cases} 0 & : n \neq s \\ \omega_n & : n = s \end{cases}$$

Suppose that $n = s$ and let $\tau_n = \sqrt{\frac{k_n}{\eta}}$ such that

$$\begin{aligned}
\omega_n &= \int_0^L (X_n(x))^2\mathrm{d}x \\
&= \frac{1}{2\tau_n\left[\cos(\tau_n L)+\cosh(\tau_n L)\right]^2}\Bigg(-L\tau_n\cos(2\tau_n L)+\tau_n L\cosh(2\tau_n L) \\
&\qquad +4\tau_n L\sin(\tau_n L)\sinh(\tau_n L)-6\cosh(\tau_n L)\sin(\tau_n L) \\
&\qquad -3\cosh^2(\tau_n L)\sin(2\tau_n L)+6\cos(\tau_n L)\sinh(\tau_n L) \\
&\qquad +3\cos^2(\tau_n L)\sinh(2\tau_n L)\Bigg).
\end{aligned} \tag{5.32}$$

Recall the possible values for k_n given by equation (5.13). Substituting the nth eigenvalue into $\tau_n = \sqrt{\frac{k_n}{\eta}}$ will cause

$$\begin{aligned}
&-6\cosh(\tau_n L)\sin(\tau_n L)-3\cosh^2(\tau_n L)\sin(2\tau_n L) \\
&+6\cos(\tau_n L)\sinh(\tau_n L)+3\cos^2(\tau_n L)\sinh(2\tau_n L)=0.
\end{aligned} \tag{5.33}$$

Hence, after some algebra, equation (5.32) will reduce to

$$\begin{aligned}
\omega_n &= \frac{L}{2\left[\cos(\tau_n L)+\cosh(\tau_n L)\right]^2}\Big[\cosh(2\tau_n L)+4\sin(\tau_n L)\sinh(\tau_n L)-\cos(2\tau_n L)\Big] \\
&= \frac{L}{2\left[\cos(\tau_n L)+\cosh(\tau_n L)\right]^2}\Big[2\sinh^2(\tau_n L)+1+4\sin(\tau_n L)\sinh(\tau_n L)-1+2\sin^2(\tau_n L)\Big] \\
&= L\left[\frac{\sinh(\tau_n L)+\sin(\tau_n L)}{\cosh(\tau_n L)+\cos(\tau_n L)}\right]^2.
\end{aligned} \tag{5.34}$$

Once again recall the possible values for k_n given by equation (5.13). Substituting the nth eigenvalue into $\tau_n = \sqrt{\frac{k_n}{\eta}}$ and evaluating using `Mathematica` gives

$$\omega_n = L\ \{1.85564, 0.964064, 1, 00155, 0.9999, \dots\}. \tag{5.35}$$

Hence when the nth eigenvalue is used (k_n), then ω_n will take the nth value in the list in equation (5.35).

Recall equation (5.19), the general solution to the Beam Equation (3.2)

$$y(x,t) = \sum_{n=1}^{\infty} G_n \bar{X}_n(x) \sin(k_n t),$$

where, from equation (5.16)

$$\begin{aligned}\bar{X}_n(x) &= \sin\left(\sqrt{\frac{k_n}{\eta}}x\right) - \sinh\left(\sqrt{\frac{k_n}{\eta}}x\right) \\ &- \left[\frac{\sin\left(\sqrt{\frac{k_n}{\eta}}L\right) + \sinh\left(\sqrt{\frac{k_n}{\eta}}L\right)}{\cos\left(\sqrt{\frac{k_n}{\eta}}L\right) + \cosh\left(\sqrt{\frac{k_n}{\eta}}L\right)}\right]\left[\cos\left(\sqrt{\frac{k_n}{\eta}}x\right) - \cosh\left(\sqrt{\frac{k_n}{\eta}}x\right)\right],\end{aligned}$$

and where G_n is an arbitrary constant. Now, recall the initial condition

$$y_t(x,0) = f(x),$$

where $f(x)$ is the initial velocity distribution of the bat as described in Chapter 3. So differentiating equation (5.19) with respect to time, evaluating at $t = 0$ and setting this equal to $f(x)$ gives

$$f(x) = \sum_{n=1}^{\infty} k_n G_n \bar{X}_n(x). \tag{5.36}$$

It has been shown that $X_n(x)$ is orthogonal with respect to $X_s(x)$. From equation (5.15), it is clear that this is also true for $\bar{X}_n(x)$ and $\bar{X}_s(x)$. Right multiplying both sides of (5.36) by $\bar{X}_s(x)$ and integrating with respect to x over the length of the bat L gives

$$\begin{aligned}\int_0^L f(x)\bar{X}_s \mathrm{d}x &= \int_0^L \sum_{n=1}^{\infty} k_n G_n \bar{X}_n \bar{X}_s \mathrm{d}x \\ &= \sum_{n=1}^{\infty} k_n G_n \int_0^L \bar{X}_n \bar{X}_s \mathrm{d}x \\ &= k_s G_s \omega_s,\end{aligned} \tag{5.37}$$

from equation (5.31). Hence

$$G_s = \frac{1}{k_s \omega_s} \int_0^L f(x)\bar{X}_s(x)\mathrm{d}x. \tag{5.38}$$

Ergo, the solution $(y(x,t))$ to the Beam equation (3.2) via the technique of Separation of Variables is given by equation (5.19)

$$y(x,t) = \sum_{n=1}^{\infty} G_n \bar{X}_n(x) \sin(k_n t),$$

where, from equation (5.16),

$$\begin{aligned}\bar{X}_n(x) = &\sin\left(\sqrt{\frac{k_n}{\eta}}x\right) - \sinh\left(\sqrt{\frac{k_n}{\eta}}x\right) \\ &- \left[\frac{\sin\left(\sqrt{\frac{k_n}{\eta}}L\right) + \sinh\left(\sqrt{\frac{k_n}{\eta}}L\right)}{\cos\left(\sqrt{\frac{k_n}{\eta}}L\right) + \cosh\left(\sqrt{\frac{k_n}{\eta}}L\right)}\right]\left[\cos\left(\sqrt{\frac{k_n}{\eta}}x\right) - \cosh\left(\sqrt{\frac{k_n}{\eta}}x\right)\right],\end{aligned}$$

and, from equation (5.13),

$$k_n = \sqrt{\frac{EI}{\gamma L^4}}\left\{(1.875)^2, (4.694)^2, (7.854)^2, \dots\right\}.$$

Also, from equation (5.38),

$$G_n = \frac{1}{k_n \omega_n} \int_0^L f(x)\bar{X}_n(x)\mathrm{d}x,$$

where, from equation (5.35),

$$\omega_n = L\ \{1.85564, 0.964064, 1, 00155, 0.9999, \dots\},$$

and $f(x)$ is as described in Chapter 3.

6 Analysis Of The Results

In this Chapter, through the use of both the Crank-Nicolson scheme from Chapter 4 and the Separation of Variables solution from Chapter 5, the results of the three different 'collision' scenarios discussed in Chapter 3.3 will be analyzed at different *Locations of Impact*. These *Locations of Impact* are: 0.45m - near the free-end of the bat, 0.25m - at the middle of the bat and 0.05m - near the handle of the bat. The different analyses to be conducted at each *Location of Impact* will be discussed in Chapter 6.1.

6.1 Analyses Used in the Model

The following analyses look at various *Locations of Impact* and will determine the behaviour of the system at these various locations under the three different scenarios discussed in Chapter 3.3. Each of the analysis techniques will be briefly discussed.

6.1.1 Initial Velocity Analysis

In each of the three collision scenarios to be analyzed in Chapter 6 for each *Location of Impact*, analyses of the initial velocity distributions will be used. These initial velocity distributions model the velocity of all points along the length of the bat immediately post-collision with the ball. These analyses will be conducted for each of the three collision scenarios.

Recall that the Separation of Variables approach in Chapter 5 gives an analytical solution to the Beam Equation (3.2) to be $y(x,t)$: the displacement of point $x \in [0, L]$ on the bat at time $t \geq 0$. The analytical solution is found using the initial velocity distribution discussed above. Then, using the analytical solution, it is possible to find the initial velocity distribution that will be used in the Crank-Nicolson scheme from Chapter 4. That is, the initial velocity distribution is given by differentiating the analytical solution with respect to time (this results in the 'velocity' function) and then setting time equal to 0. So

$$f(x) = y_t(x, 0) \tag{6.1}$$

where the subscript denotes differentiation with respect to t. This process is implemented in the second and third collision scenarios and these initial velocity distributions are subsequently implemented in the corresponding Crank-Nicolson scheme solutions. This is done to allow for the analytical and

numerical approaches to be related and hence their results compared fairly in these two scenarios. As was discussed in Chapter 3.3.1, the first collision scenario's initial velocity distribution cannot be adequately captured by the basis functions of the analytical solution due to the sharp gradient of the initial velocity function. Hence, this collision scenario is solved using only the Crank-Nicolson approach, and the (impulse-like) initial velocity distribution is passed directly to the Crank-Nicolson scheme.

To summarize: in the first collision scenario, the analytical solution is bypassed and only the numerical solution is used, with the initial velocity distribution passed directly to the Crank-Nicolson scheme. In the second and third collision scenarios, the initial velocity distributions derived in Chapters 3.3.2 and 3.3.3 are used to find the corresponding analytical solutions through the Separation of Variables technique. Then using these analytical solutions, the initial velocity distributions to be used in the Crank-Nicolson approach are derived and the numerical solutions hence obtained.

6.1.2 Displacement Analysis And Its Associated Error

The most basic but by no means least important of the analyses is the analysis of the displacement. Recall from Chapters 4 and 5 that the Beam equation (3.2) has the numerical solution $\hat{y}(x,t)$ and analytical solution $y(x,t)$; displacement of point $x \in [0,L]$ at time $t \geq 0$. For different *Locations of Impact*, the results from the three scenarios will be analyzed in terms of the displacement solutions that they produce.

Furthermore, through an error-term analysis, the displacement results will be used to compare the Crank-Nicolson approach discussed in Chapter 4 to that of the analytical Separation of Variables solution discussed in Chapter 5. At each time t_m $\forall m \in [0,M]$, the displacement of each point along the length of the bat x_n $\forall n \in [0,N]$ will be compared in the two different approaches used to solve the model. Suppose $y(x_n,t_m)$ gives the displacement of point x_n at time t_m according to the Separation of Variables approach and $\hat{y}(x_n,t_m)$ does similarly for the Crank-Nicolson approach. Then the error-term at time t_m is given by

$$Err(t_m) = \sum_{n=0}^{N} \frac{|y(x_n,t_m) - \hat{y}(x_n,t_m)|}{N} \tag{6.2}$$

This is implemented in the `Mathematica` code.

It is very important to note that the analytical solution $y(x,t)$ obtained from the Separation of Variables technique which implemented in this work con-

sists of the first 50 eigenvalues of the series solution. By definition, this is an exact solution the Beam equation (3.2). However, the series solution should have an infinite number of terms. The analytical solution presented here will be clearly contain a small inherent error from the 'true' analytical solution. Moreover, the numerical solution $\hat{y}(x,t)$ presented in this work is not compared with the 'true' analytical solution but rather with the analytical solution $y(x,t)$ presented in this work. Therefore, the difference in the two solutions will clearly also contain this small inherent error.

6.1.3 Strain Energy Analysis And Its Associated Error

Given the displacement y of a point x at time t, it is possible to calculate the strain energy in the bat at time t. From Gavin [12], the strain energy SE at time t in a beam (and so, in this case, a bat) is given by

$$SE(t) = \frac{1}{2}\int_0^L EI(y''(x,t))^2 dx \tag{6.3}$$

where L is the length of the beam, EI is the flexural rigidity of the bat and $y(x,t)$ is the solution to the beam equation (3.2) as discussed in Chapter 5. The curvature of the beam $(y''(x,t))$ at a point x and time t is the moment in the beam. A unit analysis can be conducted on this result and it is easy to find that the SI units of equation in (6.3) is $\frac{\text{kg m}^2}{\text{s}^2}$ or, equivalently, Joules.

In terms of the Crank-Nicolson method as discussed in Chapter 4, to calculate the strain energy at time t_m, the curvature of the beam at this time step is found through the use the second derivative of the displacement. The second derivative is obtained through the use of a central difference approximation. The curvature at each point $n = 0, \ldots, N$ is squared and numerical integration is implemented through use of the trapezoidal rule. In this way, using a numerical approach, the strain energy $\widehat{SE}$ in the bat can then be calculated at each point in time and this process is implemented in `Mathematica`.

Due to the sharp curvature that is experienced in the bat when the second derivative of the displacement is found, this curvature cannot be accurately captured by a three-point stencil in the numerical approach when only 100 points are used over the entire spacial domain that was used in the numerical solution of the displacement. In order to counter this problem and sufficiently capture the strain energy using the numerical scheme, a finer spatial grid is used. The finer grid will allow the three-point stencil to sufficiently capture the sharp curvatures experienced in the bat. However, this is extremely computationally expensive to implement in `Mathematica`. Therefore, the strain energy will be calculated over a much shorter time domain by the numerical

solution than was done for the numerical solution of the displacement. It is important to note that the analytical solution will not suffer from this problem due to its orthogonality condition, discussed below.

Clearly, equation (6.3) will apply directly to the analytical solution, at least in theory. To calculate the strain energy from the analytical solution in this way in `Mathematica` is very computationally expensive. However, this computational problem can be avoided by using the orthogonality condition of the analytical solution. Recall from Chapter 5 that through the Separation of Variables approach the analytical solution is given by equation (5.19):

$$\begin{aligned} y(x,t) &= \sum_{n=1}^{\infty} G_n \bar{X}_n(x) \sin(k_n t) \\ &= G_1 \bar{X}_1(x) \sin(k_1 t) + G_2 \bar{X}_2(x) \sin(k_2 t) + \dots \\ \implies y''(x,t) &= G_1 \bar{X}_1{}''(x) \sin(k_1 t) + G_2 \bar{X}_2{}''(x) \sin(k_2 t) + \dots \end{aligned}$$

where $\bar{X}_n(x)$, G_n and k_n are as described in Chapter 5. Then

$$\begin{aligned} (y''(x,t))^2 &= \Big(G_1 \bar{X}_1{}''(x) \sin(k_1 t) + G_2 \bar{X}_2{}''(x) \sin(k_2 t) + \dots \Big)^2 \\ &= (G_1)^2 (\bar{X}_1{}'')^2(x) \sin^2(k_1 t) + (G_2)^2 (\bar{X}_2{}'')^2(x) \sin^2(k_2 t) + \dots + J(x,t) \end{aligned} \tag{6.4}$$

where $J(x,t)$ is the sum of all $G_p G_q \bar{X}_p{}''(x) \bar{X}_q{}''(x) \sin(k_p t) \sin(k_q t)$ terms, where $p, q \in 1, 2, \dots$ but $p \neq q$.

Then the strain energy becomes

$$\begin{aligned} SE(t) &= \frac{EI}{2} \int_0^L (y''(x,t))^2 dx \\ &= \frac{EI}{2} \int_0^L \Big[(G_1)^2 (\bar{X}_1{}'')^2(x) \sin^2(k_1 t) + (G_2)^2 (\bar{X}_2{}'')^2(x) \sin^2(k_2 t) + \dots + J(x,t) \Big] dx \end{aligned} \tag{6.5}$$

since EI is constant in the model. Then, by using the linearity of the integration operator, consider any single, arbitrary term that could occur from equation (6.5):

$$
\begin{aligned}
&\frac{EI}{2}\int_0^L G_s G_r X''_s X''_r \sin(k_s t)\sin(k_r t)dx \\
=&\frac{EI}{2}\left[G_s G_r \sin(k_s t)\sin(k_r t)\right]\int_0^L X''_s X''_r dx \\
=&\frac{EI}{2\eta^2} G_s G_r \sin(k_s t)\sin(k_r t)k_s^2\int_0^L X_s X_r dx
\end{aligned}
\tag{6.6}
$$

by equation (5.24). Then, by the orthogonality condition given by equation (5.31), any arbitrary term from equation (6.5) will reduce as

$$
\begin{aligned}
&\frac{EI}{2}\int_0^L G_s G_r X''_s X''_r \sin(k_s t)\sin(k_r t)dx \\
=&\begin{cases} 0 & : s \neq r \\ \frac{EI}{2\eta^2}\left[\omega_n (G_s)^2 (k_s)^2 (X''_s)^2 \sin^2(k_s t)\right] & : s = r \end{cases}
\end{aligned}
\tag{6.7}
$$

where $s, r \in 1, 2, \ldots$. Therefore, the strain energy for any time $t \geq 0$ can be written as

$$
SE(t) = \frac{EI}{2\eta^2}\sum_{n=1}^{\infty}\omega_n (G_n)^2 (k_n)^2 \sin^2(k_n t) \tag{6.8}
$$

This solution for the strain energy can easily be implemented in `Mathematica` with a finite number of eigenvalues.

A similar argument to before is made here with regards to the 'true' strain energy solution obtained from the analytical solution. The analytical solution presented in this work $y(x,t)$ is obtained with 50 eigenvalues and hence contains an inherent error from the 'true' analytical solution that is obtained with an infinite number of eigenvalues. Since the strain energy solutions are calculated with the finite series analytical solution, the strain energy solution obtained from $y(x,t)$ will also contain this small inherent error.

Due to the computational cost of calculating the strain energy in the numerical solution, it is not practical to quantitatively compare the strain energy calculated from the analytical solution to the strain energy calculated from the numerical solution. However, in all cases, the strain energy solutions will be compared qualitatively.

6.1.4 Analysis Using A Fourier Transform

A Fourier Analysis is conducted on the *Location of Impact* in question over time. A Fourier Analysis is useful in this work as it provides a way to

determine the dominant frequencies in the vibration of the cricket bat. Recall that one of the definitions used in the model of a 'sweet-spot' in a cricket bat is the *Location of Impact* where the least vibrations are transmitted to the batsman's hands, in such a way as the batsman barely feels the ball hitting the bat. The beauty of a Fourier Transform and its subsequent analysis is that a *Location of Impact* that will produce small amplitudes in the power domain over relatively large frequencies could be considered to be a good *Location of Impact* as there is only weak vibrations in the bat with shorter wavelengths; the batsman is unlikely to feel many vibrations in his hands. On the other hand, a *Location of Impact* that produces larger amplitudes in the power domain over relatively small frequencies could be considered to be a poor *Location of Impact* as this would indicate large vibrations in the bat. The batsman could experience many (uncomfortable) vibrations reaching his hands in this case. It is thus hypothesized that a Fourier Analysis can thus provide a way to find the 'best' *Location of Impact* in terms of minimizing the 'sting' felt by the batsman and hence satisfying this part of the chosen definition of the sweet-spot.

It is important to note that a frequency analysis with the aim of determining the location where the least amount of energy is transferred to a batsman's hands is a tried, tested and worthwhile approach as significant results were drawn from similar approaches carried out by the likes of Penrose and Hose [21], Knowles *et al* [17], and Cross [9]. Although these approaches focused more on the physical vibrations of the bat and the analysis thereof, it is argued that the frequencies to be analysed are present because of the vibrating bat.

In terms of the Crank-Nicolson approach, the Fourier Transform is implemented on the *Location of Impact* vector. That is, from the *displacement* matrix described in Chapter 4, the row that corresponds to the *Location of Impact* is subjected to the Fourier Transform. This is implemented through the use of `Mathematica`'s `Fourier` function.

Now, for the Separation of Variables approach recall from Chapter 5 and equation (5.19),

$$y(x,t) = \sum_{n=1}^{\infty} G_n \bar{X}_n(x) \sin(k_n t).$$

The Fourier Transform is implemented on (5.19)

$$\mathcal{F}(y(x,t)) = \mathcal{F}\left(\sum_{n=1}^{\infty} G_n \bar{X}_n(x) T(t)\right) \tag{6.9}$$

where $T(t) = \sin(k_n t)$, $\mathcal{F}$ denotes the Fourier Transform and Ω is frequency, measured in Hertz. Simplifying (6.9) further gives

$$\begin{aligned}\mathcal{F}(y(x,t)) &= \sum_{n=1}^{\infty} G_n \bar{X}_n(x) \mathcal{F}(T(t)) \\ &= \sum_{n=1}^{\infty} G_n \bar{X}_n(x) \int_{-\infty}^{\infty} e^{i\Omega t} \sin(k_n t) dt \quad = \sum_{n=1}^{\infty} G_n \bar{X}_n(x) \delta(\Omega - k_n) \sqrt{\frac{\pi}{2}} i\end{aligned} \tag{6.10}$$

where $\delta(\Omega - k_n)\sqrt{\frac{\pi}{2}}i$ is the Fourier Transform of $\sin k_n t$. $\delta(\Omega - k_n)$ refers to the dirac delta function which is presented formally as

$$\delta(x) = \begin{cases} +\infty : & x = 0 \\ 0 : & x \neq 0 \end{cases}$$

Further,

$$\int_{-\infty}^{\infty} \delta(x) dx = 1.$$

So, essentially, when $\Omega = k_n$, the dirac delta function will evaluate as positive infinity, and zero otherwise.

Since dirac delta functions are present in the Fourier Transform of the analytical solution, these Transforms are omiited from the analysis in this work. The analysis into the frequencies in the bat as a result of a collision with a ball will be conducted on the Fourier Trasform from the numerical solution only.

6.1.5 Analyses Of The Pressure Distributions

Recall from Chapter 3.3 that circular and elliptical Hertzian pressure distributions are used in the second and third collision scenarios respectively, and these model the pressure exerted by the ball on the face of the bat during collision. In both of these scenarios, a pressure distribution analysis will be conducted for all three *Locations of Impact* .

6.1.6 A Note On The `Mathematica` Implementation

The programming language `Mathematica` is used to implement both the Separation of Variables approach discussed in Chapter 5 and the Crank-Nicolson

approach discussed in Chapter 4.

It is important to note that in order for the `Mathematica` code to be implemented successfully, a few compromises from the theoretical model must be introduced. Firstly, from Chapter 5, the Separation of Variables solution is complete when the sum is taken to an infinite number of terms. Clearly this is not practical in this model and the solution is calculated with the first 50 eigenvalues. It is important to note that the coefficients of the higher terms in the sum become very small. Truncation after the first 50 eigenvalues is therefore a reasonable approximation to the infinite sum.

Also, the theory dictates that analytical integration is used to calculate values of G_n in equation (5.19). However, in the second and third scenarios to be discussed in Chapter 6, the initial velocity profiles are made to be piece-wise functions, and hence difficulties arise when computing the integral analytically. To counter this, `Mathematica`'s `NIntegrate` function is used with great success.

6.2 Analyzing The Results For An Impulsive, Perpendicular Collision - Scenario 1

The results from the analyses are discussed for an impulsive, perpendicular collision between the cricket bat and the cricket ball. Recall that, as discussed in Chapter 3, this scenario models a defensive shot played by the batsman where time of the ball on the bat is considerably shorter than the time taken for a wave to propagate through the length of the bat.

In this scenario, only the results obtained from the Crank-Nicolson approach will be examined. This is because the Separation of Variables solution cannot accurately capture the basis functions required to accurately model the impulse initial velocity distribution due to the absence of high-frequency terms in the series solution.

The initial velocity distribution in this case is modelled as the impulse function, which in turn is approximated as

$$f(x) = 27 \exp\left(-\frac{(x-\upsilon)^2}{\sigma}\right) \tag{6.11}$$

where $\sigma = 10^{-5}$ is a scaling factor and $\upsilon \in [0, 1]$ is the *Location of Impact*. The coefficient of 27 is also a scaling factor and captures the velocity of the ball hitting the bat (27 m/s, approximately 100 km/h - a realistic value in a cricket match, particularly against a fast bowler). The initial velocity of all points on the bat will be no more than this amount.

Since the Separation of Variables solution is not being used in this scenario, this function $f(x)$ is passed to the `Mathematica` implementation of the Crank-Nicolson scheme immediately. In the scenarios to follow later, the initial velocity distribution for the Crank-Nicolson scheme will be derived from the Separation of Variables solution; as was discussed earlier in Chapter 6.1.1.

6.2.1 Analysis for *Location of Impact* Near the Free-End of the Bat (at 0.45m)

Figures 6.1 through 6.4 below portray the results for the collision near the free-end of the bat.

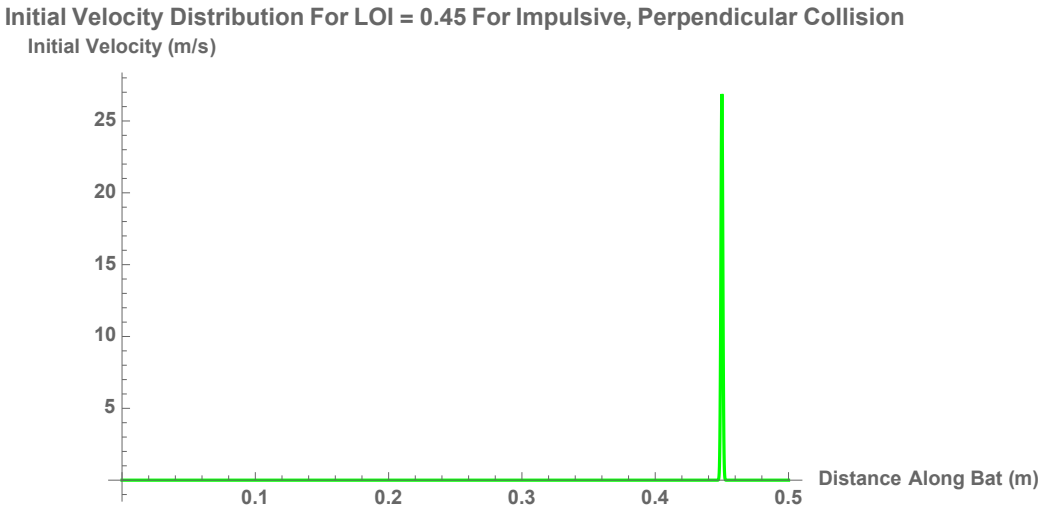

Figure 6.1: *The initial velocity distribution for Location of Impact near the free-end of the bat (0.45m) for an impulsive, perpendicular collision*

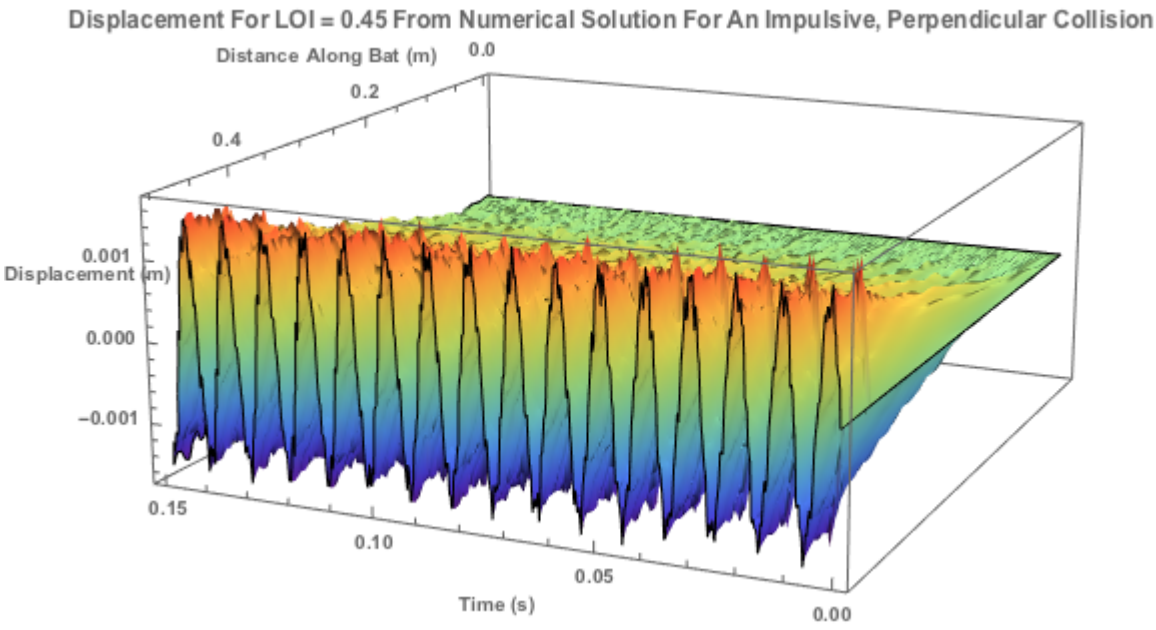

Figure 6.2: *The displacement solution for Location of Impact near the free-end of the bat (at 0.45m) for an impulsive, perpendicular collision*

Note the spike in the displacement at the *Location of Impact* from Figure 6.2 that results from the impulsive collision.

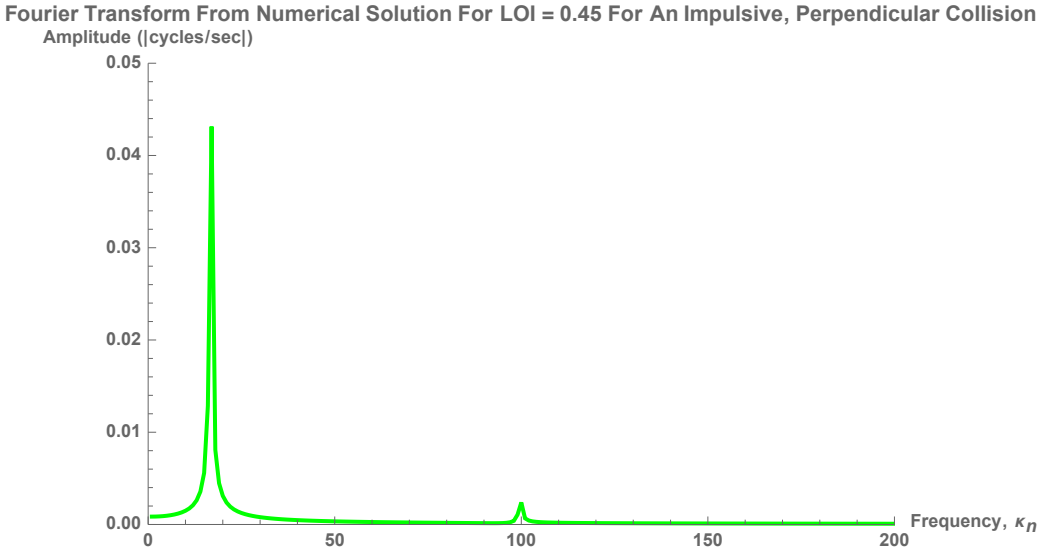

Figure 6.3: *The Fourier Transform for Location of Impact near the free-end of the bat (at 0.45m) for an impulsive, perpendicular collision*

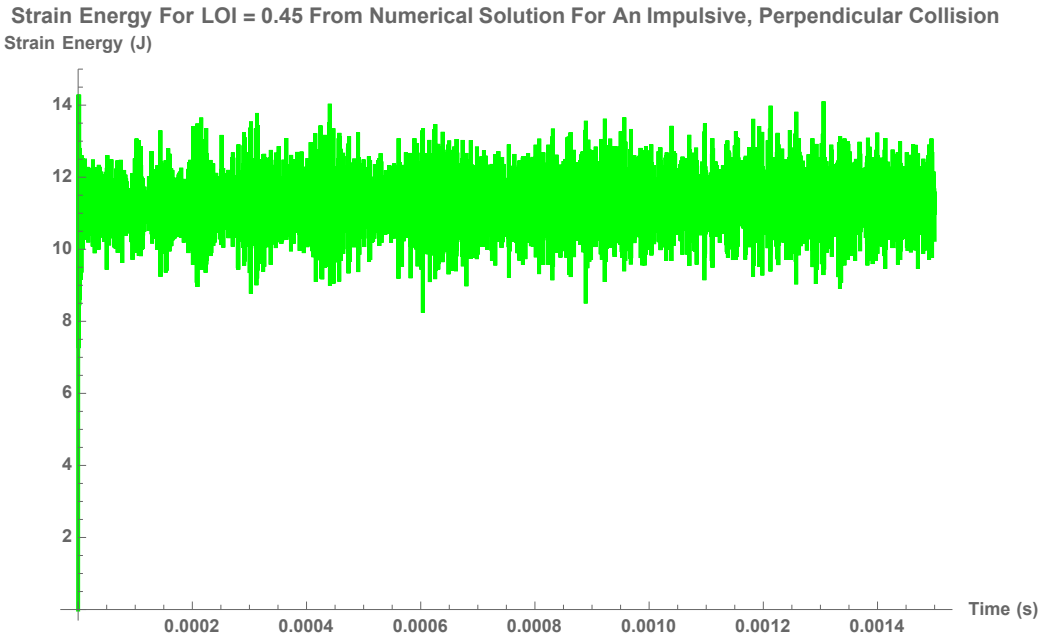

Figure 6.4: *The strain energy for Location Of Impact near the free-end of the bat (at 0.45m) for an impulsive, perpendicular collision*

6.2.2 Analysis for *Location of Impact* at the Middle of the Bat (at 0.25m)

Figures 6.5 through 6.8 below portray the results for the collision at the middle of the bat.

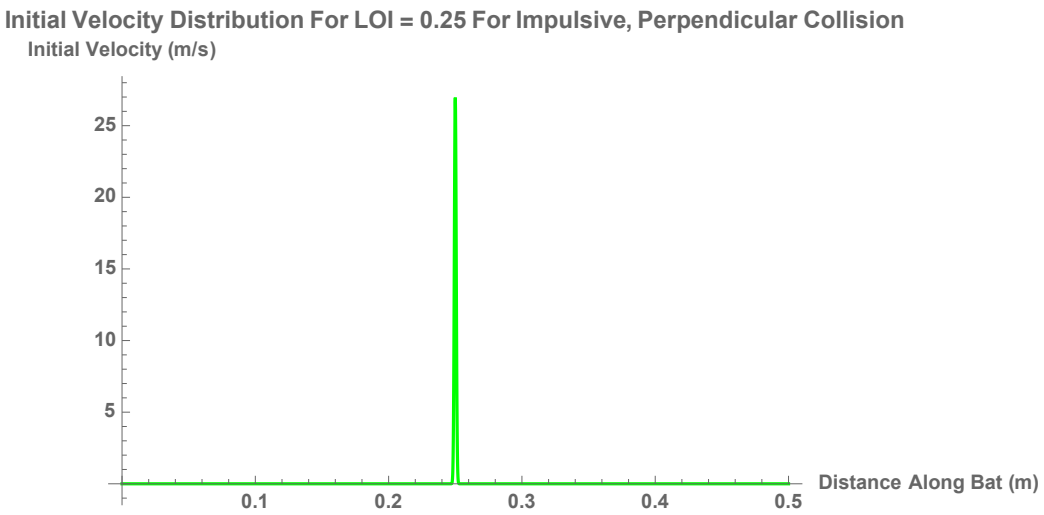

Figure 6.5: *The initial velocity distribution for Location of Impact at the middle of the bat (0.25m) for an impulsive, perpendicular collision*

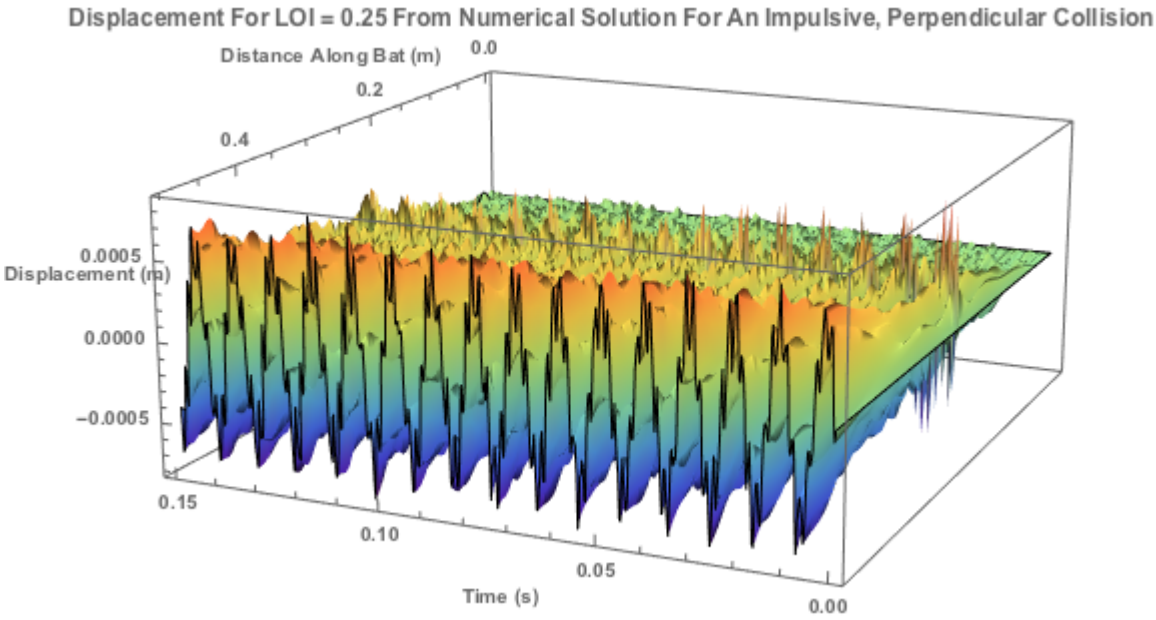

Figure 6.6: *The displacement solution for Location of Impact at the middle of the bat (at 0.25m) for an impulsive, perpendicular collision*

As with the previous *Location of Impact*, note the spike in the displacement at the *Location of Impact* from Figure 6.6 that results from the impulsive collision.

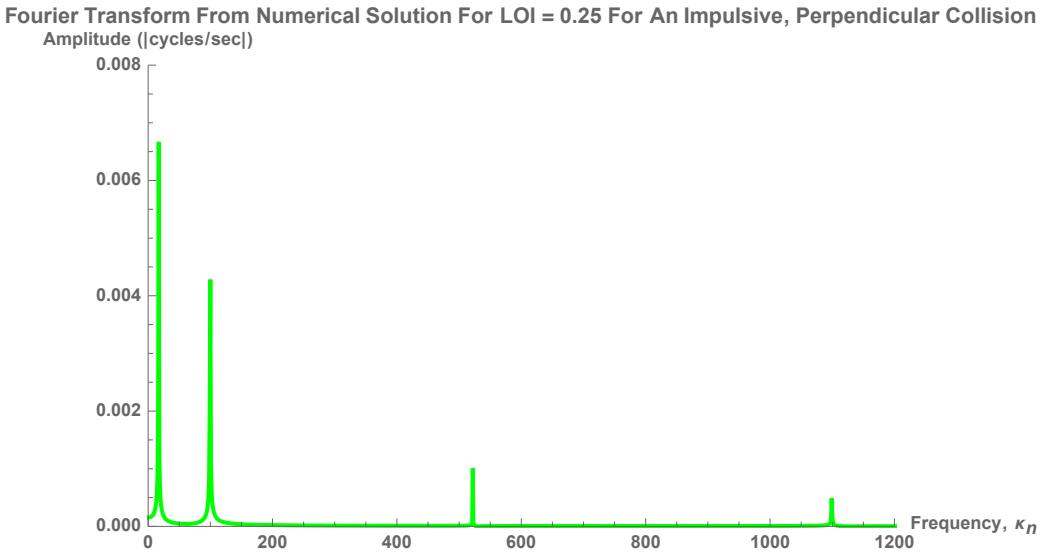

Figure 6.7: *The Fourier Transform for Location of Impact at the middle of the bat (at 0.25m) for an impulsive, perpendicular collision*

Note the significant changes in the values along both axes from Figure 6.3 to Figure 6.7.

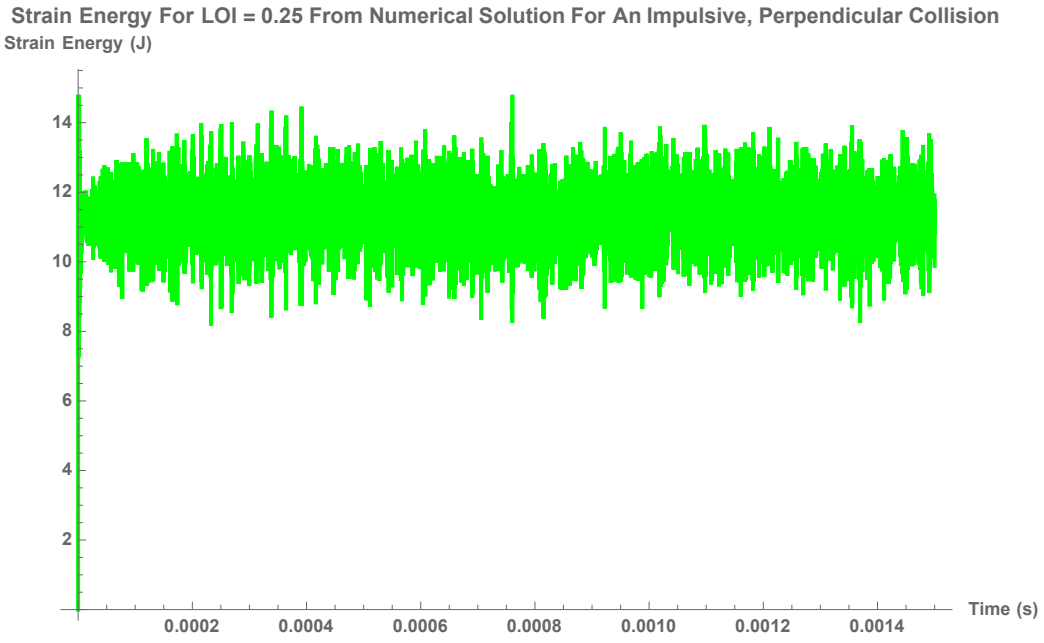

Figure 6.8: *The strain energy for Location of Impact at the middle of the bat (at 0.25m) for an impulsive, perpendicular collision*

6.2.3 Analysis for *Location of Impact* Near the Fixed-End of the Bat (at 0.05m)

Figures 6.9 through 6.12 below portray the results for the collision near the fixed-end of the bat.

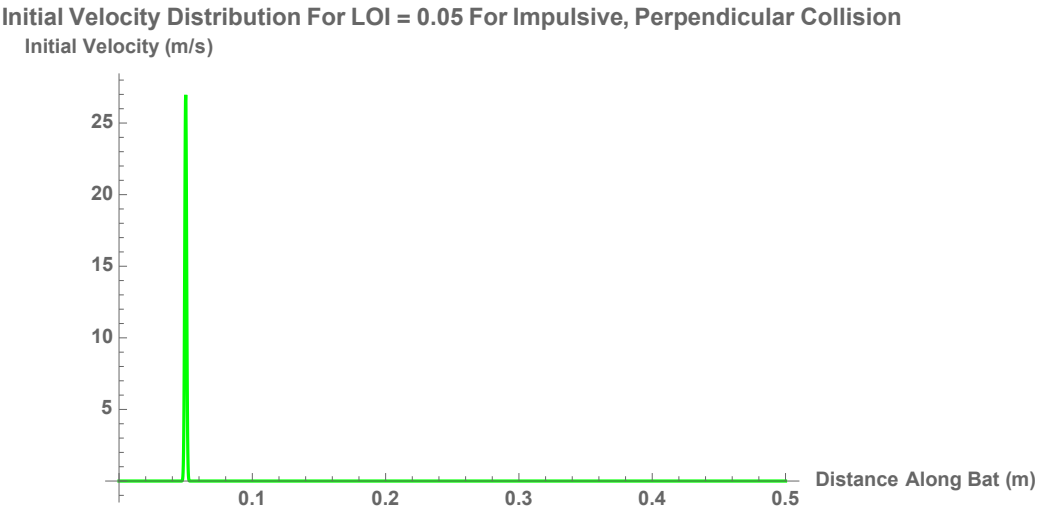

Figure 6.9: *The initial velocity distribution for Location of Impact near the fixed-end of the bat (0.05m) for an impulsive, perpendicular collision*

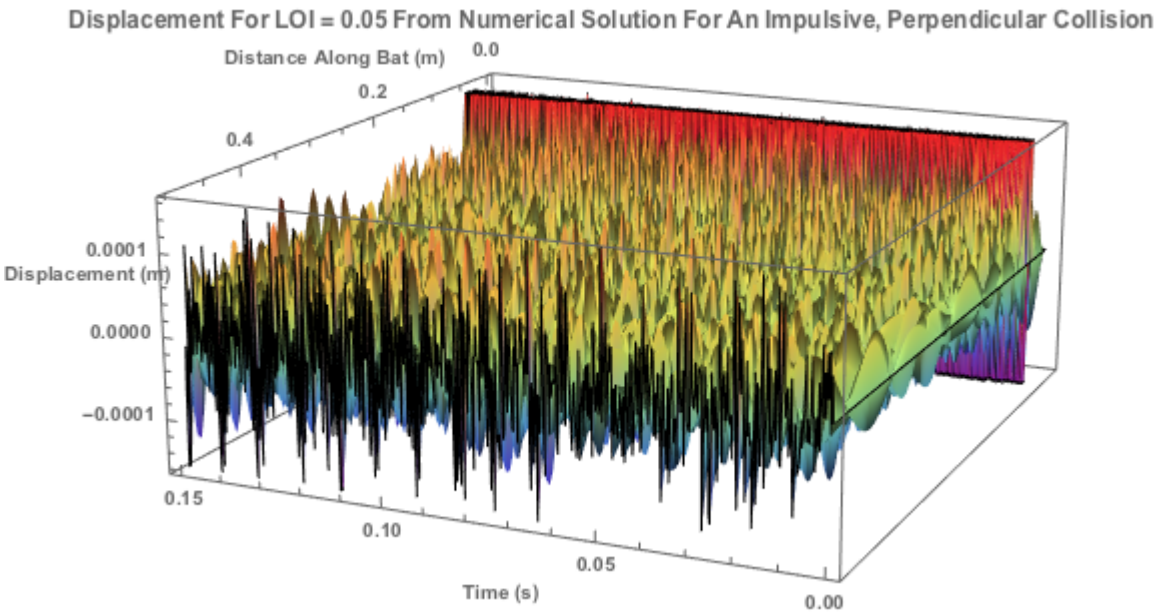

Figure 6.10: *The displacement solution for Location of Impact near the fixed-end of the bat (at 0.05m) for an impulsive, perpendicular collision*

As with the previous *Locations of Impact*, note the spike in the displacement at the *Location of Impact* from Figure 6.10 that results from the impulsive collision. This plot clearly shows the limitations of modelling the impact between a cricket ball and cricket bat as an impulsive collision.

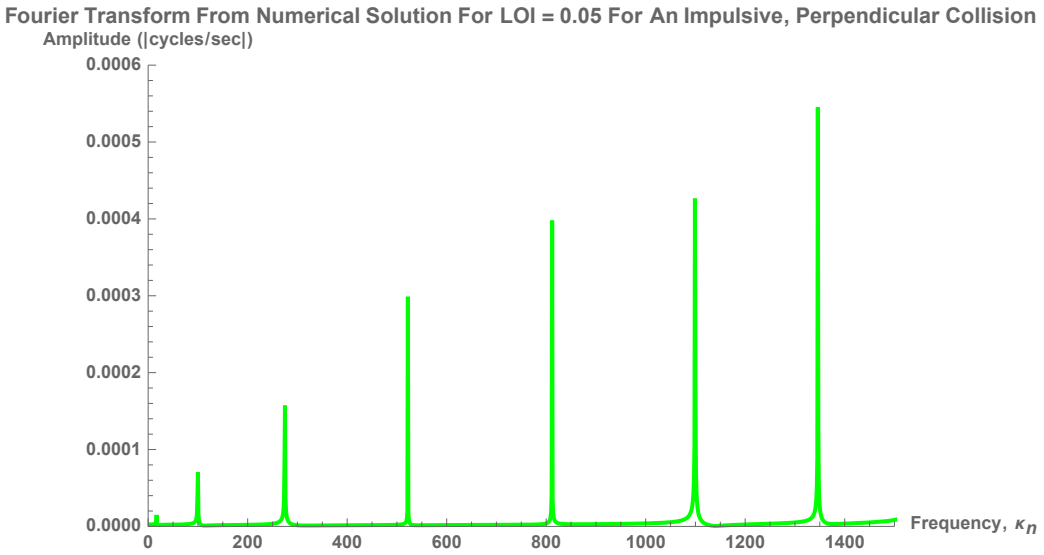

Figure 6.11: *The Fourier Transform for Location of Impact near the fixed-end of the bat (at 0.05m) for an impulsive, perpendicular collision*

Once again, note the significant changes in the values along both axes from Figures 6.3 and 6.7 to Figure 6.11.

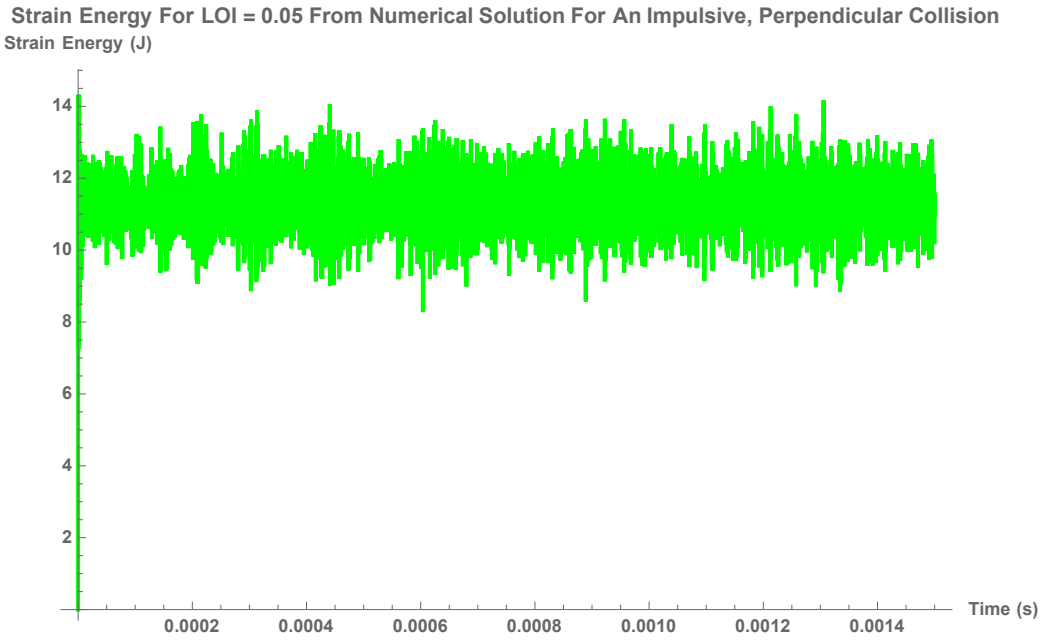

Figure 6.12: *The strain energy for Location of Impact near the free-end of the bat (at 0.05m) for an impulsive, perpendicular collision*

6.2.4 Discussion for Scenario where Collision is Impulsive and Perpendicular

Due to the characteristics of this scenario, the collision between bat and ball is not accurately modelled. These results of the model hence independently hold little value to the overall analysis and will only be used to support the more detailed and in-depth results found later in this work.

In particular, the displacement solutions from this scenario show the inadequacy of modelling a collision between a cricket bat and a cricket ball as an impulsive impact. As can be seen from Figures 6.2, 6.6 and 6.10, the relevant *Location of Impact* is displaced disproportionately compared to the other points on the bat due to the impulsive nature of the impact. It is reasoned that because the impulsive force of the collision is entirely focused at the relevant *Location of Impact*, the displacement of the *Location of Impact* is grossly exaggerated from a realistic value and is hence not accurately modelled throughout the time period.

Although the accuracy of the results in this scenario are somewhat suspect due to the impulsive impact of the ball on the bat, the scenario does serve some purpose in the sense that it introduces the basic behaviour of the model. For a *Location of Impact* near the free-end of the bat, the resultant displacement over time is large, causing a powerful, dominant signal to travel the length of the bat. For a *Location of Impact* at the middle of the bat, the displacement is considerably smaller. The frequencies present for this *Location of Impact* are not as powerful nor as dominant. The trend continues for a *Location of Impact* near the fixed-end of the bat where the displacement is the smallest out of the three *Locations of Impact*. Further, the amplitudes of the frequencies corresponding to this *Location of Impact* are very small and the high frequencies are present with no truly dominant frequency.

The strain energy in the bat for all three *Locations of Impact* is very similar over the time period from 0 seconds to 0.0015 seconds. In the numerical solution, it is necessary to calculate the strain energy over such a small time period in order to allow for the implementation of a fine spatial grid that will enable the three-point stencil to adequately capture the sharp curvature experienced in the bat. However, the fine grid used results in high computation cost and so a shorter time period must be used than when calculating the displacement solution.

The strain energy in the bat is similar across all three *Locations of Impact* after collision between the bat and the ball. This is reasonable since the ball is striking the bat with the same velocity at each *Location of Impact*. Therefore, the same amount of energy is imparted into the bat after the collision regardless of the *Location of Impact*. Across all *Locations of Impact*,

there was originally zero strain energy in the bat. Immediately post-impact with the ball, the numerical solution captures the expected jump in strain energy. Further, the strain energy in the bat remains constant over time since the model holds zero dissipative properties and no additional energy is entering into the system.

This scenario serves as a good base case for an extension into the following two scenarios, where the ball is modelled to compress against the bat during the collision. However, it is clear that because of the unrealistic displacement behaviours of the *Locations of Impact* under an impulsive impact, a collision between cricket bat and ball should not be modelled in this way.

6.3 Analyzing The Results For An Elastic, Perpendicular Collision - Scenario 2

The analysis now moves to the scenario where the ball is modelled to have compressed against the cricket bat during a perpendicular collision, and the force of the ball impacting the cricket bat actually causes the initial velocity distribution in the bat. The process of finding the initial velocity distribution was discussed in Chapter 3.3.2, and the process is implemented in `Mathematica`.

Both the analytical solution (Separation of Variables - Chapter 5) and numerical solution (Crank-Nicolson - Chapter 4) are used in this scenario and the results from each of the solutions will be compared. In this scenario, the analytical solution $y(x,t)$ is calculated using the first 50 eigenvalues of the series solution. This was found to provide sufficient accuracy.

6.3.1 Analysis for *Location of Impact* Near the Free-End of the Bat (at 0.45m)

Figures 6.13 through 6.21 below portray the results for the collision near the free-end of the bat.

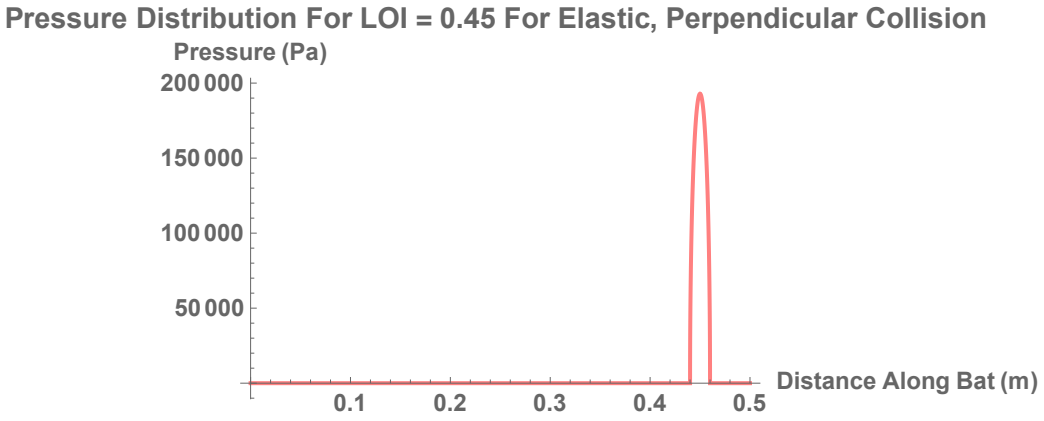

Figure 6.13: *The presure distribution caused by the ball impacting the bat for Location of Impact near the free-end of the bat (0.45m) for an elastic, perpendicular collision*

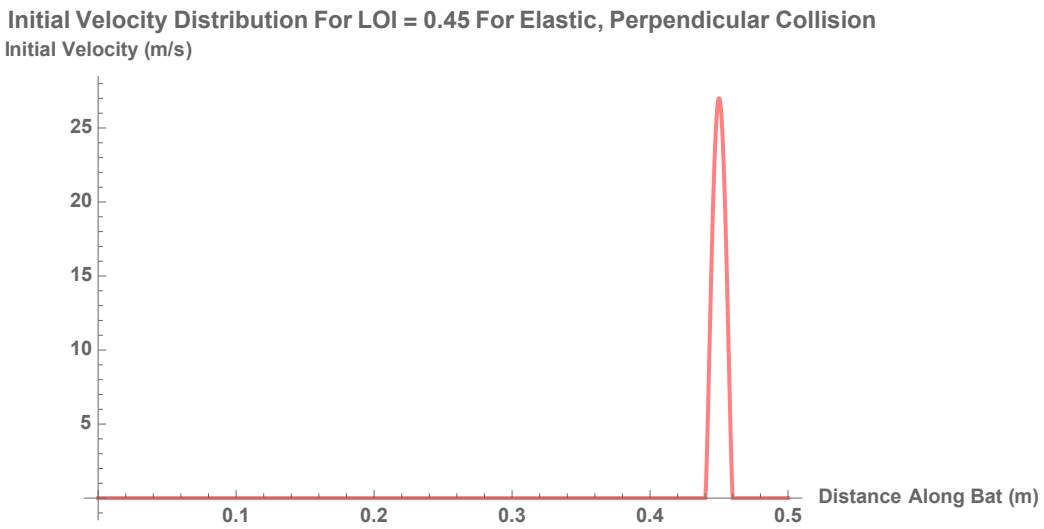

Figure 6.14: *The initial velocity distribution for Location of Impact near the free-end of the bat (0.45m) for an elastic, perpendicular collision*

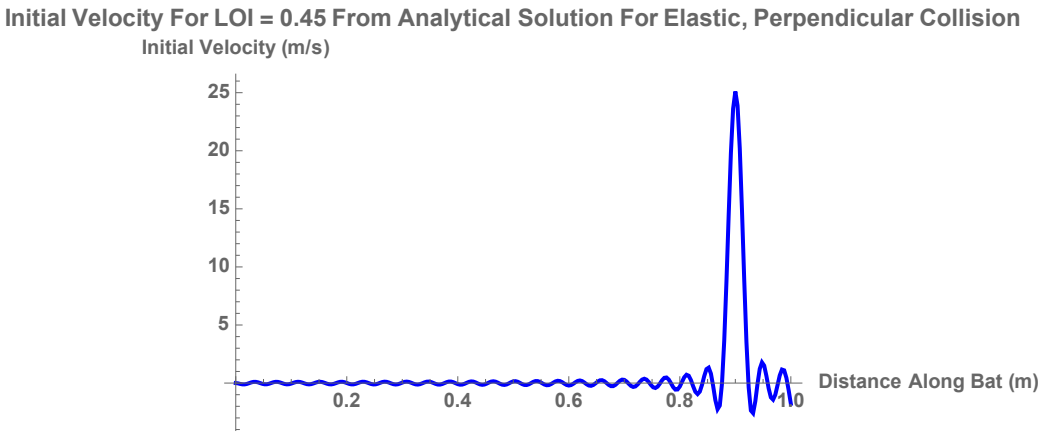

Figure 6.15: *The initial velocity distribution as derived from the analytical solution and as used in the numerical solution for Location of Impact near the free-end of the bat (0.45m) for an elastic, perpendicular collision*

It is reasoned that the tiny fluctuations around the horizontal axis in Figure 6.15 are a result of the infinite sum being approximated to the first 50 terms. Importantly, as it is suggested by Figure 6.15, the relevant initial velocity distribution that is used in the numerical solution for each *Location of Impact* is well defined by the analytical solution $y(x,t)$ by finding $y_t(x,0)$.

Note that the pressure distributions, the analytical initial velocity distribu-

tions and initial velocity distributions used in the numerical solution for the *Locations of Impact* at the middle of the bat and near the fixed-end of the bat behave similarly to what are shown in Figures 6.13, 6.14 and 6.15.

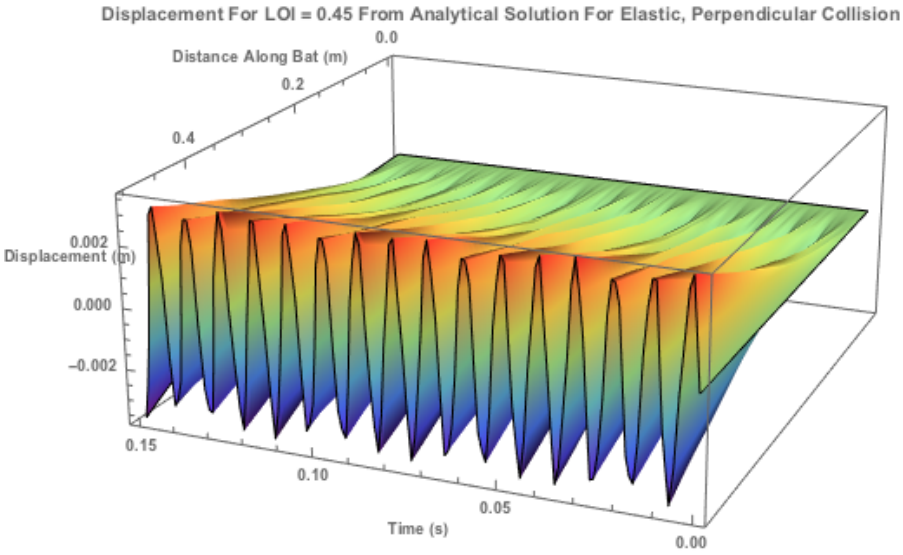

Figure 6.16: *The displacement profile from analytical solution for Location of Impact near the free-end of the bat (at 0.45m) for an elastic, perpendicular collision*

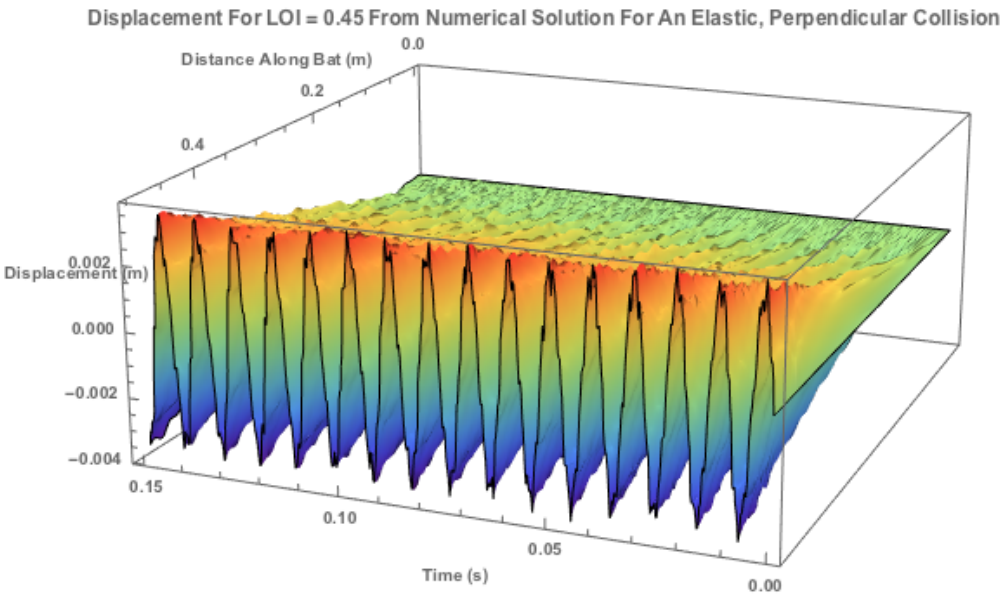

Figure 6.17: *The displacement profile from numerical solution for Location of Impact near the free-end of the bat (at 0.45m) for an elastic, perpendicular collision*

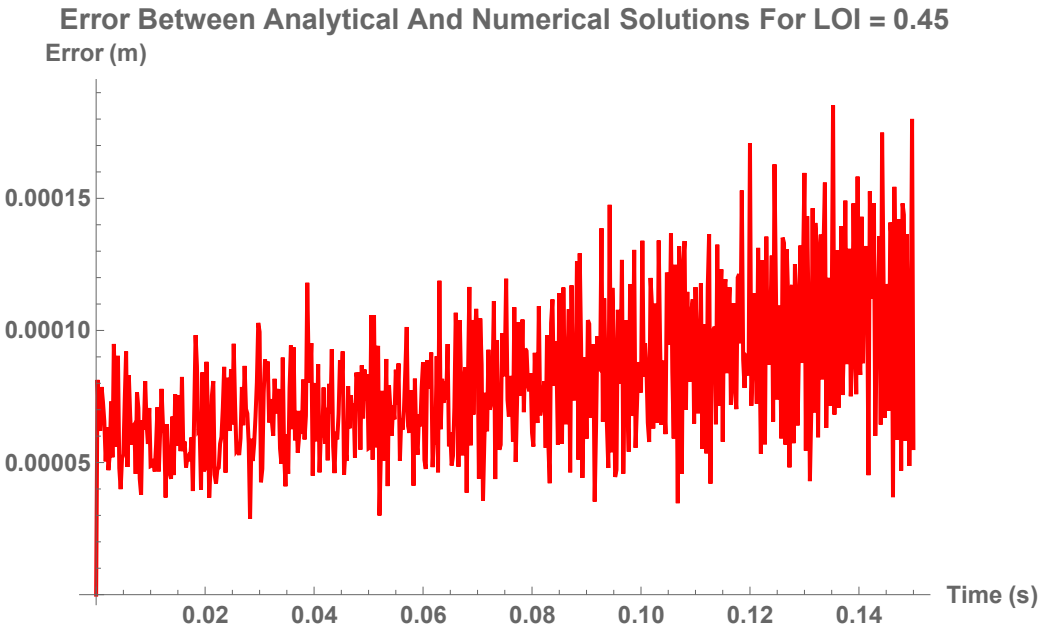

Figure 6.18: *The error between the analytical solution and the numerical solution for Location of Impact near the free-end of the bat (at 0.45m) for an elastic, perpendicular collision*

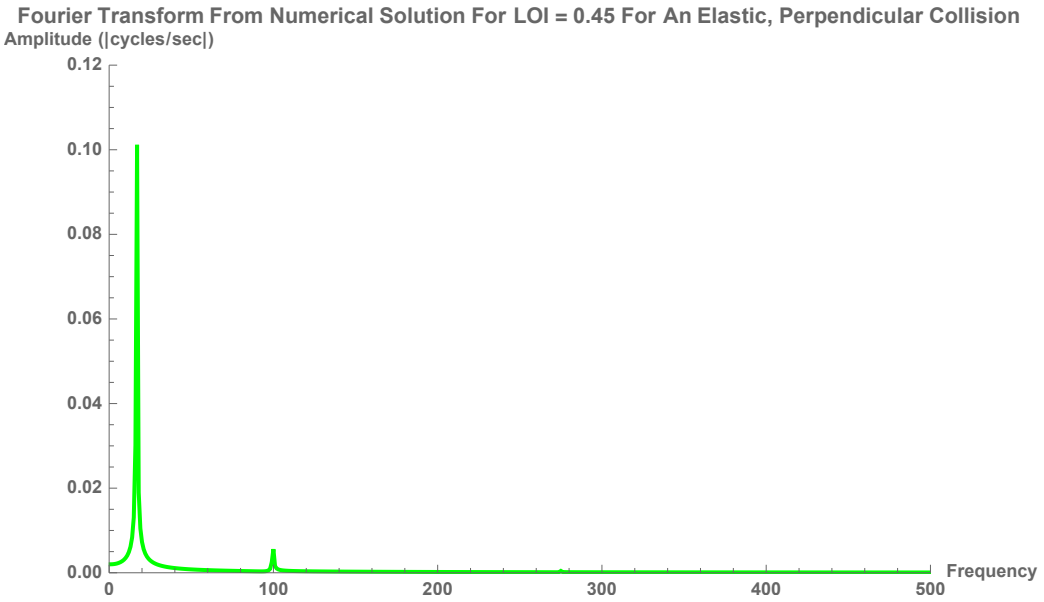

Figure 6.19: *The Fourier Transform from the numerical solution for Location of Impact near the free-end of the bat (at 0.45m) for an elastic, perpendicular collision*

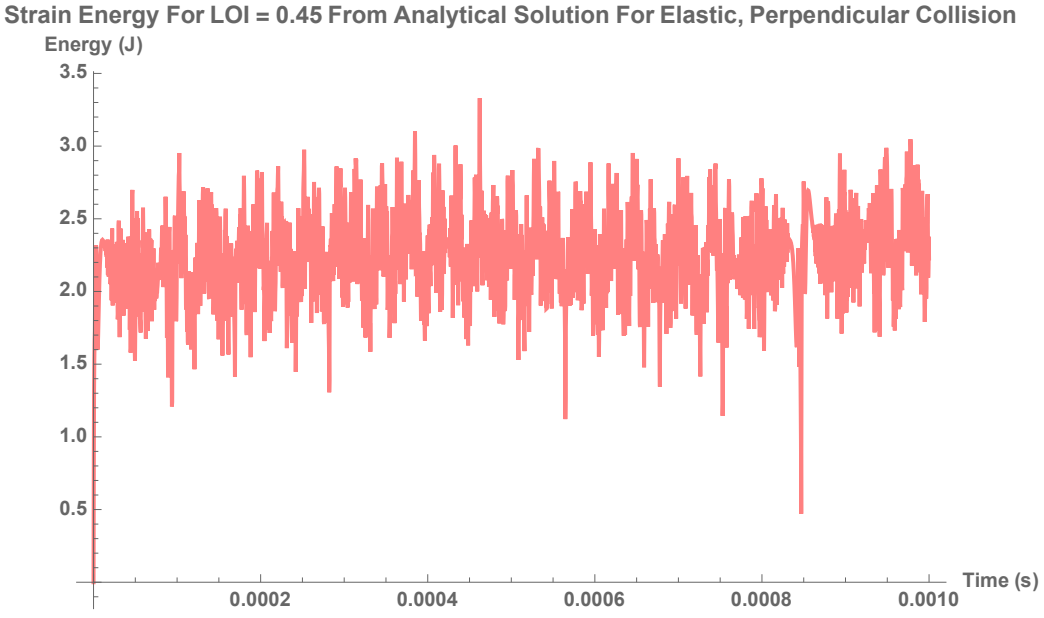

Figure 6.20: *The strain energy over the short time period from the analytical solution to be compared to the numerical solution for Location of Impact near the free-end of the bat (at 0.45m) for an elastic, perpendicular collision*

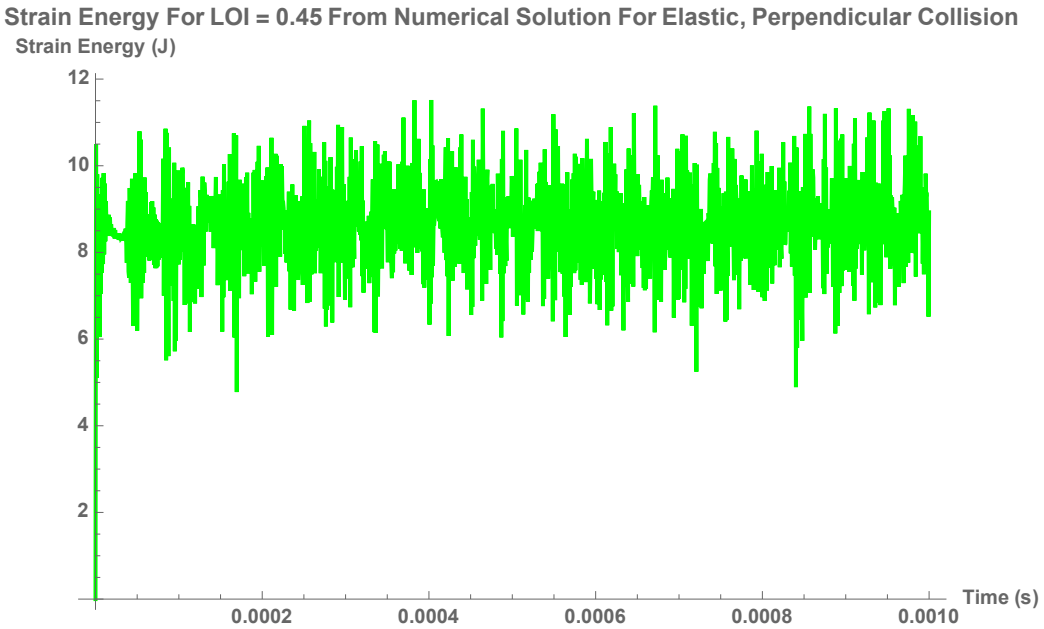

Figure 6.21: *The strain energy over the short time period from the numerical solution to be compared to the analytical solution for Location of Impact near the free-end of the bat (at 0.45m) for an elastic, perpendicular collision*

6.3.2 Analysis for *Location of Impact* at the Middle of the Bat (at 0.25m)

Figures 6.22 through 6.26 below portray the results for the collision at the middle of the bat.

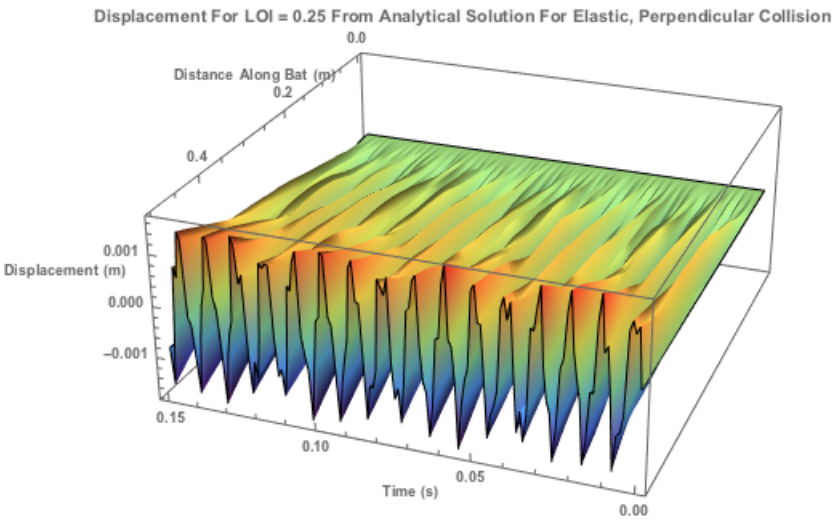

Figure 6.22: *The displacement profile from analytical solution for Location of Impact at the middle of the bat of the bat (at 0.25m) for an elastic, perpendicular collision*

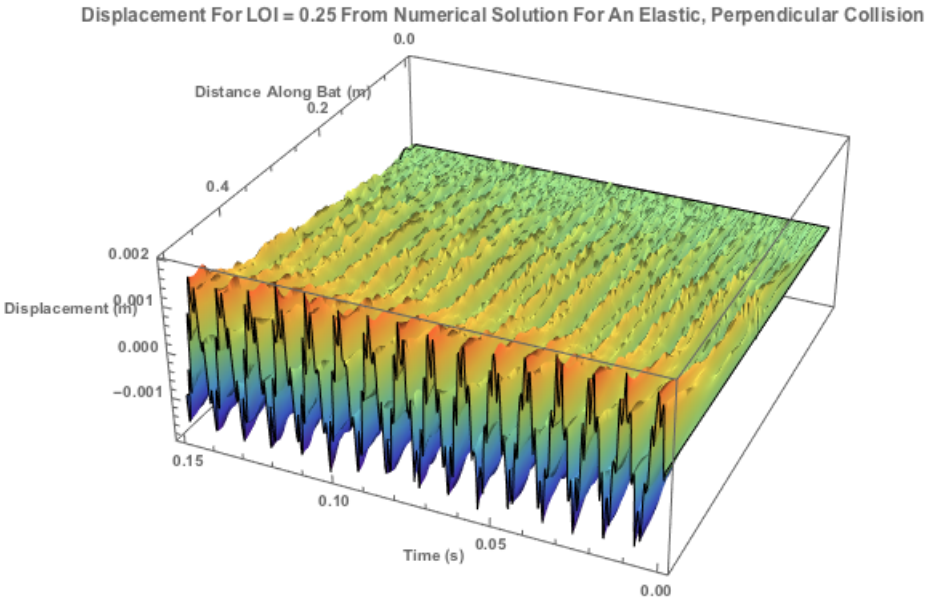

Figure 6.23: *The displacement profile from numerical solution for Location of Impact at the middle of the bat of the bat (at 0.25m) for an elastic, perpendicular collision*

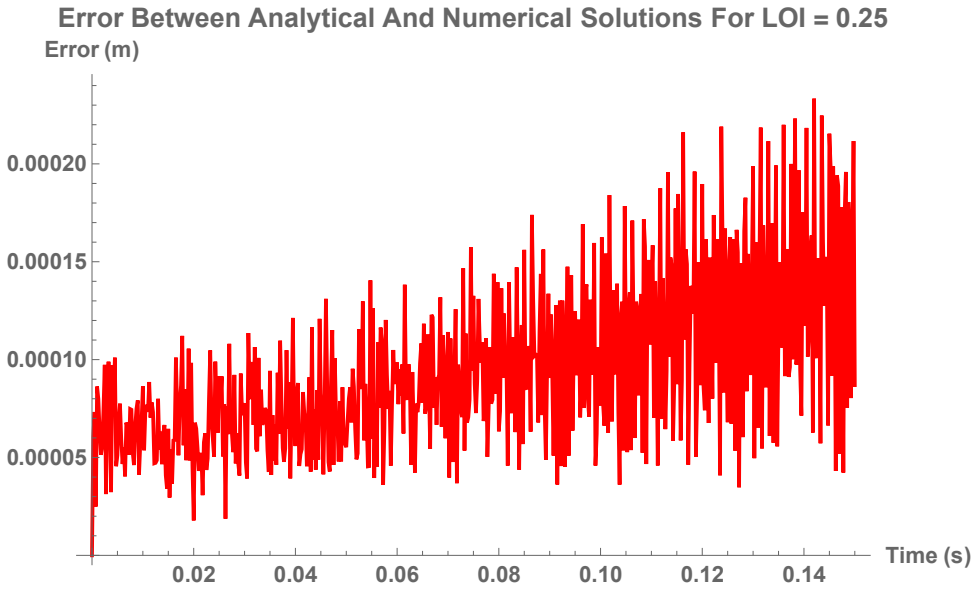

Figure 6.24: *The error between the analytical solution and the numerical solution for Location of Impact at the middle of the bat of the bat (at 0.25m) for an elastic, perpendicular collision*

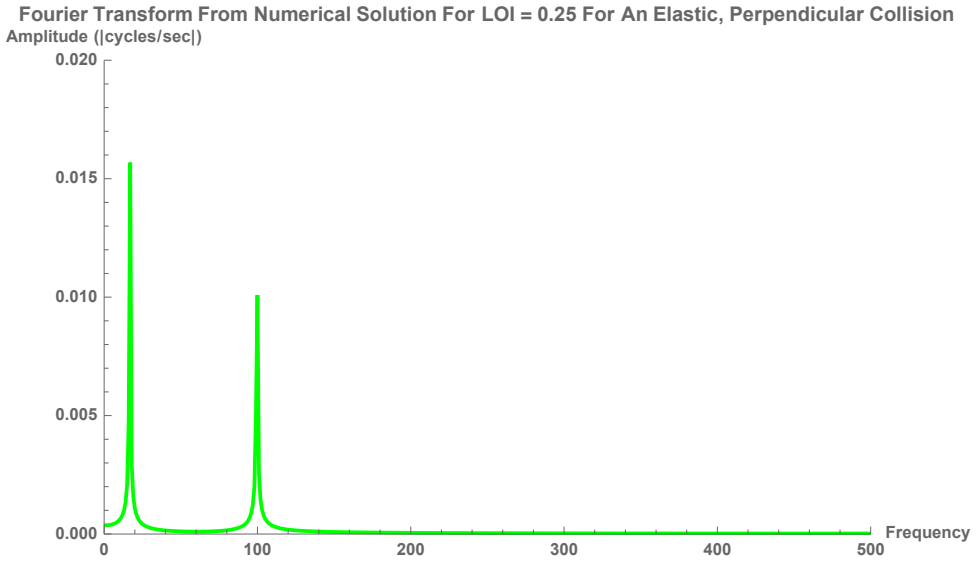

Figure 6.25: *The Fourier Transform from the numerical solution for Location of Impact at the middle of the bat of the bat (at 0.25m) for an elastic, perpendicular collision*

It is important to note the changes in the scales of the axes from Figure 6.19

to Figure 6.25.

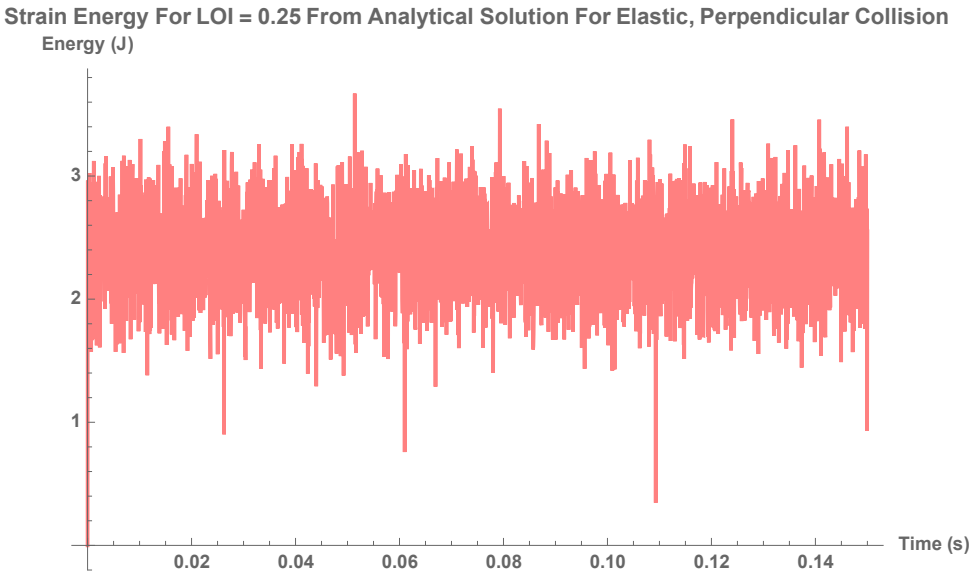

Figure 6.26: *The strain energy over the entire time period from the analytical solution for Location of Impact at the middle of the bat of the bat (at 0.25m) for an elastic, perpendicular collision*

6.3.3 Analysis for *Location of Impact* near the Fixed-End of the Bat (at 0.05m)

Figures 6.27 through 6.31 below portray the results for the collision near the fixed-end of the bat.

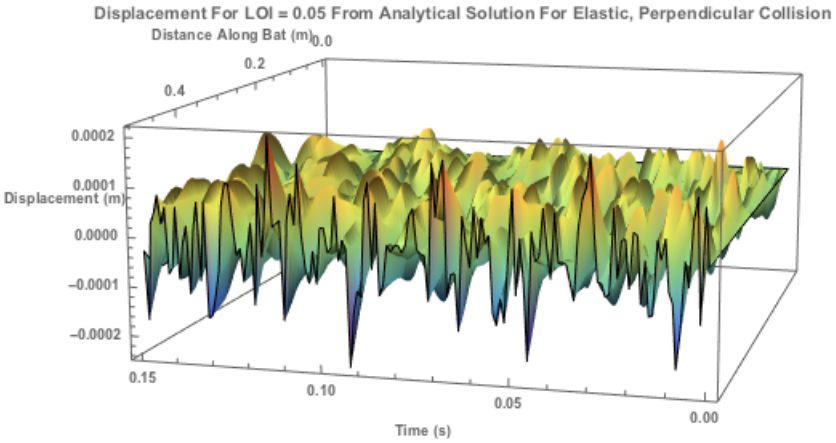

Figure 6.27: *The displacement profile from analytical solution for Location of Impact near the fixed-end of the bat of the bat (at 0.05m) for an elastic, perpendicular collision*

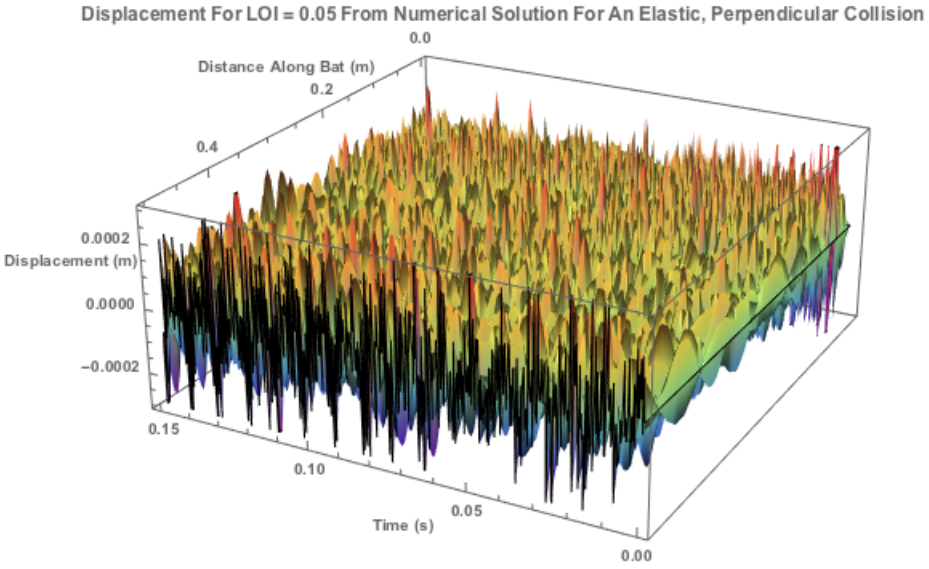

Figure 6.28: *The displacement profile from numerical solution for Location of Impact near the fixed-end of the bat of the bat (at 0.05m) for an elastic, perpendicular collision*

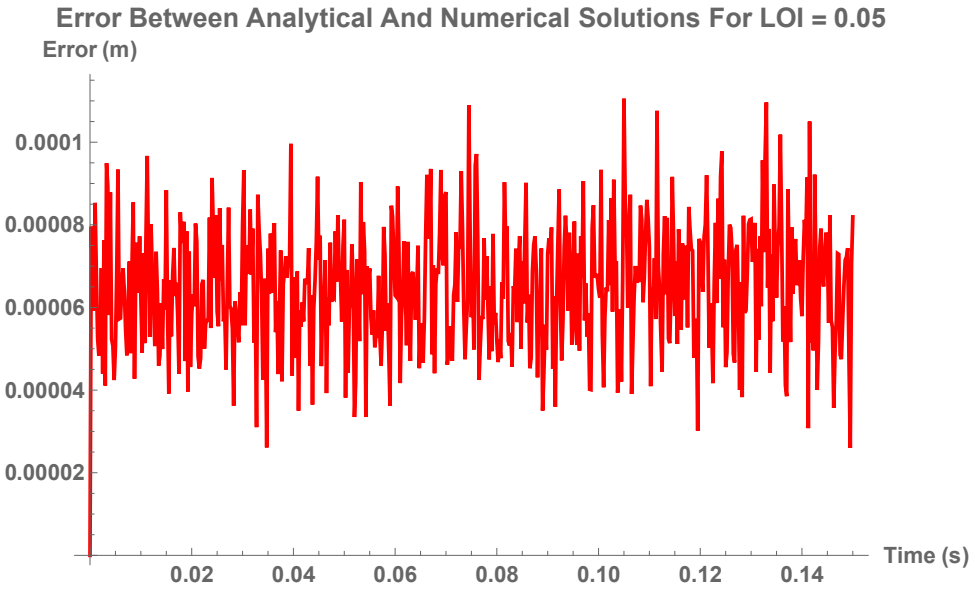

Figure 6.29: *The error between the analytical solution and the numerical solution for Location of Impact near the fixed-end of the bat of the bat (at 0.05m) for an elastic, perpendicular collision*

Figure 6.29 shows that the absolute error between the two solutions is in agreement with the theoretical bound (from the Taylor Series truncation for a finite difference approximation). However, since the values of the displacement are small, it is important to note that the relative error is large.

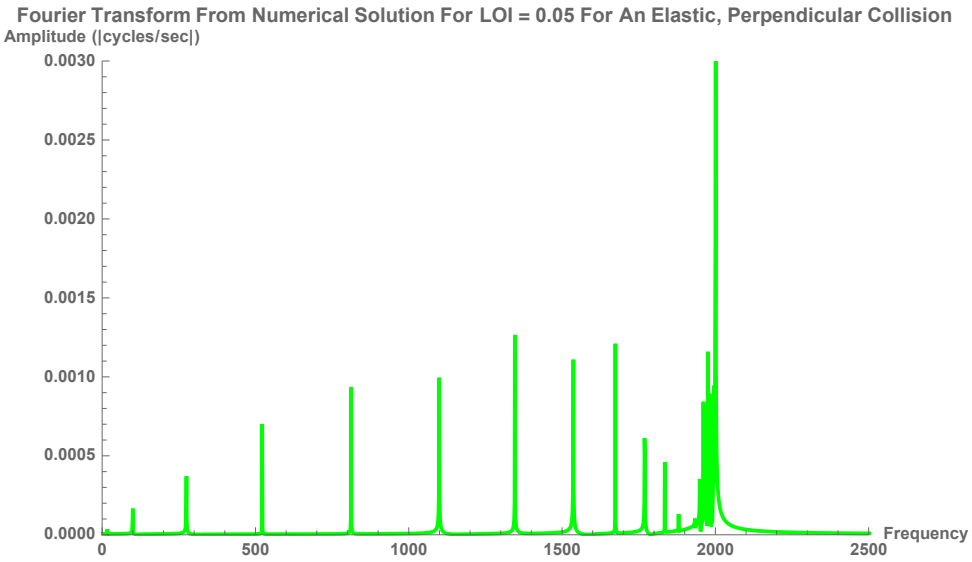

Figure 6.30: *The Fourier Transform from the numerical solution for Location of Impact near the fixed-end of the bat of the bat (at 0.05m) for an elastic, perpendicular collision*

Once again, it is important to note the changes in the scales of the axes from Figures 6.19 and 6.25 to 6.30.

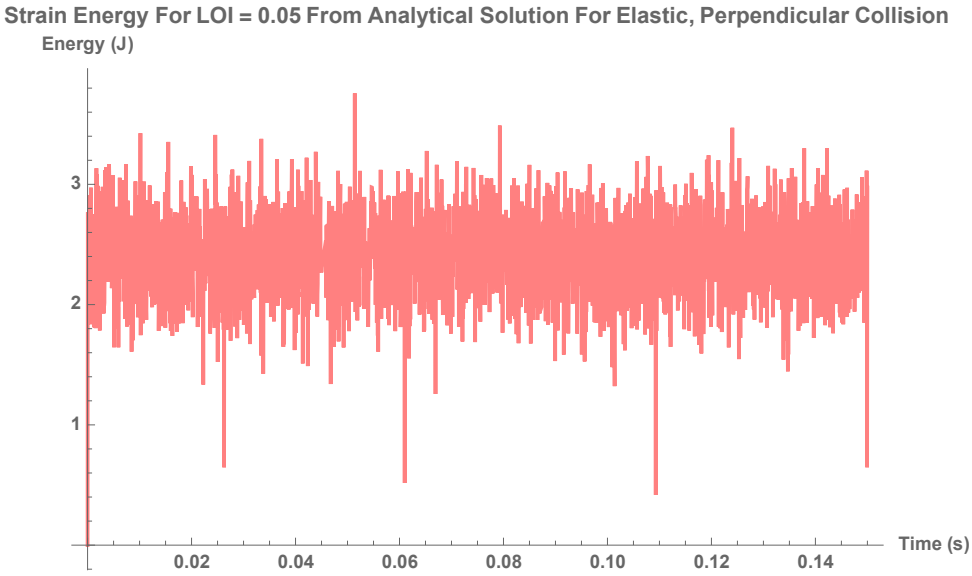

Figure 6.31: *The strain energy over the entire time period from the analytical solution for Location of Impact near the fixed-end of the bat of the bat (at 0.05m) for an elastic, perpendicular collision*

6.3.4 Discussion for Scenario where Collision is Elastic and Perpendicular

The results from this scenario suggest that modelling a collision between a cricket bat and a cricket ball as an elastic, perpendicular impact is a much better approximation of reality than in the first scenario.

For each *Location of Impact* in this scenario, the pressure distribution is symmetric about the *Location of Impact* over the length of the contact zone on the bat. The pressure exerted by the ball on the bat is in the order of 200 kPa. The parameter p_0 is chosen in such a way as for the initial velocity of the *Location of Impact* to be at most 27 m/s. The initial velocity distributions themselves are also symmetric around the the *Location of Impact* over the length of the contact zone on the bat. The symmetry of the distributions is a result of the perpendicular collision.

Unlike the previous collision scenario, the displacement profiles portray no discernible spike at the *Locations of Impact*. It is argued that this is a result of the fact that the pressure from the impact modelled in this scenario is not focussed on a single point but is rather spread over the entire length of the contact zone.

The analysis from the Fourier Transform for the numerical solution supports the corresponding discussion from the previous collision scenario. Essentially, for a *Location of Impact* near the free-end of the bat, a powerful, dominant signal is produced. This signal has a low frequency and thus a large wavelength. The signal overpowers any smaller, weaker signals in the bat and hence produces a smooth displacement profile. As the *Location of Impact* moves closer to the handle of the bat, the dominance of a single signal in the bat becomes less and higher frequencies in the bat become relatively more powerful. This results in the less smooth displacement profiles.

Considering the strain energy calculated from the analytical solutions, the amount of this energy in the bat is very similar for the entire time period across all three *Locations of Impact* after the impact of the ball on the bat. As discussed for the previous collision scenario, this is reasonable since the ball is striking the bat with the same velocity at each *Location of Impact*. Therefore, the same amount of energy is imparted into the bat after the collision regardless of the *Location of Impact*. Across all *Locations of Impact*, there was originally zero strain energy in the bat. Immediately post-impact with the ball, the expected jump in strain energy is captured. Further, the strain energy in the bat remains constant over time since the model holds zero dissipative properties and no additional energy is entering into the system.

This collision scenario allows for the first opportunity for the results of the

analytical and numerical solutions to be compared. The analytical and numerical solutions for the displacement have been compared qualitatively and are found to be in agreement. That is, the general behaviour of the solutions have been considered and the shapes of the solutions are consistent for both the numerical and analytical approach. Further, the displacement solutions are compared quantitatively as discussed in Chapter 6.1.2. This comparison shows that the numerical approach is consistent and accurate. This can be can be seen in the error plots in Figures 6.18, 6.24 and 6.29.

The behaviour of the strain energy calculated by the numerical solution (Figure 6.21) is similar to the behaviour of the strain energy as calculated by the analytical solution (Figure 6.20) over the same time period. This holds true for all *Locations of Impact*. Both strain energy solutions model the behaviour of the strain energy in the bat over time as discussed above. It is not necessary to compare the strain energy solutions quantitatively because the strain energy was derived from the displacement solutions.

Both the analytical and numerical models are adequate for modelling this collision scenario; although it is conceded that the analytical solution is more adept at modelling the strain energy and the numerical solution is more adept for the frequency analysis through the use of a Fourier Transform.

6.4 Analyzing The Results For An Elastic, Oblique Collision - Scenario 3

The analysis now moves to the scenario where the ball is modelled to have compressed against the cricket bat during an oblique collision, and the force of the ball impacting the cricket bat once again causes the initial velocity distribution in the bat. The process of finding the initial velocity distribution in this collision scenario was discussed in Chapter 3.3.3, and the process is implemented in `Mathematica`.

As with the previous collision scenario, both the analytical solution (Separation of Variables - Chapter 5) and numerical solution (Crank-Nicolson scheme - Chapter 4) are used in this collision scenario and the results from each of the solutions will be compared. In this scenario, the analytical series solution $y(x,t)$ is calculated using the first 50 eigenvalues.

The 'angle of incidence' θ between the bat and the ball is taken to be $-\frac{\pi}{6}$ radians ($-30°$). This models the batsman hitting the ball 'on-the-up' in an aggressive manner.

6.4.1 Analysis for *Location of Impact* near the Free-End of the Bat (at 0.45m)

Figures 6.32 through 6.40 below portray the results for the collision near the free-end of the bat.

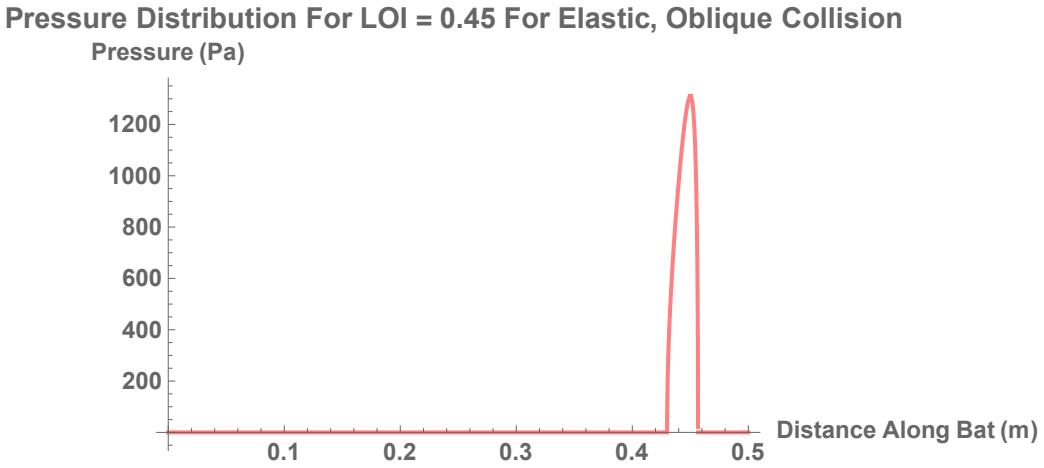

Figure 6.32: *The presure distribution caused by the ball impacting the bat for Location of Impact near the free-end of the bat (0.45m) for an elastic, oblique collision*

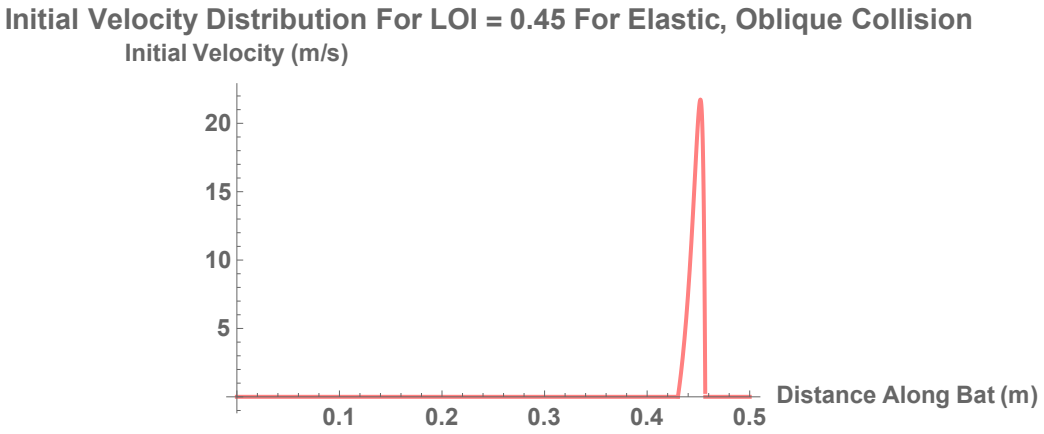

Figure 6.33: *The initial velocity distribution for Location of Impact near the free-end of the bat (0.45m) for an elastic, oblique collision*

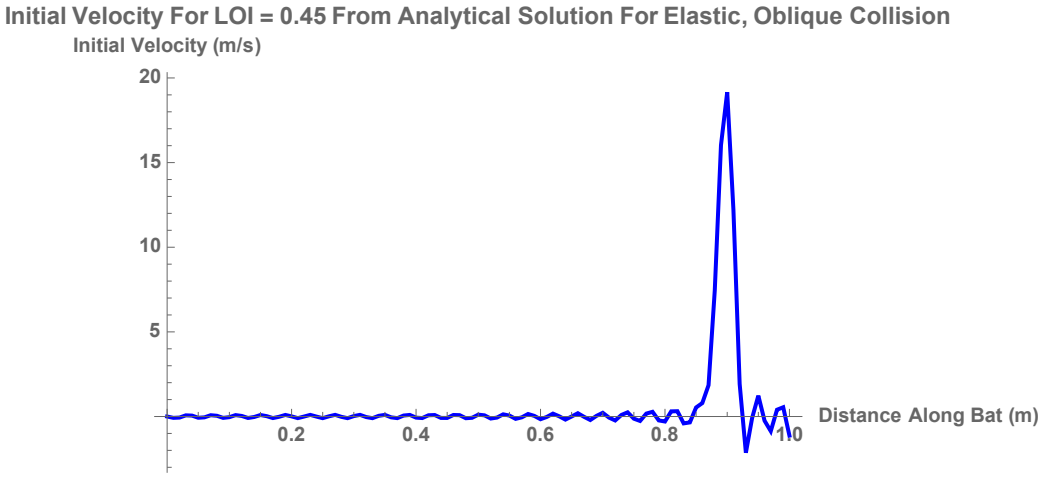

Figure 6.34: *The initial velocity distribution as derived from the analytical solution and as used in the numerical solution for Location of Impact near the free-end of the bat (0.45m) for an elastic, oblique collision*

As with the previous collision scenario, it is reasoned that the tiny fluctuations around the horizontal axis in Figure 6.34 are a result of the infinite sum being approximated to the first 50 terms. Similarly to as argued before, it is suggested by Figure 6.34 that the relevant initial velocity distribution which is used in the numerical solution for each *Location of Impact* is well defined by the analytical solution $y(x,t)$ by finding $y_t(x,0)$.

Once again note that the pressure distributions, the analytical initial velocity distributions and initial velocity distributions used in the numerical solution

for the *Locations of Impact* at the middle of the bat and near the fixed-end of the bat behave similarly to what are shown in Figures 6.32, 6.33 and 6.34.

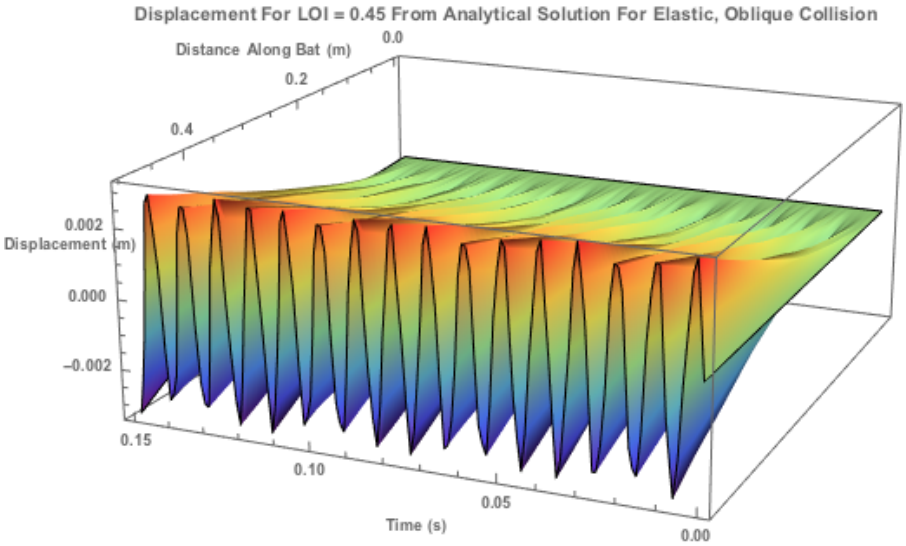

Figure 6.35: *The displacement profile from analytical solution for Location of Impact near the free-end of the bat (at 0.45m) for an elastic, oblique collision*

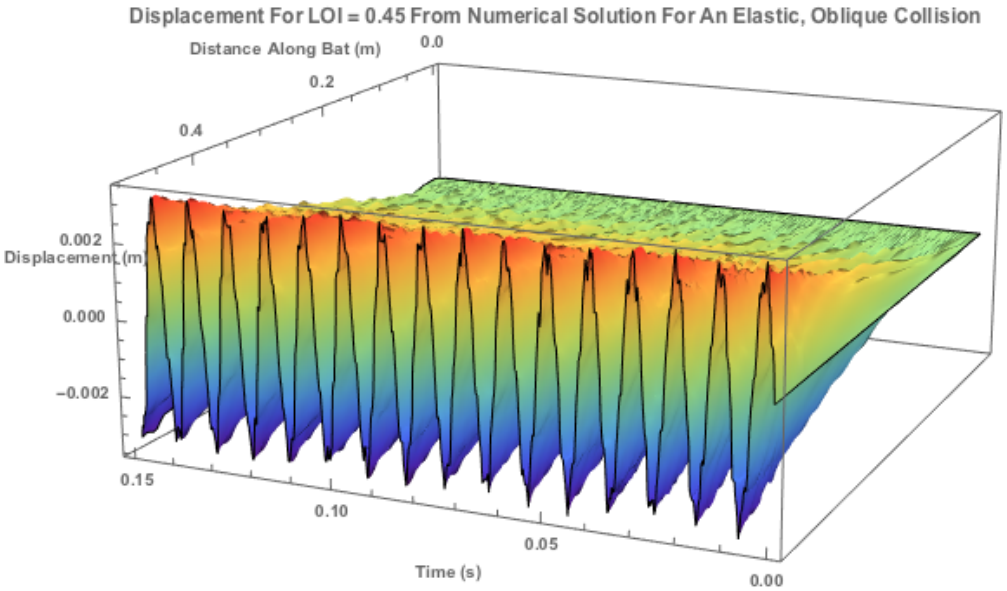

Figure 6.36: *The displacement profile from numerical solution for Location of Impact near the free-end of the bat (at 0.45m) for an elastic, oblique collision*

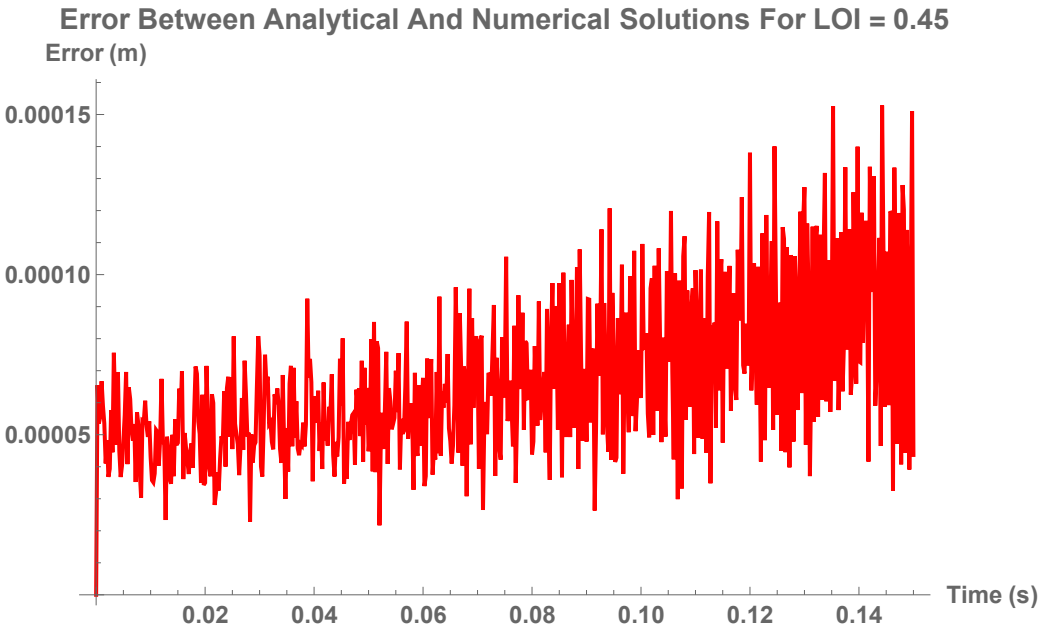

Figure 6.37: *The error between the analytical solution and the numerical solution for Location of Impact near the free-end of the bat (at 0.45m) for an elastic, oblique collision*

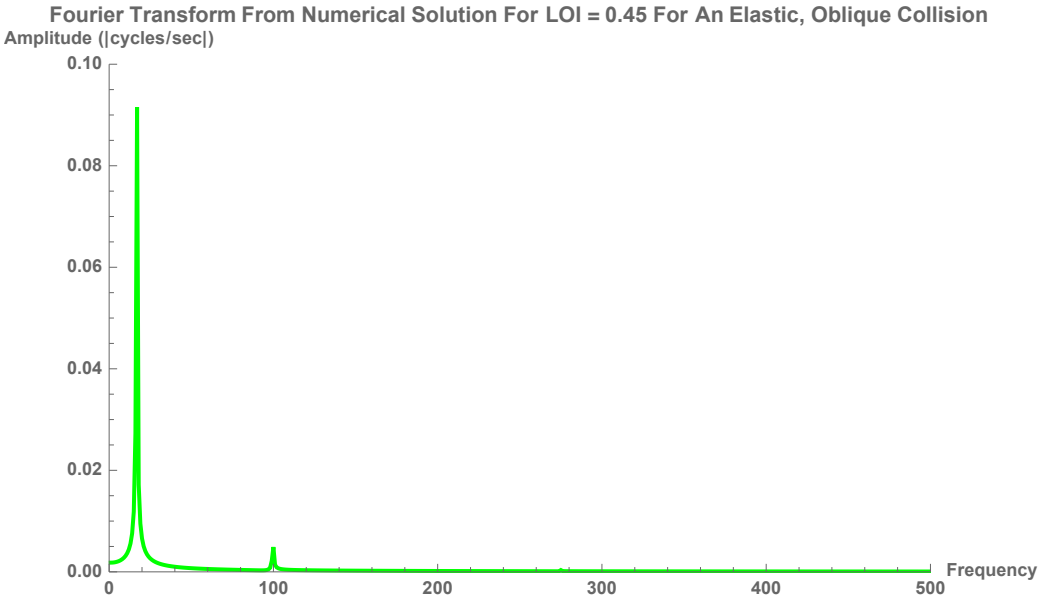

Figure 6.38: *The Fourier Transform from the numerical solution for Location of Impact near the free-end of the bat (at 0.45m) for an elastic, oblique collision*

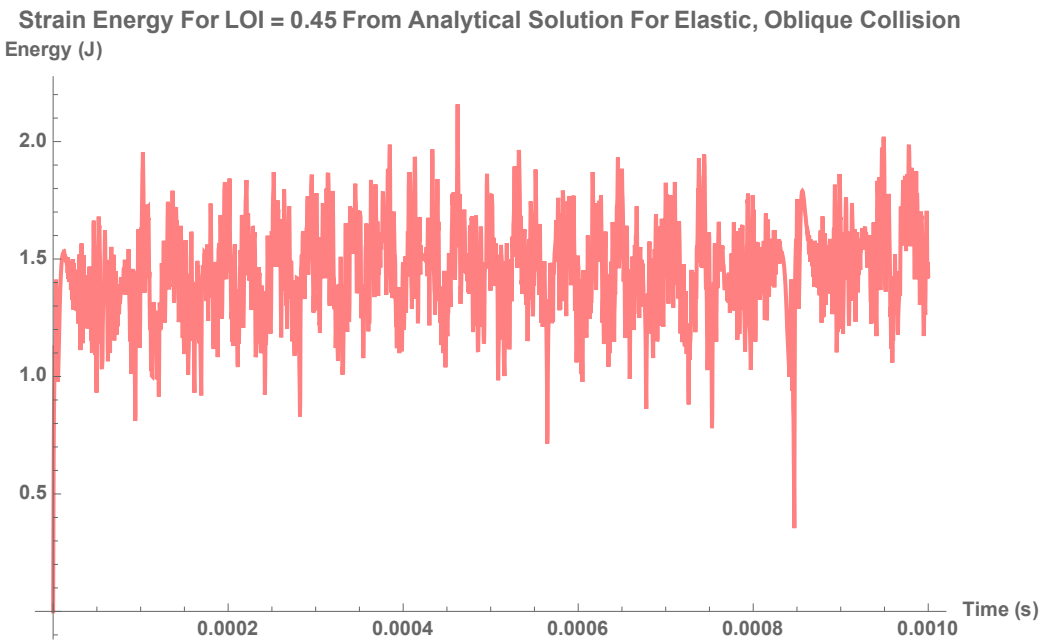

Figure 6.39: *The strain energy over the short time period from the analytical solution to be compared to the numerical solution for Location of Impact near the free-end of the bat (at 0.45m) for an elastic, oblique collision*

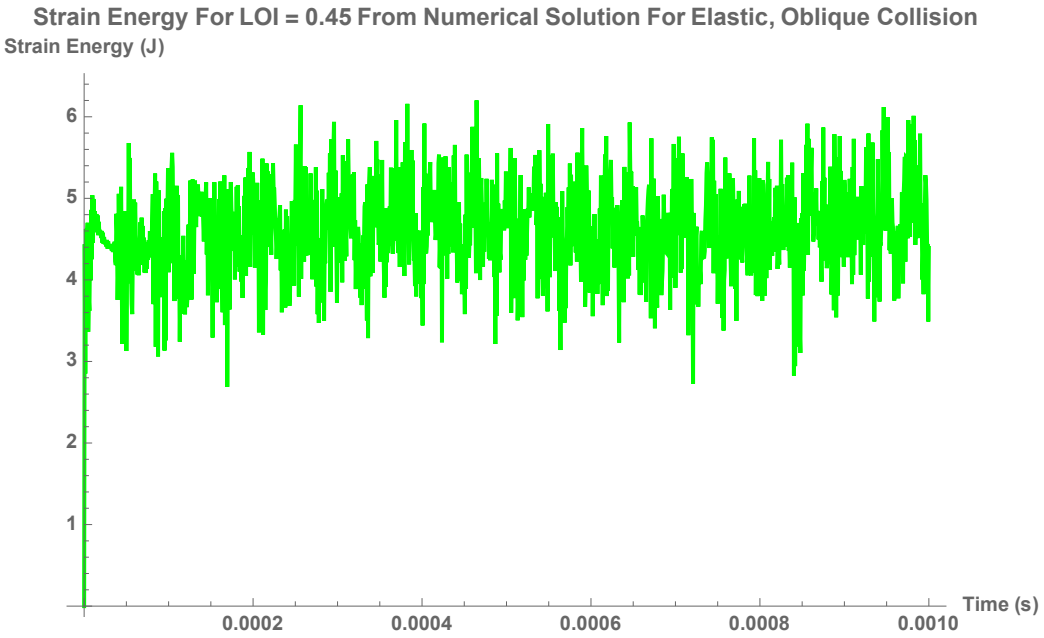

Figure 6.40: *The strain energy over the short time period from the numerical solution to be compared to the analytical solution for Location of Impact near the free-end of the bat (at 0.45m) for an elastic, oblique collision*

6.4.2 Analysis for *Location of Impact* at the Middle of the Bat (at 0.25m)

Figures 6.41 through 6.45 below portray the results for the collision at the middle of the bat.

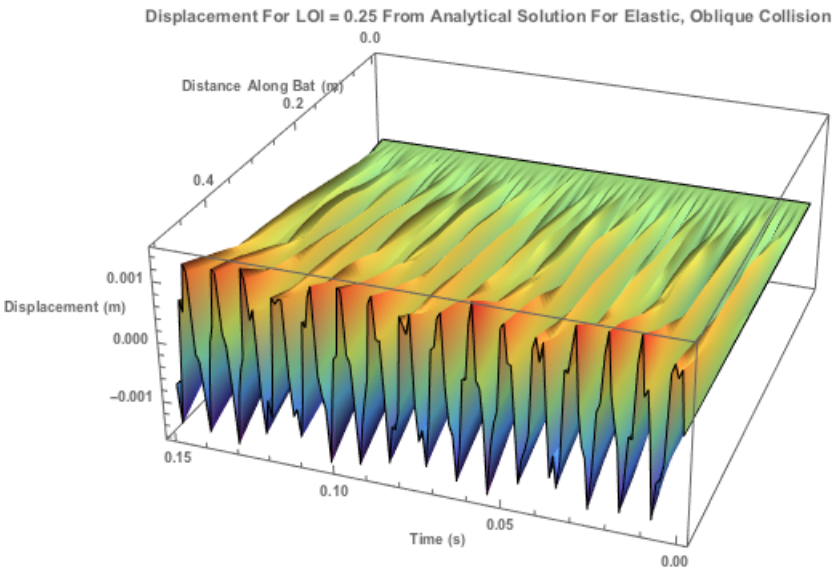

Figure 6.41: *The displacement profile from analytical solution for Location of Impact at the middle of the bat of the bat (at 0.25m) for an elastic, oblique collision*

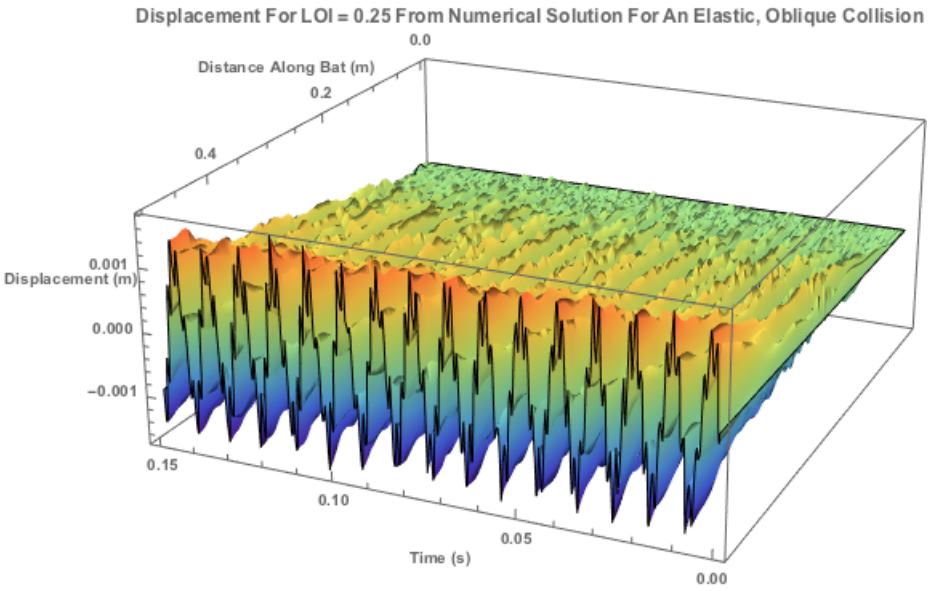

Figure 6.42: *The displacement profile from numerical solution for Location of Impact at the middle of the bat of the bat (at 0.25m) for an elastic, oblique collision*

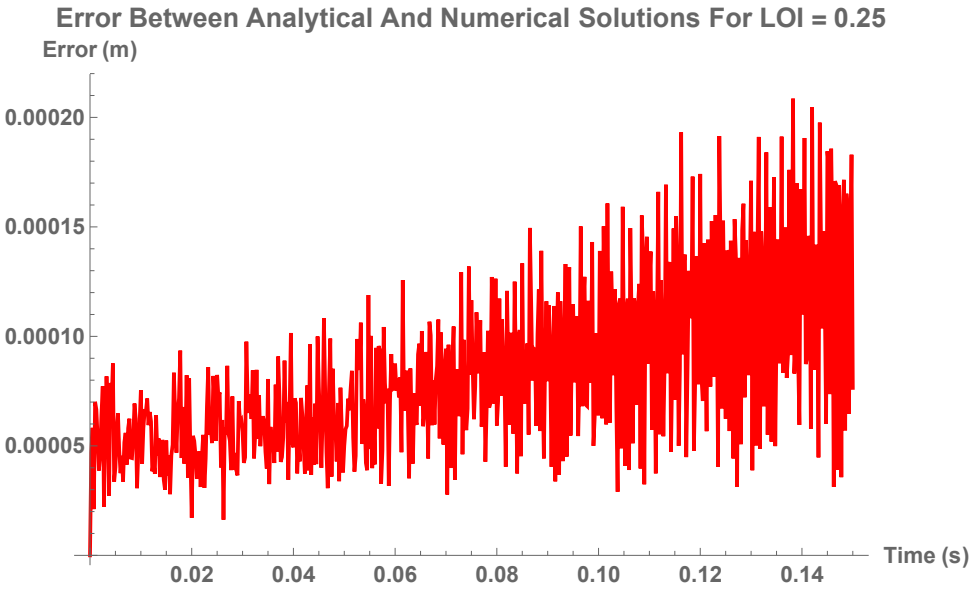

Figure 6.43: *The error between the analytical solution and the numerical solution for Location of Impact at the middle of the bat of the bat (at 0.25m) for an elastic, oblique collision*

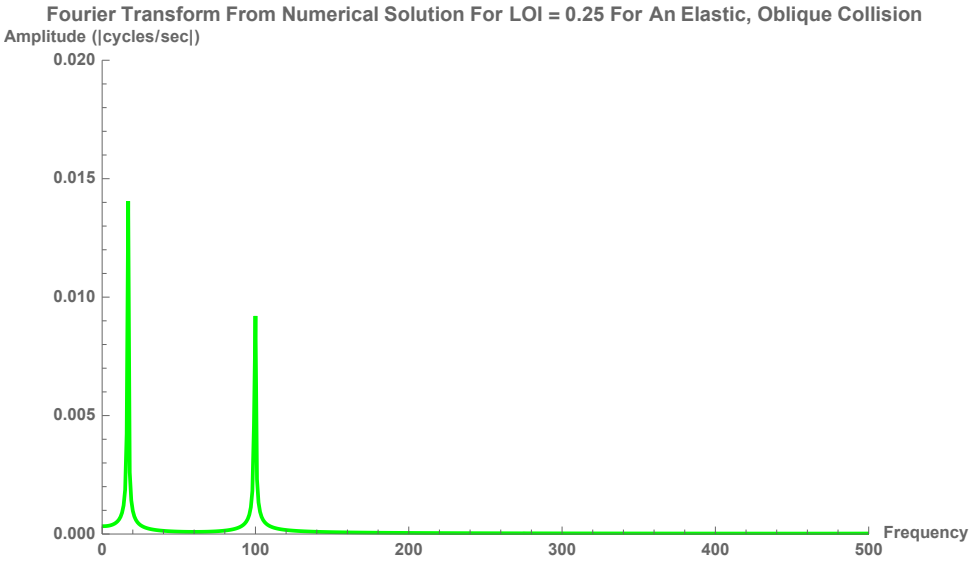

Figure 6.44: *The Fourier Transform from the numerical solution for Location of Impact at the middle of the bat of the bat (at 0.25m) for an elastic, oblique collision*

It is important to note the changes in the scales of the axes from Figure 6.38

to Figure 6.44.

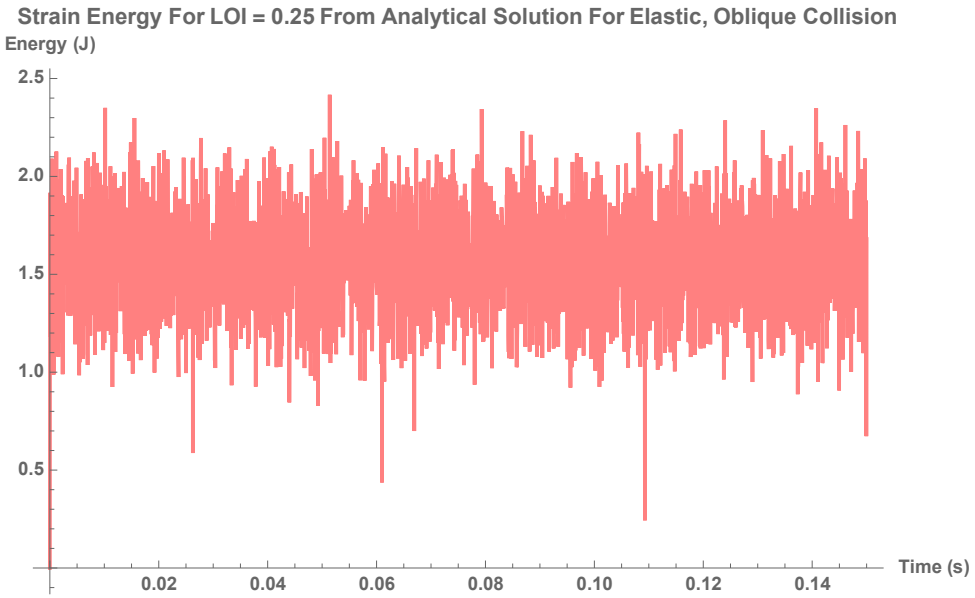

Figure 6.45: *The strain energy over the entire time period from the analytical solution for Location of Impact at the middle of the bat of the bat (at 0.25m) for an elastic, oblique collision*

6.4.3 Analysis for *Location of Impact* near the Fixed-End of the Bat (at 0.05m)

Figures 6.46 through 6.50 below portray the results for the collision near the fixed-end of the bat.

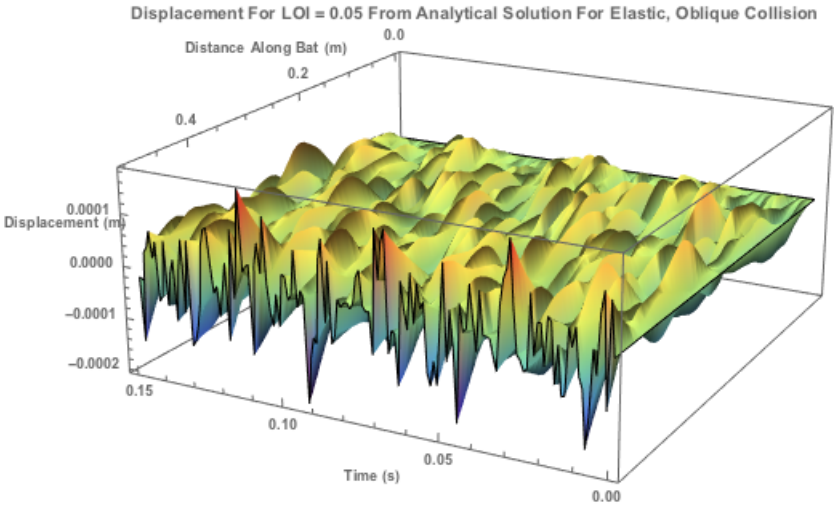

Figure 6.46: *The displacement profile from analytical solution for Location of Impact near the fixed-end of the bat of the bat (at 0.05m) for an elastic, oblique collision*

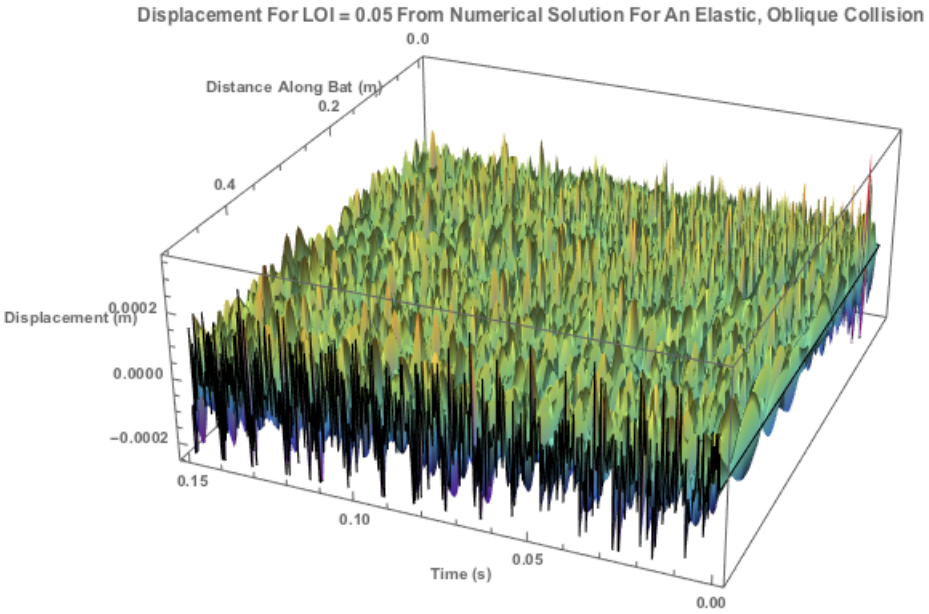

Figure 6.47: *The displacement profile from numerical solution for Location of Impact near the fixed-end of the bat of the bat (at 0.05m) for an elastic, oblique collision*

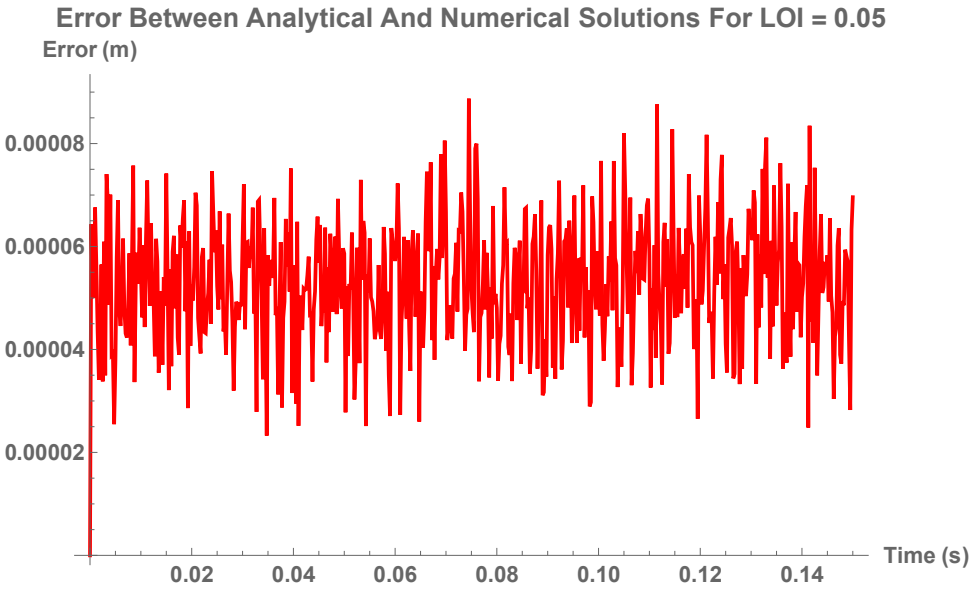

Figure 6.48: *The error between the analytical solution and the numerical solution for Location of Impact near the fixed-end of the bat of the bat (at 0.05m) for an elastic, oblique collision*

In a similar discussion to that of the previous collision scenario, Figure 6.48 shows that the absolute error between the two solutions is in agreement with the theoretical bound (from the Taylor Series truncation for a finite difference approximation). However, since the values of the displacement are small, it is important to note that the relative error is large.

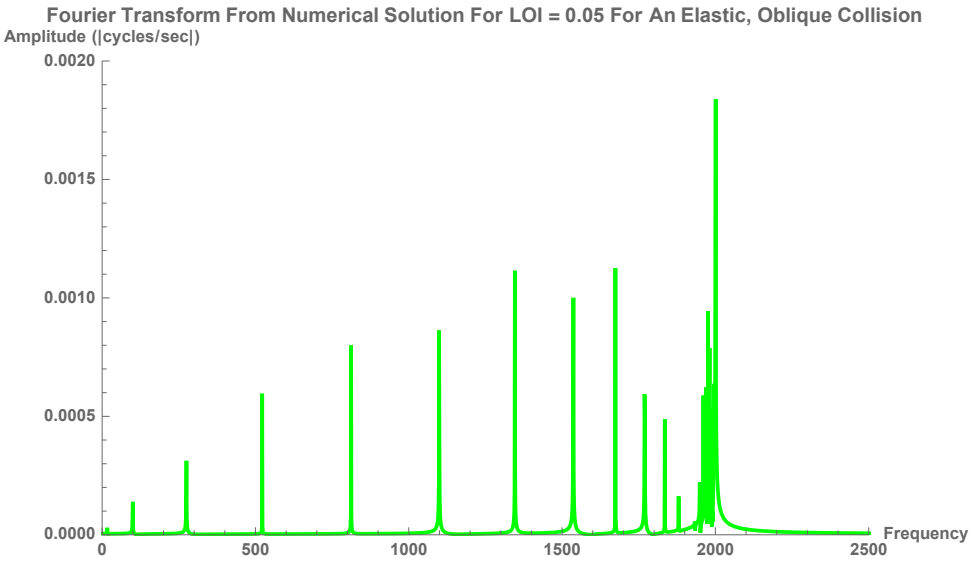

Figure 6.49: *The Fourier Transform from the numerical solution for Location of Impact near the fixed-end of the bat of the bat (at 0.05m) for an elastic, oblique collision*

Once again, it is important to note the changes in the scales of the axes from Figures 6.38 and 6.44 to 6.49.

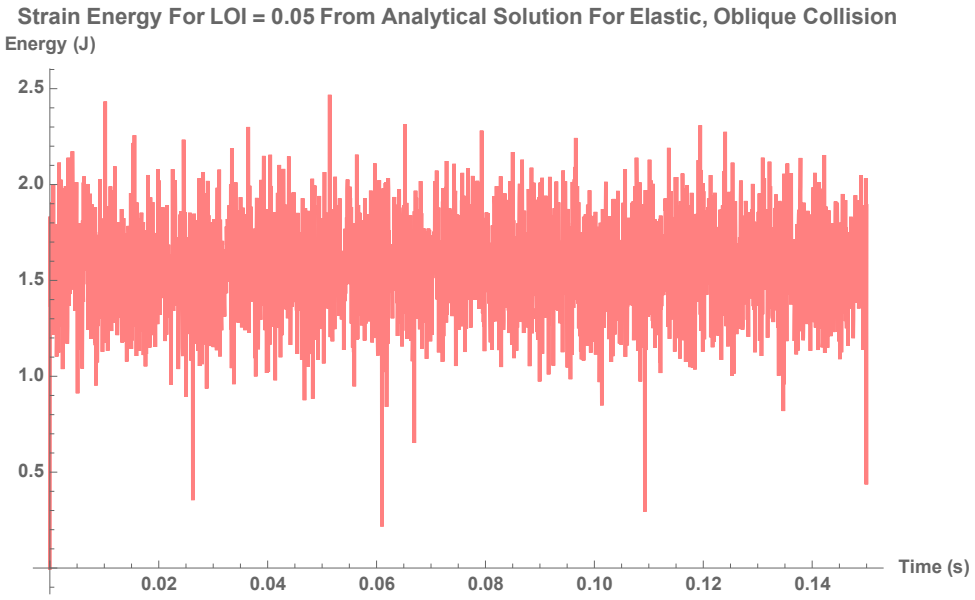

Figure 6.50: *The strain energy over the entire time period from the analytical solution for Location of Impact near the fixed-end of the bat of the bat (at 0.05m) for an elastic, oblique collision*

6.4.4 Discussion for Scenario where Collision is Elastic and Oblique

The results from this scenario suggest that modelling an upward collision between a cricket bat and a cricket ball as an oblique, elastic impact is a good approximation of reality for the type of shot that is being played.

Unlike the previous collision scenairo, the pressure distributions are non-symmetric about the *Location of Impact* over the length of the contact zone on the bat. As a result of the impact of the ball on the bat being modelled in an upward direction, the pressure is exerted more towards the free-end of the bat for each *Location of Impact*. This can be seen in the pressure distribution given by Figure 6.32. As a result of the oblique collision, the pressure distribution has a greater gradient towards the free-end of the bat and less towards the fixed-end of the bat. The pressure exerted by the ball on the bat is considerably smaller than in the previous collision scenario due to the fact that the collision is oblique and not direct. Once again, the value for p_0 is chosen in such a way as for the initial velocity of the *Location of Impact* to be at most 27 m/s. The initial velocity distributions themselves are also non-symmetric around the the *Location of Impact* over the length of the contact zone on the bat. This non-symmetric property of the distributions is a result of the oblique collision between the bat and the ball.

Unlike the first collision scenario and similarly to the previous collision scenario, the displacement profiles portray no discernible spike at the *Locations of Impact*. Identically to previously, it is argued that this is a result of the fact that the pressure from the impact modelled in this scenario is not focussed on a single point but is rather spread over the entire length of the contact zone.

The analysis from the Fourier Transform for the numerical solution supports the corresponding discussion from the previous two collision scenarios. For a *Location of Impact* near the free-end of the bat, a powerful, low frequency signal is produced. This dominant signal produces a smooth displacement profile. As the *Location of Impact* moves closer to the handle of the bat, the dominance of a single signal in the bat becomes less and higher frequencies in the bat become relatively more powerful. This results in smooth displacement profiles.

The strain energy in the bat is, in general, smaller than that of the previous collision scenarios. This is understandable since the collision is oblique and hence more glancing than direct. The amount of this energy in the bat from the analytical solution is very similar for the entire time period across all three *Locations of Impact* after the impact of the ball on the bat. As discussed for the previous two collision scenarios, this is reasonable since the ball is striking the bat with the same velocity at each *Location of Impact*. Therefore, the same amount of energy is imparted into the bat after the collision regardless of the *Location of Impact*. Across all *Locations of Impact*, there was originally zero strain energy in the bat. Immediately post-impact with the ball, the expected jump in strain energy is captured. Further, the strain energy in the bat remains constant over time since the model holds zero dissipative properties and no additional energy is entering into the system.

The displacement solutions from the numerical approach and the analytical approach are compared once again. Qualitatively, the solutions are in agreement. That is, the general behaviour of the solutions have been considered and the shapes of the solutions are consistent for both the numerical and analytical approach. Further, the displacement solutions are compared quantitatively as discussed in Chapter 6.1.2. This comparison shows that the numerical approach is consistent and accurate. This can be can be seen in the error plots in Figures 6.37, 6.43 and 6.48.

As with the previous collision scenario, the behaviour of the strain energy calculated by the numerical solution (Figure 6.40) is similar to the behaviour of the strain energy as calculated by the analytical solution (Figure 6.39) over the same time period. This holds true for all *Locations of Impact*. Both strain energy solutions model the behaviour of the strain energy in the bat over time as discussed above. As mentioned previously, it is not necessary to

compare the strain energy solutions quantitatively because the strain energy was derived from the displacement solutions.

Similarly to the previous collision scneario, both the analytical and numerical models are adequate for modelling this collision scenario; although analytical solution is more adept at modelling the strain energy and the numerical solution is more adept for the frequency analysis through the use of a Fourier Transform, as was the case in the previous collision scenario.

7 Discussion of the Results

Analysis into the displacement solutions of the numerical and analytical approaches provide the first insights into the main conclusions of this work. These solutions form the foundation of the overall analysis as all subsequent analyses are derived from these two solutions.

In general, the displacement solutions are intuitive and, for the second and third collision scenarios, agreeable with real-life scenarios. A *Location of Impact* near the free-end of the cricket bat provides greater displacement of the bat post-collision with a ball than a *Location of Impact* near the fixed-end of the bat. Further, the displacement profile of the bat post-collision with a ball for a *Location of Impact* near the free-end of the bat is generally smoother than for a *Location of Impact* near the fixed-end of the bat. A *Location of Impact* at the middle of the bat illustrates the transition between the cases of the two *Locations of Impact* near the two ends of the bat. Here, the displacement magnitude is less than for a *Location of Impact* near the free-end of the bat and more than for a *Location of Impact* at the fixed-end of the bat. Further, the displacement profile is less-smooth than for a *Location of Impact* near the free-end and smoother than for a *Location of Impact* near the fixed-end of the bat. These are intuitive and expected results.

These results can be further justified by examining the frequencies present in the bat at the *Location of Impact* post-collision with the ball. Such an analysis is achieved through the use of a Fourier Transform. For a *Location of Impact* near the free-end of the bat, a large, dominant signal with a low frequency is produced. This low frequency, long wavelength signal overpowers all other signals in the bat and results in the high amounts of displacement and its corresponding smooth profile. For a *Location of Impact* near the fixed-end of the bat, no truly dominant signals are produced. However, a number of high frequency, short wavelength signals with substantially smaller amplitude are present in the bat post-collision with ball. These signals interact with each other and result in small displacement magnitudes and 'non-smooth' displacement profiles.

Recall that the sweet-spot in this work was defined by the two-part definition: 1) the *Location of Impact* on a cricket bat that transfers the maximum amount of energy into the batted ball and 2) the *Location of Impact* that transfers the least amount of energy to the batsman's hands post-impact with the ball; minimizing the unpleasant stinging sensation felt by the batsman in his hands.

Consider the second part of this definition. For a *Location of Impact* near the free-end of the bat, it is clear that a powerful signal is produced in the bat. This signal will travel to the hands of the batsman (at the fixed-end of

the bat) and, as a result of the strength of this signal, the batsman will feel an unpleasant stinging sensation in his hands. Conversely, for a *Location of Impact* near the fixed-end of the bat, the many high frequency signals with small amplitudes that are produced post-collision with the ball will interact with each other and, to a large extent, cancel each other out. The batsman will feel only a slight stinging sensation in his hands when these signals reach the fixed-end of the bat. It is hence argued that the second part of the definition has been satisfied for a *Location of Impact* near the fixed-end of the bat. This is the primary result of this work.

The first part of the definition is discussed with the use of the analysis of the strain energy in the bat for each *Location of Impact*. As depicted by the various strain energy analyses in Chapters 6.2, 6.3 and 6.4, the strain energy in the bat is very similar for each *Location of Impact* in a particular collision scenario. As discussed previously, this is a reasonable result since the amount of energy entering into the bat due to the collision with the ball is the same regardless of the *Location of Impact*. Further, since the model does not contain any dissipative properties and no other energy is entering the system post-collision with the ball, the strain energy in the bat remains constant over time.

Therefore, an energy analysis such as this, conducted only on the strain energy in the bat itself, is inadequate for satisfying the first part of the definition of the sweet-spot since the strain energy in the bat appears to be independent of the *Location of Impact*. A more sophisticated analysis into the energy of the entire system - and into the energy in the batted ball, in particular - is required for satisfaction of the first part of the definition.

It is hypothesized that such an analysis will reveal that maximum energy in the batted ball will occur for a *Location of Impact* of near the free-end of the bat. However, it is clear from the above discussion that this *Location of Impact* will violate the second part of the definition of the sweet-spot. In fact, these two concepts of minimizing the sting with the *Location of Impact* near the fixed-end of the bat (as it is shown in this work) and maximizing the energy in the batted ball with the *Location of Impact* near the free-end of the bat (as it is hypothesized) are at odds with each other for finding the sweet-spot as it defined in this work.

It is therefore further hypothesized that a trade-off between these concepts will lead to the sweet-spot to be at some point between the free- and fixed-ends of the bat - although not necessarily at the middle of the bat. It is postulated that, once a sophisticated analysis for the strain energy in the whole system is developed, a sound and well-defined optimisation problem will be able to model this trade-off and fully determine the sweet-spot on the cricket bat.

8 Conclusion

The primary objective of this work was to determine the ideal hitting location (the 'sweet-spot') of a cricket bat when it hits a cricket ball. The model used in this work is based upon a two-part definition of the 'sweet-spot': 1) the *Location of Impact* on a cricket bat that transfers the maximum amount of energy into the batted ball and 2) the *Location of Impact* that transfers the least amount of energy to the batsman's hands post-impact with the ball; minimizing the unpleasant stinging sensation felt by the batsman in his hands.

As discussed in Chapter 3, the cricket bat was modelled by the Euler-Bernoulli Beam Equation under the boundary and initial conditions introduced in the same Chapter. In order to implement the model, both a numerical approach and an analytical approach were used to solve the equation and derive the subsequent analyses.

The analytical solution was constructed using a Separation of Variables approach. The numerical solution was constructed through the use of a Crank-Nicolson finite difference scheme. The numerical scheme was shown to be stable, consistent and therefore, via the Lax Thereom, convergent. Further, the scheme was shown to be in agreement with the analytical solution since the error between the two solutions were within the theoretical bands discussed in Chapter 4.2.

The solution of the approaches modelled the displacement of all points on the cricket bat over time. The solutions were reasonable and intuitive for different *Locations of Impact* and allowed for deeper analyses of the strain energy and frequencies at the *Locations of Impact* to be conducted.

The results from the strain energy analysis proved insufficient to adequately determine the sweet-spot. This is because the strain energy present in the bat is independent of the *Location of Impact*. This is likely due to the assumption of constant flexural rigidity (EI) throughout the bat. A more sophisticated analysis is required into the energy of the entire system (bat and ball) in order for the first part of the definition of a sweet-spot to be satisfied.

The frequency analysis through the use of a Fourier Transform was particularly significant to the main result of this work. An analyses into the frequencies present in the bat for different collision scenarios demonstrated that a *Location of Impact* near the fixed-end of the bat satisfied the second part of the two-part definition of the sweet-spot. More precisely, the frequency analysis showed that a *Location of Impact* near the fixed-end of the bat transferred the least amount of energy to the batsman's hands post-collision with the ball. This is because of the occurrence of rapid, small amplitude signals

caused as a result of the collision near the fixed-end of the bat.

As discussed in Chapter 2, Penrose and Hose [21] asserted that the point on the bat that provides the greatest velocity to the batted ball is dependent on the vibrational properties of the bat. Based on the analyses done in this work, particularly with regard to the frequency analysis, it is agreed that the 'sweet-spot' of a cricket bat is significantly dependent on the bat's vibrational properties; although this conclusion will stop short of saying that the 'sweet-spot' is entirely dependent on these properties based on the fact that these analyses did not consider the bat's true mass, inertial or density properties. Penrose and Hose also suggest that these vibrational properties should be more deeply and carefully considered by cricket bat manufacturers. The results of the frequency analyses discussed in this work do indeed support this conclusion made by Penrose and Hose. Considering the results that have been drawn from simple frequency analyses in Chapter 6, the results that could be found with a more in-depth frequency analysis of a model that more accurately models a cricket bat are potentially vast.

Further, since it is clear from these results that the vibrational properties play a significant role in the performance of a cricket bat, it is argued that it is not a good approach to model a cricket bat as a rigid object, as was done by Brearley *et al.* [3] and Brody [4]. As noted by Adair [1], the cricket bat is flexible over the time scale of the bat-ball collision. A rigid bat assumption implies that there is no flexibility in the cricket bat and it is argued that significant properties of the bat-ball collision and the mechanics thereafter are lost. Hence, extreme caution should be exercised when using results that have been obtained from modelling a cricket or baseball bat as a rigid object.

It is recommended that if similar or extended work is to be done in this area then the studies by the likes of Penrose and Hose [21], Knowles *et al.* [17], Hariharan and Srinivasan [14], Cross [9] and Jaramillo *et al.* [15] should be considered to be of particular importance to due to the emphasis on the vibrational qualities of the cricket bat.

It is important to note that shots modelled by this work are limited to shots where the ball contact time on the bat is considerably shorter than the time taken for the wave generated in the bat as a result of the collision with the ball to travel the length of the bat and return to the point of collision.

The work done in this project can be extended or improved in a number of ways. Firstly, as was noted by Knowles *et al.*, it is not ideal to use a clamped boundary condition to model the batsman's grip on the bat. During a cricket shot, the batsman obviously has a lot more maneuverability in his hands than a clamped boundary condition suggests. In addition, it is noted that the geometry of a cricket bat changes significantly at the fixed-end of the bat. The

boundary condition may not model reflections of signals at this point realistically. It is noted that a more realistic boundary condition would add more value to this work. Secondly, despite the success that the results in Chapter 7 indicate for the approximation of a Crank-Nicolson scheme in the model, it is hypothesized that a more sophisticated numerical scheme could be implemented in the model to find the numerical solution even more accurately. Thirdly, it is noted that there are very clear limitations of modelling the cricket bat as a one-dimensional beam. This work could definitely be extended to model a two- or three-dimensional cricket bat. Finally, it is clear that the assumptions that the bat has constant density and flexural rigidity could be heavily taxing on the modelling of a real-life cricket bat. It is hypothesized that more realistic assumptions with regards to these parameters could lead to more realistic behaviour of the bat post-collision with the ball.

9 References

[1] Robert K. Adair. The Physics of Baseball. *Physics Today*, pages 26–35, May 1995.

[2] Rob Bower. The Sweet Spot Of A Cricket Bat For Low Speed Impacts. *International Sports Engineering Association*, (15):53–60, 2012.

[3] M.N. Brearley, J.C. Burns, and N.J. De Mestre. What Is The Best Way To Hit A Cricket Ball? *International Journal Of Mathematical Education In Science And Technology*, 21(6):949–961, 1990.

[4] H. Brody. The Sweet Spot Of A Baseball Bat. *American Journal Of Physics*, 54(7):640–643, 1985.

[5] Anthony M.J. Bull. A Performance Comparasion Between Two Cricket Bat Designs, 2008.

[6] M.J. Carré, D.M. James, and S.J. Haake. Impact Of A Non-homogeneous Sphere On A Rigid Surface. *Proceedings Of The Institution Of Mechanical Engineers*, 2004.

[7] Marylebone Cricket Club. *Law 5 (The Ball)*, 2013. `http://www.lords.org/mcc/laws-of-cricket/laws/law-5-the-ball/`.

[8] CodeCogs. *Shear Force and Bending Moment*, 2011. `http://www.codecogs.com/library/engineering/materials/shear-force-and-bending-moment.php`.

[9] Rod Cross. The Sweet Spot Of A Baseball Bat. *American Journal Of Physics*, 66(9):772–779, September 1998.

[10] Rod Cross. The Bounce Of A Ball. *American Association Of Physics Teachers*, 67(3):222–227, March 1999.

[11] Bengt Fornberg. Generation of Finite Difference Formulas on Arbitrarily Spaced Grids. *Mathematics Of Computation*, 51(184):699–706, 1988.

[12] Henri P. Gavin. Strain Energy in Linear Elastic Solids. *Department of Civil and Environmental Engineering, Duke University*, 2015.

[13] F. Gutaj. A Comparasion Of Methods For Modelling The Dynamics Of A Cricket Bat. *Journal Of Mechanical Engineering Science*, 218(12):1457–1468, December 2004.

[14] V. Hariharan and (Dr) PSS Srinivasan. *Inertial And Vibrational Characteristics Of A Cricket Bat*. Department of Mechanical Engineering-PG, Kongu Engineering College, India.

[15] Paola Jaramillo, (Dr) Ronald S. Adrezin, John T. Reinard, Kevin S. Manarky, (Dr) Robert D. Celmer, and (Dr) Devdas Shetty. "Sweet Spot" or "Sweet Zone"? Modal Analysis Of A Wooden Baseball Bat For Design Optimization. *Journal Of Dynamic Systems And Control*, 2003.

[16] Kenneth Langstreth Johnson. *Contact Mechanics*, page 60. Cambridge University Press, 1987.

[17] S Knowles, Ft Brooks, and J.S.B Mather. *Novel Design Of Sports Equipment Through Impact Vibration Analysis*. Department of Mechanical Engineering, University of Nottingham, UK, 1996.

[18] Leonard Meirovitch. *Fundamentals Of Vibrations*. McGraw-Hill Higher Education, 2001.

[19] Peter McLeod Michael F. Land. From Eye Movements to Actions: How Batsmen Hit The Ball. *Nature Neuroscience*, 3(12):1340–1345, December 2000.

[20] L. Pauchard and S. Rica. Contact And Compression Of Elastic Spherical Shells: The Physics Of A 'Ping-Pong' Ball. *Philosophical Magazine*, 78(2):225–233, 1998.

[21] J.M.T Penrose and D.R Hose. An Impact Analysis Of A Flexible Bat Using An Iterative Solver. *Journal Of Sport Sciences*, 17(8):677–682, 1999.

[22] (Dr) Daniel A. Russel. The Sweetspot Of A Hollow Baseball Or Softball Bat, 2004.

[23] The Engineering Toolbox. *Speed of Sound in some Common Solids*, Accessed in 2015. `http://www.engineeringtoolbox.com/sound-speed-solids-d_713.html`.